Master's thesis

NTNU
Norwegian University of Science and Technology
Faculty of Engineering
Department of Geoscience and Petroleum

Håkon Myhre Aftret og Vetle Martnes Daleng

Suitability of Thermosyphon as a Ground Freezing Technology in Longyearbyen

Master's thesis in Geotechnology
Supervisor: Randi Kalskin Ramstad
Co-supervisor: Malte Jochmann, Aleksey Shestov and Henrik Holmberg

June 2022

NTNU
Norwegian University of
Science and Technology

Håkon Myhre Aftret og Vetle Martnes Daleng

Suitability of Thermosyphon as a Ground Freezing Technology in Longyearbyen

Master's thesis in Geotechnology
Supervisor: Randi Kalskin Ramstad
Co-supervisor: Malte Jochmann, Aleksey Shestov and Henrik Holmberg
June 2022

Norwegian University of Science and Technology
Faculty of Engineering
Department of Geoscience and Petroleum

NTNU
Norwegian University of
Science and Technology

Preface

This master's thesis is written as the final work of the Master of Science in Geotechnology with a specialization in Rock Mechanics and Engineering Geology. The paper is written for the Department of Geoscience and Petroleum at the Norwegian University of Science and Technology (NTNU) in Trondheim, Norway.

We would like to thank our main supervisor, Randi Kalskin Ramstad, for her assistance during the writing of this thesis and for forming such an interesting topic for the thesis. The input from our co-supervisors is also greatly appreciated. Thanks to Malte Jochmann for his feedback during the semester and for collecting rock samples on Svalbard. Assistance and discussions regarding modeling and results from Aleksey Shestov has been a great advantage during this study. Henrik Holmberg also deserves gratitude for his input and discussion during this work.

Lastly, we would like to thank our friends and fellow students in Trondheim for 5 fantastic years.

Trondheim, June 2022.

Håkon Myhre Aftret og Vetle Martnes Daleng

Sammendrag

Nedkjøling av grunnen er i mange tilfeller nødvendig ved bygging av infrastruktur i arktiske områder for å unngå tining av permafrost. Tining av løsmasser og berg reduserer materialets trykkfasthet, som igjen kan gi setninger og skader på konstruksjoner. I avsidesliggende områder som Longyearbyen er energi kostbart og har høye CO2-utslipp. Det er derfor viktig å sikre at energien utnyttes så effektivt som mulig. Termosifonger er tofasede varmevekslere som kan utnytte kald luft til å kjøle ned bakken uten behov for ekstra energi. Målet med denne oppgaven er å vurdere termosifongers egnethet for nedkjøling av grunnen i Longyearbyen. Det er flere potensielle bruksområder, inkludert kjøling for vindmøllefundamenter, bygninger, geotermiske brønner og annen infrastruktur. Egnethet for kjøling ved bruk av termosifong i dagens og fremtidig klima er vurdert ut fra beregninger i programvaren COMSOL. For fremtidig klima er det vurdert to CO2-utslippsscenarier, RCP45 og RCP85. RCP45 er et middels utslippsscenario med moderat økning i lufttemperatur, RCP85 er scenarioet med størst utslipp og høyest temperaturøkning. Den numeriske modellen inkluderer en simulering med et bygningsfundament på permafrost.

Modellering viser reduserte temperaturer i grunnen ved installasjon av termosifonger. Effekten reduseres for høyere lufttemperaturer med fremtidige klimaendringer. Høye utslipp, RCP85, vil føre til omfattende tining av permafrost, og termosifonger blir ikke sett på som egnet for slike temperaturer. For dagens klima- og moderate utslipp, RCP45, kan termosifonger gi passiv kjøling og effekten er tilstede gjennom vinteren. Om sommeren vil ikke termosifonger gi kjøling på grunn av høye lufttemperaturer. På grunn av dette anses en hybrid termosifongløsning, med mulighet for å for å gi aktiv kjøling, i tillegg til passiv kjøling, som en gunstigere løsning. Denne studien antyder at termosifonger har potensial til å bli brukt for nedkjøling av grunnen i Longyearbyen.

Abstract

Ground cooling is necessary in many cases when constructing infrastructure in Arctic areas to avoid permafrost thawing, settlements, and damage to constructions. Thawing of soil and rock decreases the compressive strength of the material. In remote areas such as Longyearbyen energy is expensive and comes with high CO2 emissions. For this reason, it is essential to ensure that energy is not wasted and utilized as efficiently as possible. Thermosyphons are two-phased heat exchangers that utilize cold air to cool the ground without the need for additional energy. The goal of this thesis is to review the suitability of thermosyphons as a ground freezing technology in Longyearbyen. There are several potential applications including ground freezing for windmill foundations, buildings, geothermal wells and other infrastructure. Establishing a numerical model in the commercial software, COMSOL, the study evaluates thermosyphon cooling for today's climate and future climate, for two CO2 emissions scenarios, RCP45 and RCP85. RCP45 is a middle emission scenario with a moderate increase in air temperature, and RCP85 is the worst-case emission scenario with the highest temperature increase. The numerical model includes a building foundation case.

Results from modeling shows lower ground temperatures with thermosyphons in operation. The effect is reduced for higher air temperatures with future climate change. High emissions, RCP85, will lead to extensive thawing of permafrost, and thermosyphons are will not be suitable for such temperatures. For today's climate and mid-range emissions, RCP45, thermosyphons can provide cooling passively and the effect is present during winter. During summer thermosyphons can not provide cooling due to warm air. Therefore, a hybrid thermosyphon solution, with the option to provide active cooling, in addition to passive cooling, is considered a favorable solution. This study suggests that thermosyphons have the potential to be used for ground freezing in Longyearbyen.

Contents

List of Figures

List of Tables

1 Introduction

1.1 Background

Mean annual air temperatures in the Arctic have been increasing over the past decades and are expected to increase in the future. This will affect the environment and the permafrost in these areas. Warmer temperatures will increase the active layer depth and make the permafrost more sensitive. When constructing buildings and other infrastructure in permafrost precautions must be taken to ensure that the permafrost does not thaw. Finding an efficient and environmentally friendly solution to prevent permafrost thawing is essential to preserve the permafrost with low emissions. Using a thermosyphon is a possible option to cool down permafrost and prevent thawing.

A thermosyphon is a two-phase heat exchanger that can utilize cold air to cool down and preserve permafrost. Thermosyphons are advantageous in the way that they can provide cooling from the temperature difference between the ground and the air alone, without the need for additional energy. With the climate in Longyearbyen, the temperature is low during large parts of the year which ensures there is potential for thermosyphon to be sufficient as a ground cooling technology. The technology is in itself green and thermosyphons can be combined with other renewable energy sources. Thermosyphons can be combined with heat pumps, work as foundation cooling for windmills or prevent permafrost thaw when establishing geothermal wells. Thermosyphons have previously been used for cooling under buildings and railroads as both passive solutions and hybrid solutions with the option to provide cooling using a heat pump.

The topic of this thesis is relevant as a contribution to the transition to more clean energy use. This is in line with the long-term strategy to phase out coal and use more renewable energy in Longyearbyen (Regjeringen, 2021). This study is also relevant for other Arctic communities with similar challenges as Svalbard. Electricity is often provided from diesel in Arctic areas which are both expensive and negative for the climate (de Witt et al., 2019). Countries having energy policies for renewable energy in the Arctic include Alaska, Greenland, and Canada, with goals of reducing cost and emissions (de Witt et al., 2019).

1.2 Aim and Objectives

The aim of this thesis is to evaluate the suitability of thermosyphon as a ground cooling technology in Longyearbyen. The study will include today's climate and

temperature from future climate projections. The thermal impact of thermosyphons for different temperatures will be compared. The goal is to address potential applications of thermosyphons and see if this is a suitable option for Svalbard.

The following objectives are of interest to achieve this:

- Review thermal conditions of permafrost in Svalbard and the expected impact of future climate changes.
- Introduce the technology and review applications for thermosyphons.
- Build a finite element model (FEM) to evaluate the thermal impact of thermosyphons and discuss the suitability as a ground cooling option in Longyearbyen.
- Compare thermosyphon cooling for today's air temperatures with expected temperatures from future climate predictions.

1.3 Limitations

The main limitations for this thesis are uncertainties regarding the modeling. When building a numerical model it is necessary to make assumptions and simplifications. The model should represent the physical real-world problem as accurately as possible, but uncertainty is introduced. The modeling is simplified and done in 2 dimensions, thus end effects for the thermosyphons are not accounted for. Still, 2D is considered to be sufficient to evaluate the suitability of thermosyphons. The thermosyphon heat transfer used in the model comes from an empiric equation from theory and it is a simplification of the actual heat transfer as shown in the theory section. The ground surface boundary condition is challenging to describe accurately. The ground surface boundary is affected by several factors and the necessary data is not available. The resolution of the wind and air temperature data is in days which also introduces inaccuracy for both the ground surface boundary and the thermosyphon boundary. Temperatures and wind speed vary throughout the day and average data will not necessarily give the same output as data sampled with finer resolution. The wind data can be different from the actual wind speed for a specific site, both topography, and infrastructure impact wind speed locally. Wind affects both the ground surface boundary and the thermosyphon heat sink.

Future climate projections are complex and come with uncertainties. Different climate models give different estimates and the variation between the coldest and hottest estimations are significant. The mean temperature is used in this study,

but it is still important to be aware of uncertainties that follow projections for climate towards the end of the century. The uncertainty of future temperatures and simplifications of the ground surface boundary also give an expected deviation for the initial conditions used in the simulation with future climate. One should also keep in mind the horizontal grid of the climate simulation being 0.44°, approximately 50km, which can reduce accuracy due to factors such as topography and sea-ice and atmosphere interaction that affect the climate locally (Hanssen-Bauer et al., 2019).

1.4 Structure

The thesis is structured into chapters with sections and subsections. Chapter 2 presents the theory for the thesis. This includes permafrost and its thermal characteristics, and the climate in Longyearbyen. The theory chapter also presents the theory for thermosyphons. The driving forces for a thermosyphon and heat transfer through the heat exchanger are presented. Different solutions and applications for thermosyphons are also shown in Chapter 2. Chapter 3 introduces the methodology of this thesis. The collection of climate data for the thesis is addressed. Background and theory behind the tests for the thermal properties of rock. Chapter 3 also introduces and explains the numerical model setup. This includes an explanation of finite element modelling (FEM) and the choices for the numerical model. Chapter 4 presents the results from the simulations. Chapter 5 is a discussion of the presented results. Chapter 6 provides a summary and conclusion of the study. Chapter 7 presents recommendations for further work on the subject to expand and improve on this study.

2 Theory

2.1 Permafrost

2.1.1 What is Permafrost?

Permafrost is present if the ground holds a temperature of below 0 ° C for two consecutive years (Flyen & Mattson, 2017). This implies that the air temperature must be below 0°C on average for the permafrost to develop. In reality, the temperature needs to be lower than - 2°C for the permafrost to have any significant extension (French, 2017). The climate providing such low temperatures is found in a northern latitude, typically in areas such as Russia, Canada, and Svalbard, but also in central Norway such as Jotunheimen (Flyen & Mattson, 2017). The vertical extension of permafrost can be from a few meters to 1500 meters (Flyen & Mattson, 2017). The top layers of the ground will thaw during parts of the year due to seasonal temperature variations, this upper part is called the active layer. The thickness of the active layer changes from year to year, and the depth will depend on the local temperatures, typically depth is a few centimeters to more than 1 meter. In Longyearbyen, the active layer is approximately 1.5 meters (Instanes & Rongved, 2018). Towards greater depth one can expect the ground is not affected by seasonal changes in air temperature, this depth is called zero annual amplitude (ZAA). At ZAA the temperature is constant through the season, but the temperature can change over time due to a change in the climate. An illustration of layering, zero annual amplitude, and the temperature towards depth is shown in Figure 1.

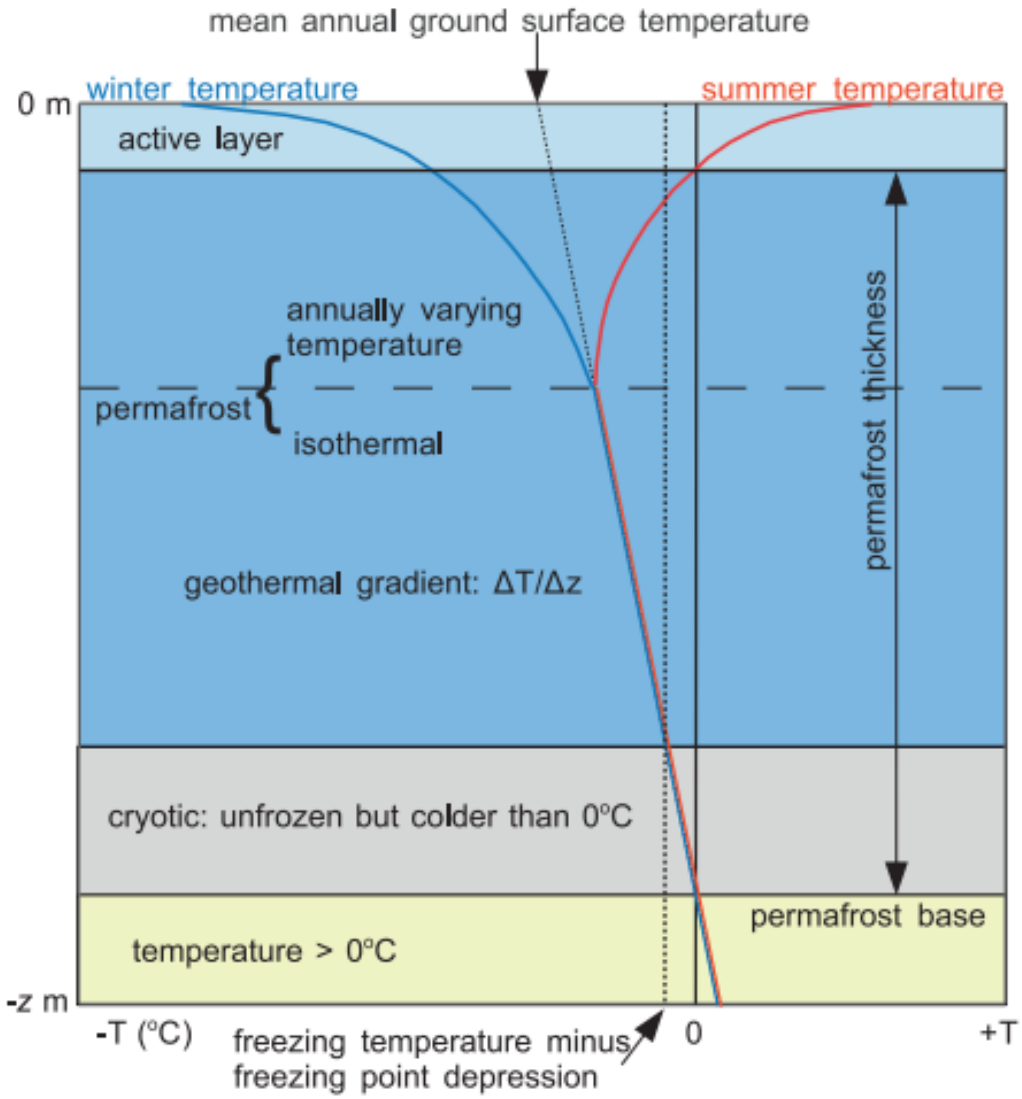

Figure 1: Layers and temperature of permafrost towards depth (van Huissteden, 2020).

From Figure 1 one can notice the cryotic layer where the permafrost is colder than 0°, but not frozen. Since permafrost is defined from temperature alone, the permafrost does not have to be frozen hard to be defined as permafrost. Thus to preserve the frozen characteristics of the ground the permafrost might have to be held at lower temperatures than 0°C.

The temperature of the permafrost is determined by climatic factors such as air temperature, snow coverage, wind and radiation, and the thermal properties of the (Johansson et al., 2006). The ground surface temperature will have a daily and an annual fluctuation which is related to the temperatures towards depth. Both surface temperature and temperature at depth are illustrated in Figure 2.

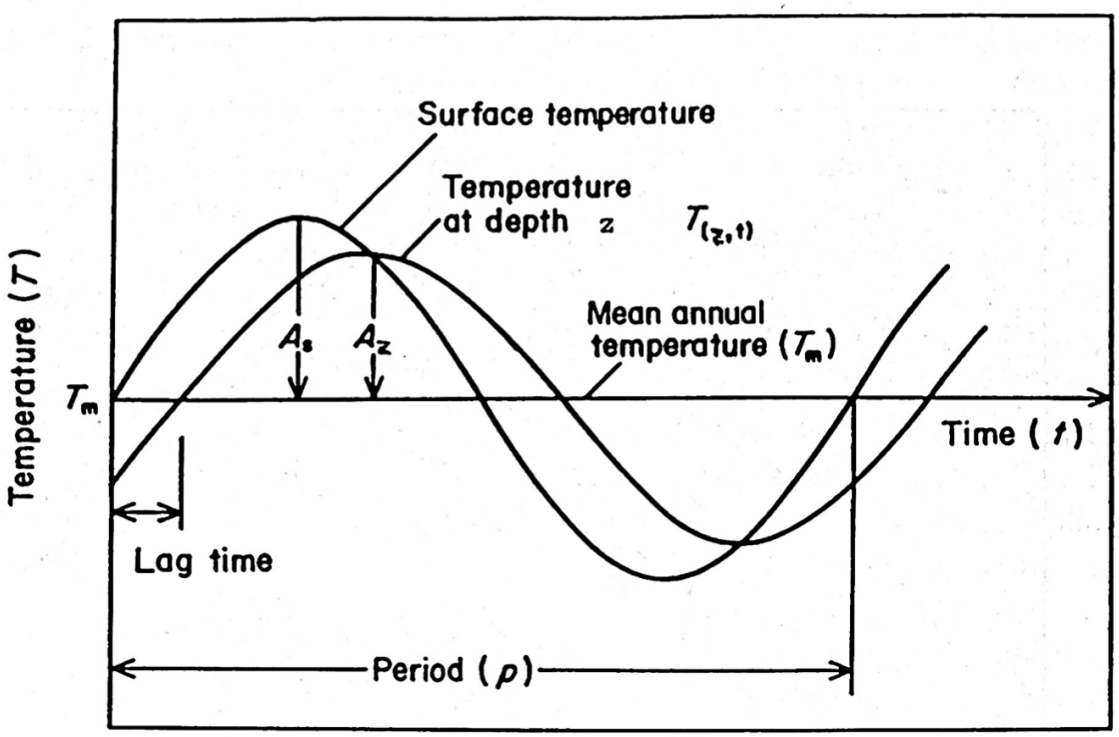

Figure 2: Sinusoidal fluctuation of the surface and permafrost temperature over time (Andersland & Ladanyi, 1994).

From Figure 2 one can notice the delay in the ground temperature as a shift in the sinusoidal function. The ground surface temperature can be estimated using Equation 1 (Andersland & Ladanyi, 1994). This gives an estimate of the surface temperature for a given time.

$$T_{s,t} = T_m + A_s \left(sin \frac{2\pi t}{p} \right) \tag{1}$$

Where:

- $T_{s,t}$ = Surface temperature [K]
- T_m = Mean annual temperature [K]
- A_s = Surface temperature amplitude [K]
- p = Period [Day]
- t = Time [Day]

When assessing temperatures of the permafrost with respect to the depth, a time delay for temperature change at depth compared to the ground surface temperature

must be taken into account. The reason for this delay will be the time it takes the heat to reach depth z. For a homogeneous soil with no change of state the ground thermal regime can be estimated using Equation 2 (Andersland & Ladanyi, 1994). The heat flux from the deeper soil temperature is neglected.

$$T_{z,t} = T_m + A_s exp\left(-z\sqrt{\frac{\pi}{\alpha_u p}}\right) sin\left(\frac{2\pi t}{p} - z\sqrt{\frac{\pi}{\alpha_u p}}\right) \tag{2}$$

Where:

- $T_{z,t}$ = Temperature for a given depth and time [K]
- α_u = Thermal diffusivity $[m^2/Day]$

To synchronize the coldest day with the lowest point in Figure 2, a phase lag, ϕ, must be added to Equation 2 (Andersland & Ladanyi, 1994). Without including the phase lag, the day with the coldest air temperature would not correlate with the ground surface temp. With the phase lag, the temperature at a given time of the year and at a given depth can be estimated with Equation 3.

$$T_{z,t} = T_m + A_s exp\left(-z\sqrt{\frac{\pi}{\alpha_u p}}\right) - cos\left(\frac{2\pi t}{p}(1-\phi) - z\sqrt{\frac{\pi}{\alpha_u p}}\right) \tag{3}$$

Where:

- ϕ = Phase lag [Day]

2.1.2 Permafrost in Longyearbyen

The depth of permafrost in Svalbard ranges from 100 meters in valleys and near the coast, to 500 meters in mountain areas. The main factors for permafrost thickness include air temperature, topography, snow cover, lithology, geothermal heat flow, and distance to ocean (Humlum et al., 2003). Svalbard has low annual average temperatures and the snow cover is not thick. In 2018, the annual 30 year average temperature was - 3.9°C (Gilbert et al., 2019). The average precipitation is observed to be 196 mm in the period 1971 - 2000 (Isaksen et al., 2017). Cold air temperatures and low precipitation grant good conditions for permafrost. The ocean is warm compared to the permafrost and therefore there are large differences in permafrost depth in near coastal areas compared to mountain areas.

For construction and cooling purposes the future conditions and characterization

of the permafrost in Longyearbyen are important. Increased air temperatures and increased temperature in the permafrost reduce the compressive strength of the ground and increase the chance of settlements. When using thermosyphons or other cooling operations, warmer temperatures demand more cooling. The ground temperatures, as well as the air temperatures, are predicted to increase in the future towards 2100 (Instanes & Rongved, 2018). Despite increased temperatures, the permafrost is most likely present also in 2100. A warmer climate will also lead to warmer permafrost, but the change in ground temperature is delayed compared to air temperature. The temperature of the permafrost at 10 meters depth increased by 0.06-0.15°C in the period 2009-2018 (Hanssen-Bauer et al., 2019). Warmer ground temperatures also lead to greater depth in the active layer, and an increase of 1 meter, to a total of 2.5 meters depth, is likely in 2100 (Instanes & Rongved, 2018). In Longyearbyen center the ground temperature at 10 and 20 meters is modeled by and predicted to increase (Instanes & Rongved, 2018):

- At 10 meters depth the temperature is expected to increase by 1.6°C, from -3.9°C to -2.3 from 2017 to 2100.
- At 20 meters depth the temperature is expected to increase by 1°C, from -4.2°C to -3.2°C from 2017 to 2100.

2.1.3 Thawing of Soil and Bedrock

Thawing of soil and bedrock is a concern for buildings and other infrastructure in Longyearbyen, as well as other Arctic areas. The compressive strength is reduced in both soil and bedrock when the temperature of the permafrost increases and thawing happens. Frozen soil has proven to have higher strength than unfrozen soil. The strength has been shown to be 8 times greater for frozen sand with the same conditions (Ladanyi & Andersland, 2004). Frozen soil has poor draining abilities, meaning that permafrost thawing potentially can cause increased pore pressure and over-saturated soil causing further instabilities, especially in ice-rich soil.

Areas, where permafrost sits in the bedrock, can be exposed to many of the same problems as areas with permafrost in soil. If the bedrock is ice-rich and has fractured permafrost thawing can cause instability problems due to volume reduction when the ice thaws. If the bedrock in addition has ice lenses, where one can expect thawing, the issues can be more significant. In addition to this, the strength of bedrock is greater when frozen rather than unfrozen. The friction angle of frozen bedrock is shown to be greater than that of unfrozen bedrock (Krautblatter et al., 2013).

2.2 Climate in Longyearbyen

The climate in Longyearbyen has been showing warmer air temperatures over the past decades. This affects the permafrost due to warmer mean annual temperatures. The temperature is projected to keep increasing in the future. It is important to assess this climate change as it affects both the permafrost and the effect of thermosyphons. Increased temperatures will affect the characteristics of permafrost and make it more sensitive. Thermosyphons are dependent on the temperature difference between the permafrost and air temperature to provide cooling, thus changes in both air temperature and permafrost temperature may affect the cooling potential of thermosyphon. Changes in the climate include other aspects of the climate than just air and permafrost temperature, but these two factors are seen as the most relevant for this thesis.

2.2.1 Introduction

The climate in Svalbard and Longyearbyen is cold and the precipitation is low. The average annual temperature in the period 1971-2000 was -5.9°C and yearly precipitation was approximately 200mm (Hanssen-Bauer et al., 2019). The mean annual air temperature in Svalbard has increased steadily in the latest 40-50 years. The increase in the observed mean annual temperature is 3-5° since 1971, with higher temperature change in the winter season than summer season (Hanssen-Bauer et al., 2019). Temperatures from 1976 - 2021, from Norwegian Centre for Climate Services (MET, 2022), are plotted in Figure 3 and show the increase in air temperature in the latest decades.

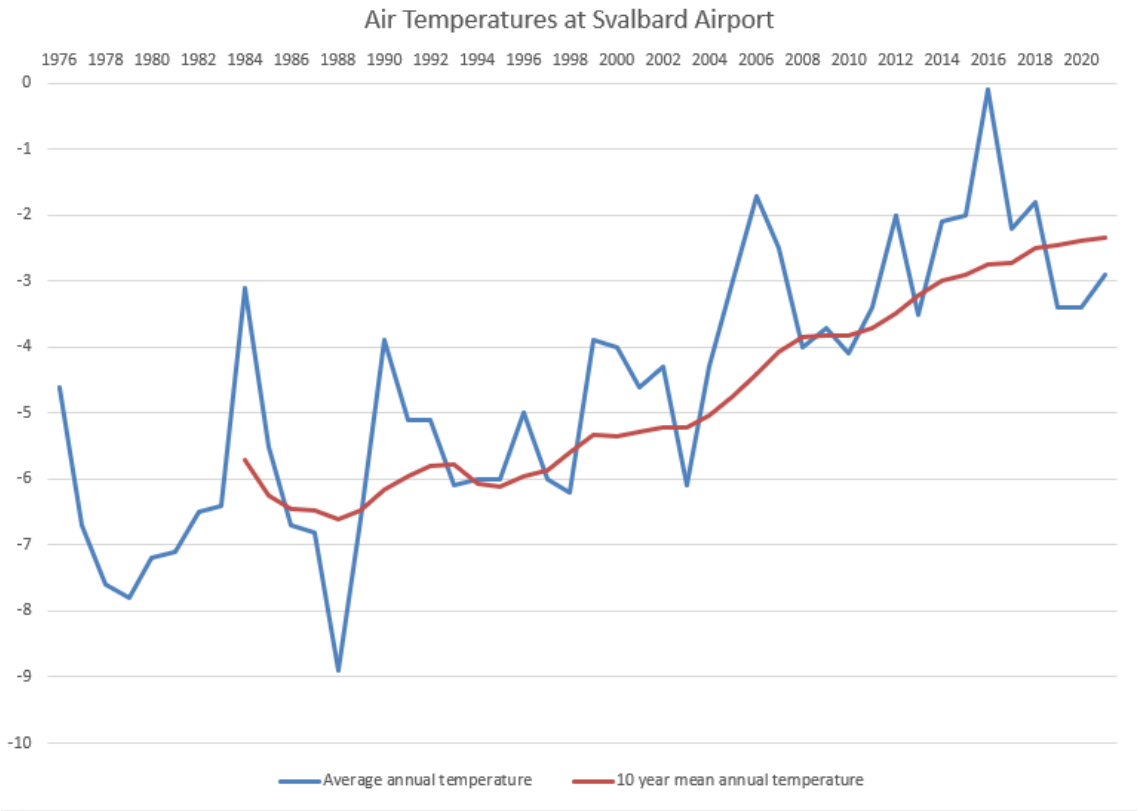

Figure 3: Average annual and 10-year mean annual temperatures at Svalbard airport from 1976-2021. Plotted using data from MET (2022).

For meteorological weather data, the closest measurement station to Longyearbyen is located at Svalbard Airport. One can use this temperature data from Svalbard airport to analyze and compare the historical temperatures for Longyearbyen. According to MET the temperature correction needed to compare Svalbard airport and Longyearbyen is 0°C (Instanes & Rongved, 2018). Average temperatures from 1961 to 2015 for a 30-year span at Svalbard Airport are shown in Table 1. This Table indicates the bigger change in temperature in winter compared to the summer season. The period 1961-1990 compared to 1986-2015 shows an increase in 1.1 °C for summer and 3.2 °C for the winter season.

Table 1: Average temperatures at Svalbard Airport, annual and for seasons. "DJF", "MAM", "JJA", "SON" - short for the months included in each season. Modified from: Isaksen et al. (2017)

.

	Average Temperature [°C] at Svalbard Airport		
	1961-1990	**1971-2000**	**1986-2015**
Annual Average	-6.7	-5.9	-4.6
Winter DJF	-15.0	-14.0	-11.8
Spring MAM	-10.8	-9.6	-8.2
Summer JJA	4.1	4.5	5.2
Autumn SON	-5.2	-4.7	-3.5

2.2.2 Future Climate in Svalbard and Longyearbyen

Several report reports are written regarding both permafrost and the climate in Svalbard and how it is predicted to change towards 2100. Climate in Svalbard 2100 by Hanssen-Bauer et al. (2019), Forventede klimaendringers påvirkning på byggegrunn i Longyearbyen-området (Expected Change in Climate Affects Construction in Longyearbyen Area) Instanes and Rongved (2018) and Klimascenarioer for Longyearbyen-området, Svalbard (Climate Scenarios for Longyearbyen area, Svalbard) (Isaksen et al., 2017) are reviewed especially, to assess future climate and permafrost in Longyearbyen. The reports have some common data from Arctic CORDEX. The reports evaluate different emission scenarios with, RCP2.6, RCP4.5, and RCP8.5. RCP2.6 is the scenario with the biggest cuts in CO_2 emissions, this scenario considers big reductions in emissions from 2020. RCP4.5 predicts climate change with reductions in greenhouse gasses from 2040. RCP8.5 predicts the future climate in a scenario with a very low reduction in emissions from today's level.

Climate in Svalbard 2100

The report Climate in Svalbard 2100 predicts the change in climate from 1971-2000 to 2071-2100. This report uses Arctic regional climate models and a fine-scale atmospheric climate model, COSMO-CLM (Hanssen-Bauer et al., 2019). For the period 1971-2000 the average temperature at Svalbard airport was -5.9°C.

For the scenario with the lowest reduction in CO_2 emissions, RCP8.5, the mean

annual air temperature is estimated to increase by almost 10°C. This will mean that the annual mean temperature at the end of the century is 4.1°C. For the scenario with a reduction in CO_2 emissions from 2040, RCP4.5, the temperatures do not increase to the same extent. For this lower emissions scenario, the increase in mean annual temperature is estimated to be 7°C. With a 7°C increase, the mean annual temperature in the period 2071-2100 is 1.1°C. From the report, one can also note an increase in expected precipitation with future climate change. The increase in precipitation is 65% and 45% for RCP8.5 and RCP4.5 respectively.

This report reviews ground temperature modeling. For the scenario with emissions RCP8.5, the upper parts of the permafrost are projected to thaw before 2100. Modeling of ground temperature from the report suggests permafrost thawing down to a depth of at least 5 meters depth in near costal and low altitude areas, while the permafrost is still intact below 10 meters. The report concludes that the upper parts of the permafrost will thaw completely in some scenarios between RCP4.5 and RCP8.5. Hanssen-Bauer et al. (2019) state the following in their report:

> For most of the lowland landscape in western Svalbard, all available modeling results suggest that the limit between "permafrost remains (at least partly)" and "the upper meters of the permafrost thaws completely" towards the end of the century will be somewhere between the emission scenarios RCP4.5 and RCP8.5. (p.11)

Climate Scenarios for Longyearbyen Area, Svalbard

This report estimates future climate change in Svalbard with 1971-2000 as a reference period. The estimates stretch as far as 2200, but the main focus is towards 2100. The report uses the emission scenarios RCP4.5, RCP8.5, and RCP 2.6, the latter being a low emission scenario for big cuts in emissions from 2020. The increased temperatures mentioned are in comparison with the reference period, 1971-2000, if not stated otherwise. The average temperature for the reference period is the same as in Climate in Svalbard 2100, -5.9°C.

The report utilizes several models and simulations to predict future temperatures. The results give different estimates, but the report presents estimations based on a selection of methods and models. For the lowest emission scenario, RCP2.6, the yearly average temperature towards the middle of the century increases by 4.0°C. Towards the end of the century, 2071-2100, the models show an increase of 3.6°C. This indicates little change and stable temperatures for the low emissions scenario in the period 2050-2100. For the middle emission scenario, RCP4.5, the temperature is

expected to increase by 4.6°C for the period 2031-2060. For the period 2071-2100, the models predict an increase by 6.5°C for RCP4.5. For the highest emission scenario, RCP8.5, the temperature increase is higher. The temperature is predicted to increase by 5.3°C for the period 2031-2060. The temperatures keep increasing throughout the century and estimated temperatures in the period 2071-2100 are 9.2°C higher than the reference period. An overview of the predicted temperature changes are listed in Table 2, both annual average and seasonal changes are shown for both mid and end-of-century predictions.

Table 2: Temperature change in °C for different emission scenarios, by season and annual for the periods 2031-2060 and 2071-2100. Modified from Isaksen et al. (2017)

	Temperature Change [°C]					
	2031-2060			**2071-2100**		
	RCP2.6	**RCP4.5**	**RCP8.5**	**RCP2.6**	**RCP4.5**	**RCP8.5**
Annual Average	4.0	4.6	5.3	3.6	6.5	9.2
Winter (DJF)	5.5	6.8	7.8	5.7	9.1	13.4
Spring (MAM)	3.7	4.5	5.3	3.7	6.7	9.7
Summer (JJA)	1.3	1.9	2.2	1.1	2.6	4.0
Autumn(SON)	4.3	5.1	5.6	4.2	6.7	9.4

These increases in annual temperature entail average annual temperatures above 0° for both RCP4.5 and RCP8.5 in the period 2071-2100. For the lowest emission scenario, average temperatures are -1.9° and -2.3° for the periods 2031-2060 and 2071-2100 respectively. The temperature in 2031-2060 is -1.3° for RCP4.5 and -0.6° for RCP8.5, considering predicted temperature increases. Annual average temperatures for both 2031-2060 and 2071-2100, based on predicted temperature changes Isaksen et al. (2017), are summarized in Table 3.

Table 3: Predicted average annual temperatures in Longyearbyen in the periods 2031-2060 and 2071-2100. Modified from Hanssen-Bauer et al. (2019).

	Average Annual Temperature [°C]		
	RCP2.6	**RCP4.5**	**RCP8.5**
2031-2060	-1.9	-1.3	-0.6
2071-2100	-2.3	0.6	3.3

Expected Change in Climate Affects Construction in Longyearbyen Area

The main focus of this report written by Instanes and Rongved (2018), is the ground conditions in Longyearbyen. The report evaluates ground thermal modeling based on the middle emissions scenario, RCP4.5. The data used for the modeling is Arctic CORDEX. The ground thermal analysis is done with the software Temp/W from Geo-Slope International ltd. This software utilizes a finite element method.

The report reviews geothermal modeling at three locations in the Longyearbyen area, Sentrum, Skjæringa, and Forskningsparken. For all three locations, the modeling indicates warmer ground temperatures at 10 meters and 20 meters in depth. Increased depth of the active layers is also predicted for all locations. A summary of ground temperatures in 2017 and predicted temperatures in 2100, at 10 meters and 20 meters depth is presented in Table 4.

Table 4: Ground temperatures in 2017 and predicted temperatures in 2100. Modified from Instanes and Rongved (2018).

	Modeled Mean Annual Temp. [°C]		Modeled Ground Temperature [°C]				Depth of Active Layer	
			10 m depth		20 m depth			
	2017	2100	2017	2100	2017	2100	2017	2100
Sentrum	-3.7	-0.4	-3.9	-2.3	-4.2	-3.2	1-1.5 m	ca. 2.5 m
Skjæringa	-3.7	-0.4	-2.8	-1.1	-3.1	-1.4	ca. 1.5 m	ca. 2.5 m
Forskningsparken	-3.7	-0.4	-3.6	-1.9	-3.7	-2.7	ca. 1.5 m	ca. 2.5 m

2.2.3 Wind Conditions

The most common wind direction at Svalbard Airport is south-easterly winds (Dobler, 2019). Wind direction and wind speed are predicted to have only minor changes in future climate (Hanssen-Bauer et al., 2019). In addition, the predictions for wind are large, and local winds are affected by topography and infrastructure. For this reason, one might find it acceptable to use historical wind speed for future climate simulations.

2.3 Ground Surface Thermal Characteristics

2.3.1 Ground Surface Energy Balance

The energy balance between the air and ground surface can be divided into solar radiation, longwave radiation, sensible heat, and latent heat. This ground heat flux can be calculated from Equation 4 (Andersland & Ladanyi, 1994).

$$q_g + aq_{sw} + q_{lw} + q_h + q_e = 0 \tag{4}$$

Where:

- q_g = Ground heat flux $[J/(m^2 s)]$
- q_{sw} = Net flux solar radiation $[J/(m^2 s)]$
- q_{lw} = Net flux long wave radiation $[J/(m^2 s)]$
- q_h = Net heat convection to air $[J/(m^2 s)]$
- q_e = Heat flux from evaporation $[J/(m^2 s)]$
- a = Absorptivity

The net solar radiation is the amount of heat flux from the sun that reaches the ground surface. This will depend on the position of the sun, weather, and albedo. When solar radiation hit the ground surface, some will be converted into heat energy. And the emitted energy that is released from the ground surface is known as longwave radiation (Geo Slope, 2021).

The heat convection is the transport of heat between two materials with different temperatures. It will mainly depend on the temperature difference between the air and the ground, but also on wind speed and roughness of the ground surface. The

heat flux from evaporation and condensation describes the released, or absorbed, amount of energy within a phase change (Geo Slope, 2021).

2.3.2 n-Factor Boundary Condition

The ground surface temperature can also be found by using the empirical surface n-factor. For engineering, this method has been commonly used, making it possible to simulate without knowing all the site-specific data. The seasonal n-factor for thawing and freezing can be calculated as shown in Equation 5 and 6, respectively.

$$n_f = \frac{I_{sf}}{I_{af}} \tag{5}$$

$$n_t = \frac{I_{st}}{I_{at}} \tag{6}$$

Where:

- I_{af} and I_{sf} = Freezing air and surface index, respectively
- I_{at} and I_{st} = Thawing air and surface index, respectively

The magnitude of these factors depends on the ground and climatic conditions. In Table 5 some examples of n-factors are presented.

Table 5: Approximate n-factors for different surface types (Geo Slope, 2014).

Surface type	$\mathbf{n}_f$	$\mathbf{n}_t$
Soil surface with spruce trees, brush and moss over peat	0.29	0.37
Soil surface with brush and moss over peat	0.25	0.73
Turf	0.5	1.0
Snow	1.0	-
Gravel	0.6-1.0	1.3
Gravel northern conditions	0.9-0.95	
Asphalt pavement	0.29-1.0	1.4-2.3
Asphalt pavement northern conditions	0.9-0.95	
Concrete pavement	0.25-0.95	1.3-2.1
Concrete pavement northern conditions	0.7-0.9	

It is then possible to estimate the ground temperature by using the n-factor for a given surface type and Equation 7 (Geo Slope, 2014).

$$T_{Ground} = (\text{n-factor})(T_{air} - T_{Phase}) + T_{Phase} \tag{7}$$

Where:

- T_{air} = Air temperature [K]
- T_{Phase} = Phase change temperature for water [K]

2.4 Thermal Properties of Soil and Rock

2.4.1 Thermal Conductivity

Thermal conductivity is a material parameter that describes a material's ability to transfer heat through conduction. A material with a low thermal conductivity transmits heat at a slower rate. The thermal conductivity can be expressed as Equation 8 (Cengel & Ghajar, 2014). Which is derived from Fourier's law of heat conduction.

$$k = \frac{QX}{A\Delta T} \tag{8}$$

Where:

- k = Thermal conductivity [W/(mK)]
- Q = Heat flux [W/m^2]
- ΔT = Temperature gradient. ΔT = T$_1$ - T$_2$ [K]
- A = Cross-section area [m^2]
- X = Thickness or length the heat flux passes through [m]

An illustration of the thermal heat flow and the parameters from Equation 8 are shown in Figure 8.

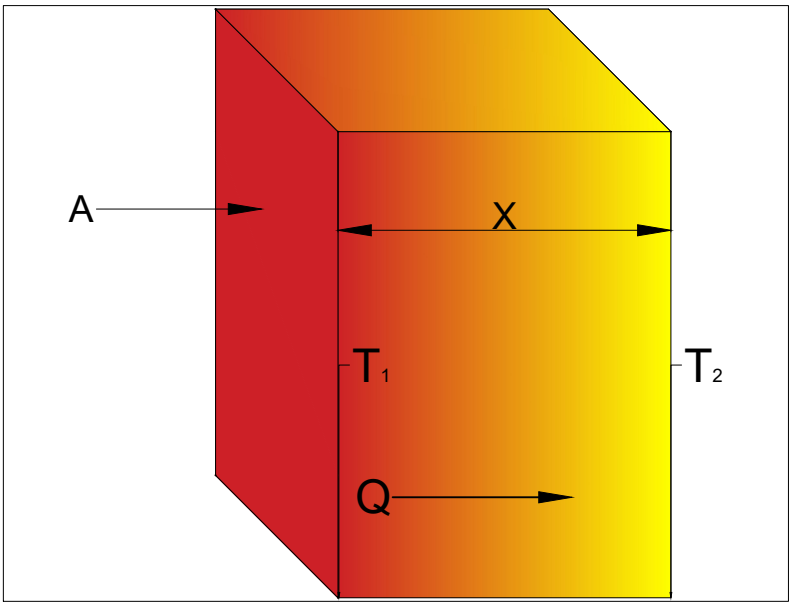

Figure 4: An illustration to heat flow and parameters to determine the thermal conductivity of a material. Modified from: Cengel and Ghajar (2014).

For soil, the thermal conductivity will depend on the characteristics of the soil. The effective thermal conductivity of soil depends on temperature, water content, thermal properties of the minerals, porosity, and fluid saturation (Bratlie, 2018). These factors are often correlated and will influence each other.

The effective thermal conductivity can be found by Equation 9, where the effective thermal conductivity is found as a weighted geometrical mean of the thermal conductivity of soil, water, ice and air (Johansen, 1975):

$$k_{eff} = k_s^{1-n} \cdot k_i^{nS_w(1-\phi)} \cdot k_w^{nS_w\phi} \cdot k_a^{n(1-S_w)} \tag{9}$$

Where:

- k_{eff} = effective thermal conductivity $[W/(mK)]$
- k_s, k_i, k_w and k_a = Thermal conductivity for solid, ice, water and air, respectively $[W/(mK)]$
- S_w = Water saturation

- ϕ = Volumetric fraction of water content
- n = Porosity

When it comes to estimate the thermal conductivity of soil, k_s, the geometric mean from Equation 10 can be used (Johansen, 1975):

$$k_s = k_q^q \cdot k_o^{1-q} \tag{10}$$

Where:

- k_q = Thermal conductivity of quartz $[W/(mK)]$
- k_o = Thermal conductivity of other minerals $[W/(mK)]$
- q = fraction of quartz

The thermal conductivity of the soil can be difficult to estimate because of the content of the rock soil. In Table 6 the thermal conductivity for some materials is listed. The thermal conductivity of quartz is almost eight times higher than clay and therefore a significant factor for the thermal conductivity of the soil.

Table 6: Thermal conductivity of selected materials (Andersland & Ladanyi, 1994).

Material	Thermal Conductivity
Air ($10°C$)	0.026
Ice ($0°C$)	2.21
Water ($0°C$)	0.56
Clay, dry	0.9
Sand, dry	1.1
Rock, typical	2.2
Shale	1.5
Quartz	8.4

2.4.2 Latent Heat of Fusion

The latent heat of fusion is defined as the amount of heat that is required to change the phase of a medium. At the temperature of phase change for a medium this latent heat is the energy needed to change the structure of the medium. For the case of permafrost, the phase change is from solid to liquid and vice versa. When H_2O changes phase from liquid to solid, the water freezes, 334 kJ/kg is released, and when the ice melts the same amount is required. In other words, when ice warms up

and reaches 0°C it will need 334 kJ/kg to change to a liquid phase. This implies that additional energy is required to thaw the permafrost, and the latent heat resists the thawing of permafrost.

For phase changes in frozen ground, freezing, and thawing, the required energy depends on the total amount of water. For a given ground the volumetric latent heat of fusion is shown in Equation 11 (Andersland & Ladanyi, 1994).

$$L = \rho_d L' \frac{w - w_u}{100} \tag{11}$$

Where:

- L = Latent heat [kJ/m^3]
- ρ_d = Dry soil density [kg/m^3]
- L' = Latent heat for water, 334 [kJ/kg]
- w = Total water content
- w_u = Unfrozen water in frozen ground

For sands and gravel it is acceptable to set the unfrozen water content, $w_u = 0$ (Bekele & Sinitsyn, 2017).

2.4.3 Heat Capacity

Specific heat capacity, $kJ/(kgK)$, is defined as the energy required to increase the temperature of a one unit mass of a material by one degree. This can be found by summing up the heat capacity, multiplied by the mass fraction, from the different parts of the soil. Multiplying the specific heat capacity with the density of a material will yield the volumetric heat capacity, $kJ/(m^3K)$.

In fine graded soils, like silt and clay, unfrozen water will have a gradual decrease over a longer temperature interval. This will indicate a different heat capacity than heat capacity calculated from mass fractions. Considering latent heat from unfrozen water, one can use Equation 12 to calculate the apparent heat capacity using heat capacity from the different materials of the soil, and adding a term for the latent heat (Andersland & Ladanyi, 1994). For fine graded soil, the heat capacity will gradually increase with temperature because water has higher heat capacity compared to ice.

$$c_a = c_s + c_i(w - w_u) + c_u w_u + \frac{1}{\Delta T}\int_{T_1}^{T2} L\frac{\partial w_u}{\partial T} dT \tag{12}$$

Where:

- c_a = Apparent heat capacity $[kJ/(kgK)]$
- c_s, c_w, c_i and c_{air} = Heat capacity for solids, water, ice and air, respectively $[kJ/(kg/K)]$
- T = Temperature [K]
- w_u = Unfrozen water content

For engineering purposes, it is common to use specific heat of material to calculate the volumetric heat capacity. Specific heat capacity is the ratio of the mineral compared to water. The specific heat capacity for soil, water, and ice are 0.17, 1.0, and 0.5, respectively. Using Equation 13 and 14 the frozen and unfrozen volumetric heat capacity can be calculated (Andersland & Ladanyi, 1994).

$$c_{vu} = \frac{\rho_d}{\rho_w}(0.17 + 1.0\frac{w}{100})c_{vw} \tag{13}$$

$$c_{vf} = \frac{\rho_d}{\rho_w}(0.17 + 1.0\frac{w_u}{100} + 0.5\frac{w - w_u}{100})c_{vw} \tag{14}$$

Where:

- c_{vu} and c_{vf} = Volumetric heat capacity for unfrozen and frozen soil $[MJ/m^3K]$
- c_{vw} = Volumetric heat capacity for water - 4.187 $[MJ/m^3K]$
- ρ_d and ρ_w = Density for soil and water $[kg/m^3]$

2.4.4 Thermal Diffusivity

Thermal diffusivity is defined as the ratio of the heat transported into the material and the temperature increase this heat is creating (Andersland & Ladanyi, 1994). In other words, the thermal diffusivity of a material measures how fast the temperature of the material changes. From Equation 15 thermal diffusivity is given as the ratio between thermal conductivity and the product of the density and the specific heat capacity (Andersland & Ladanyi, 1994):

$$\alpha = \frac{k}{\rho \cdot c} \tag{15}$$

Where:

- α = Thermal diffusivity $[m^2/s]$
- k = Thermal conductivity $[W/(mK)]$
- ρ = Bulk density $[kg/m^3]$
- c = Heat capacity $[J/(kgK)]$

The thermal diffusivity of ice is $11.2{\cdot}10^{-14}$ m^2/s, for water it is lower with a thermal diffusivity of approximately $1.4{\cdot}10^{-14}$ m^2/s. Thus the thermal diffusivity is reduced if the frozen ground thaws. This is because the thermal conductivity will increase and the heat capacity will decrease when ice changes phase to water for increased temperature. Lower thermal diffusivity for thawed soil implies that the heat transfer happens at a lower rate, thus the temperature changes slower.

2.4.5 Longyearbyen

When modeling the suitability of thermosyphon as a freezing technology in Longyearbyen, both rock and soil can be relevant. The literature from earlier geotechnical surveys indicates that silty sand and silty clay are the dominating component in soil in Longyearbyen. In addition, there are some alternating layers of sand. The thermal properties of soil can change considerably within small distances and within the same soil (Heller, 2021). For this thesis, the evaluation of thermosyphon is not for a specific site. Therefore, the thermal properties of soil in Table 7 are taken from results from Longyearbyen (Bekele & Sinitsyn, 2017). The table shows that the water/ice content in soil is 30%, for hard rock this will most likely be lower. The water in hard rock will to a greater extent be linked to fracture systems and ice lenses. From rock samples at Endalen, a water/ice content of 5% has been found (Etzelmüller et al., 2011).

Table 7: Thermal properties for soil (dense silty sand) in Longyearbyen, Svalbard. Collected at 30-40 meters altitude at Longyearbyen Vei 232.16 (Bekele & Sinitsyn, 2017).

Unfrozen thermal conductivity [W/mK]	Frozen thermal conductivity [W/mK]	Water/ice content [%]	Frozen heat capacity [J/(kgK)]	Unfrozen heat capacity [J/(kgK)]	Density [kg/m^3]
1.8	1.6	30	800	2056	1800

Structures in areas with permafrost will generally have a limited lifespan. Especially in areas where there is a large abundance of ice-rich loose material, it will over time lead to settlement damage due to creep settlements. These deformations will be expensive, and it is therefore recommended to set the maximum service life to 30-50 years (Instanes & Rongved, 2018). For Longyearbyen, these will be the areas where it is not possible to take advantage of the bedrock because it is too deep.

2.5 Thermosyphon

2.5.1 Working Principles

Two-phased closed thermosyphons are closed systems driven by natural processes. The driving forces in a closed thermosyphon are gravity and buoyancy effects induced by the temperature difference in the system. This makes it possible for thermosyphons to provide a cooling effect without the need for a pump, any mechanical system, or energy demand. In the most basic case, a thermosyphon consists of a pipe with three parts, a condenser, an adiabatic section, and an evaporator. An illustration of a simple thermosyphon is shown in Figure 5.

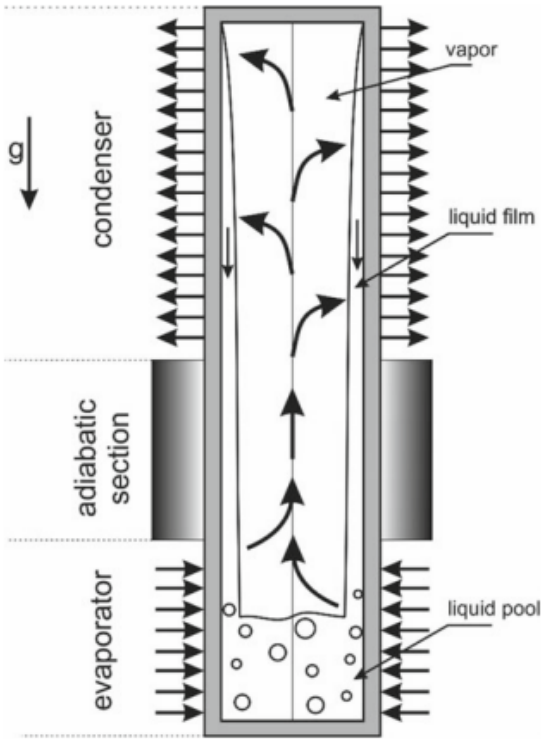

Figure 5: Working principle of a thermosyphon (Mantelli, 2021).

A thermosyphon must have the condenser above the evaporator to work. The working fluid in a closed-loop thermosyphon boils and evaporates in the evaporator and thus cooling down this part of the thermosyphon, due to the latent heat of evaporation. The vapor will rise in the system due to buoyancy effects. In the condenser the vapor cools down and condenses, thus heating the condenser. After condensing, the working fluid will flow downwards along the walls of the thermosyphon as gravity will transport the fluid down to the evaporator. With the condenser at the top and the evaporator at the bottom, the cooling happens at the bottom of the thermosyphon, and heat is released from the condenser. Thus the temperature must be warmer in the evaporator section than in the condenser section for a thermosyphon to provide cooling. The vapor transports heat from the evaporator and up to the condenser part of the thermosyphon. Most of the cooling is provided by the latent heat of evaporation when the working fluid evaporates. This makes a thermosyphon efficient as a cooling device while using only natural convection (Mantelli, 2021).

2.5.2 Heat Transfer Through a Thermosyphon

The heat transfer of a thermosyphon is dependent on a temperature difference between the evaporator and the condenser and is affected by several other factors.

The performance of a thermosyphon can be described by Equation 16 or Equation 20 (Long & Zarling, 2004).

$$Q = \frac{T_s - T_a}{R} \tag{16}$$

Where:

- Q = Heat transfer for the thermosyphon [W]
- T_a = Air temperature around the condenser [K]
- T_s = Soil temperature around the evaporator [K]
- R = The total thermal resistance [K/W]

When the temperature in the ground is lower than the air temperature, the working fluid in the thermosyphon circulates and thus there will be no cooling from the thermosyphon. This is because the gas is warmer in the condenser and has a lower density, thus it can not move downwards. This results in very little heat transfer due to the low conductivity of the gas (Abdalla et al., 2015). In other words the heat transfer, Q = 0 when $T_s < T_a$.

The total thermal resistance can be described as:

$$R = R_s + R_{we} + R_{ce} + R_e + R_c + R_{cc} + R_{wc} + R_f \tag{17}$$

Where:

- R_s = resistance of soil
- R_{we} = resistance of evaporator wall
- R_{ce} = resistance of the condensate in the evaporator
- R_e = resistance of evaporation
- R_c = resistance of condensation
- R_{cc} = resistance of the condensate in the condenser
- R_{wc} = resistance of the condenser wall
- R_f = resistance of the condenser

The thermal resistance of R_f and R_s are large in comparison to the rest of the resistances, thus making the sum of these an acceptable simplification for the total

thermal resistance. This gives Equation 18.

$$Q = \frac{T_s - T_a}{R_s + R_f} \tag{18}$$

Where on can express R_f as:

$$R_f = \frac{1}{Aeh} \tag{19}$$

Where:

- A = Area of condenser
- h = heat transfer coefficient, dependent of air velocity and characteristics of the condenser.
- e = fin efficiency, dependant on fin geometry, material and the heat transfer coefficient, h.

eh can be decided empirically from fin test data, wind velocity and exposure, typical values in the range 6 - 30 W/mK (Long & Zarling, 2004). The heat transfer in the condenser, is a result of convection. For this reason, wind speed is important for the efficiency of the thermosyphon. This implies that the placement of the thermosyphon is important, and one should consider installing the condenser so that snow accumulation is avoided if possible. The value for heat transfer, Q, is for the entire length of the evaporator. This is important to keep in mind when evaluating the dimensions of the evaporator and the cooling effect necessary for a specific project. Heat transfer can also be expressed using thermal conductance.

Expressed with thermal conductance:

$$Q = C * (T_s - T_a) \tag{20}$$

where:

- C = conductance of the thermosyphon [K/W]

The conductance of the thermosyphon can be seen as a measure of its performance. GEO-SLOPE International Ltd. has developed the software TEMP/W and describes the heat transfer into the thermosyphon as given in the equation. This heat transfer is for a unit length, and for modeling and actual installation one must divide the effect by the surface area of the evaporator 21 (Geo Slope, 2014).

$$Q = P(T_g - T_{air}) \tag{21}$$

Where:

- P = the performance characteristic of the thermosyphon.
- T_g = temperature of the ground
- T_{air} = temperature of the air

And one can express the performance characteristic, P, from Equation 22. This relation is found by experimentation done by Arctic Foundations Inc. (Geo Slope, 2014).

$$P = (2.54 + 4 * wind^{0.62})area \tag{22}$$

Where:

- P = the performance for the entire pipe length [W/K].
- wind = wind speed [m/s].
- area = surface area of the condenser [m^2].

From the equations above one can see several factors affecting the performance of a thermosyphon, but some simplifications makes it less complicated. The most important factors to consider regarding the performance are the following (Long and Zarling (2004) as cited in Plaxix (2017)):

- Thermal conductance of evaporator
- Soil thermal properties
- Air temperature
- Size of the evaporator

2.5.3 Design of Thermosyphon

Working Fluid

Different working fluids are used and have been reviewed for thermosyphons. Because of the sensitivity of the thermosyphon, the working fluid must be selected to the intended use and performance (Badache et al., 2019). CO_2, NH_3, freon, propane, and butane have all been used in thermosyphons, where CO_2 and NH_3 are the

most common working fluids (Wagner, 2014). The focus on environmentally friendly refrigerants has been more critical in the last decades. This has led to an increase in the research on natural refrigerants. CO_2 is considered ideal as an environmentally friendly refrigerant. It is non-flammable, has low toxicity, and has a low global warming potential and depletion potential (Kim et al., 2004). NH_3 works well as a working fluid for ground-coupled thermosyphons, but it is toxic, making it less preferable in some areas. For ground-coupled thermosyphon, ammonia is suitable because of its phases change at a low temperature (Mantelli, 2021). But it is an unstable gas and reactions can lower the thermal performance over time.

When choosing a working fluid for a thermosyphon, the vapor pressure of the working fluid needs to be carefully considered. For the optimal effect of the thermosyphon, the working fluid needs to be at the right temperature. The vapor pressure for CO_2 is shown in Figure 6. Most of the heat transfer in the thermosyphon occurs at evaporation and condensation, in other words, at a saturation state. The vapor pressure should be based on the ground temperature nearby the thermosyphon (Badache et al., 2019).

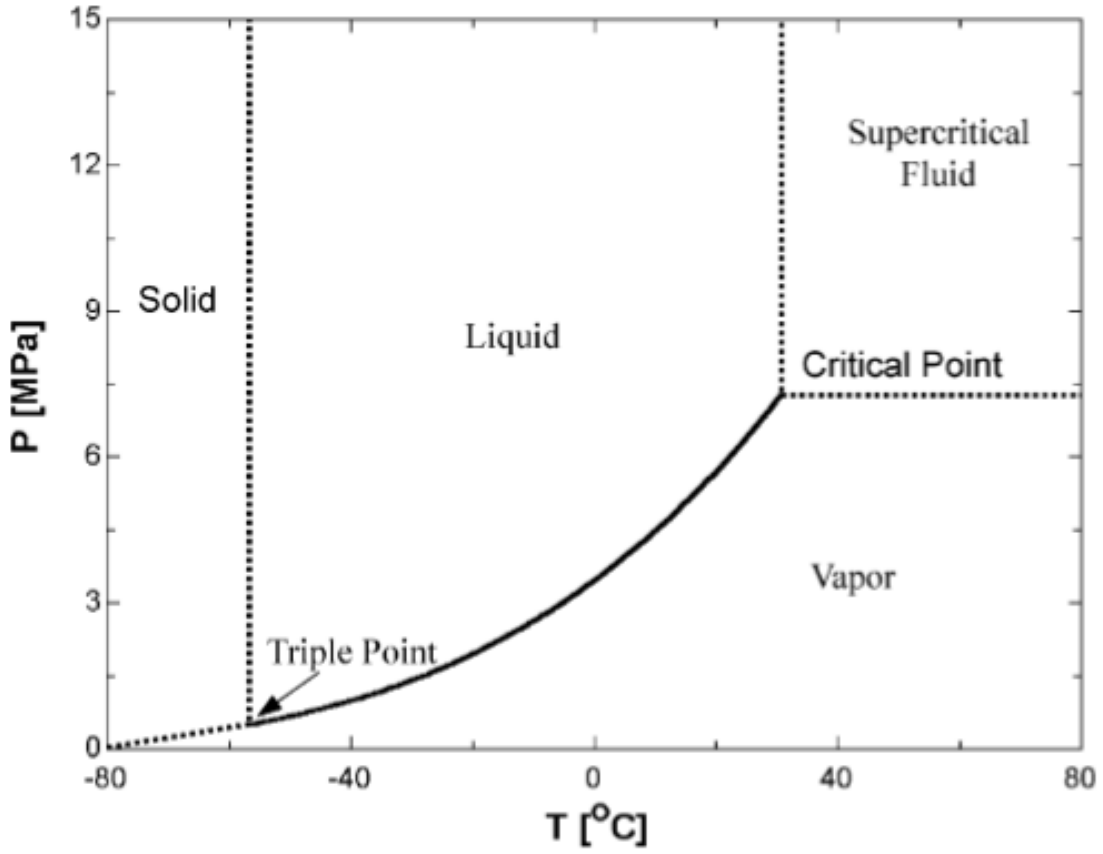

Figure 6: Vapor pressure for CO_2 (Kim et al., 2004).

The pressure in the thermosyphon might need adjustments during the lifespan of the thermosyphon. The reason for this is to secure that the vapor pressure is appropriate if the air temperatures change with a warmer climate in the future. By doing this, the thermosyphon can continue to work optimally even if the ambient temperatures change.

Casing materials

When choosing a casing design, the first thing to consider is the contact between the casing and the working fluid. If the casing and the working fluid react chemically it can result in a non-condensable gas in the thermosyphon. The non-condensable gas can block off a part of the condenser and reduce the efficiency of the thermosyphon (Mantelli, 2021). It is also essential to ensure that the casing can hold the high vapor pressure, which demands a more robust casing. If the working fluid is ammonia then the casing should not be made of cooper, this could lead to corrosion (Badache et al., 2019).

Evaporator

The evaporator of a thermosyphon can be loops or pipes. For this thesis, the focus with regards to modeling will be on steel pipe evaporators. For flat pipes, the outside diameter of the evaporator should be 2cm according to the Canadian Standards Association (CSA, 2014). Bigger diameters are also used, from the theory diameters in the range of 3-7.5 cm are also recommended (Badache et al., 2019). The length of the pipes can vary from a few meters up to 400m (Badache et al., 2019). The distance between the evaporator pipes should be determined with regards to the cooling effect needed and the radiator capacity, common spacing is 1-2 meters (CSA, 2014).

Radiator

The radiator is the part of the thermosyphon that sits above ground. The size of the radiator is important for the cooling effect provided by the thermosyphon. Typical sizing is an outer diameter of 9 cm and a surface area in the range of 13-19.5 m^2, the use of bigger radiators is also possible if needed (CSA, 2014). For optimal effect, the radiator should be placed in a windy location, with low solar radiation.

Construction and Monitoring

When using thermosyphon as a ground freezing device there are some aspects that need to be considered. Some points are presented under (CSA, 2014):

- The construction should be done during the appropriate time of the year,

usually in the summer months.

- During construction of the thermosyphon, disturbances of the permafrost should be kept to a minimum. The more disruptions that are made, the more important it becomes to let the systems run for some time before further construction begins. This should be at least one winter.
- Install measuring equipment for later temperature measurements.

The monitoring should start already under the construction. This is important to see that the thermosyphons actually provide the effect required to maintain the permafrost. Such a monitoring process should include the following (CSA, 2014):

- Inspections for damages to the thermosyphons, at least before the winter.
- Measuring the temperature at the condenser through the winter, to see if the thermosyphon is working. If they are working it should be a temperature difference between the air and the condenser.
- Monitoring of deformations and settlements for the constructions.

2.5.4 Different Types of Thermosyphon

The convection cycle of a thermosyphon can be maintained in three different ways:

- Passive
- Active
- Hybrid

A passive thermosyphon is able to function without external power. For a passive thermosyphon to provide cooling the air temperature must be lower than the ground temperature. An active thermosyphon is coupled permanently with a heat pump. The advantage of this is that the thermosyphon can provide cooling even when the air temperatures are higher than the ground temperatures and thus making it possible to use in more temperate climates. The disadvantage of an active thermosyphon is the demand for energy to provide cooling. If the active and passive methods are combined it is called a hybrid thermosyphon. With a hybrid solution, there is the possibility to use the thermosyphon passively when the temperature allows it and then use a heat pump when it is required. A hybrid thermosyphon will function without power for most of the year in a cold climate, but having the option to also

run the thermosyphon actively, one can provide cooling also during warmer parts of the year. There have not been done many studies on hybrid thermosyphons, but a study that was performed in Fairbanks, Alaska, showed good results in the creation of an artificially frozen barrier (Wagner, 2013). The hybrid thermosyphon is usually built as a regular passive thermosyphon, but with a mechanical cooling unit as shown in Figure 7 (Zueter et al., 2021).

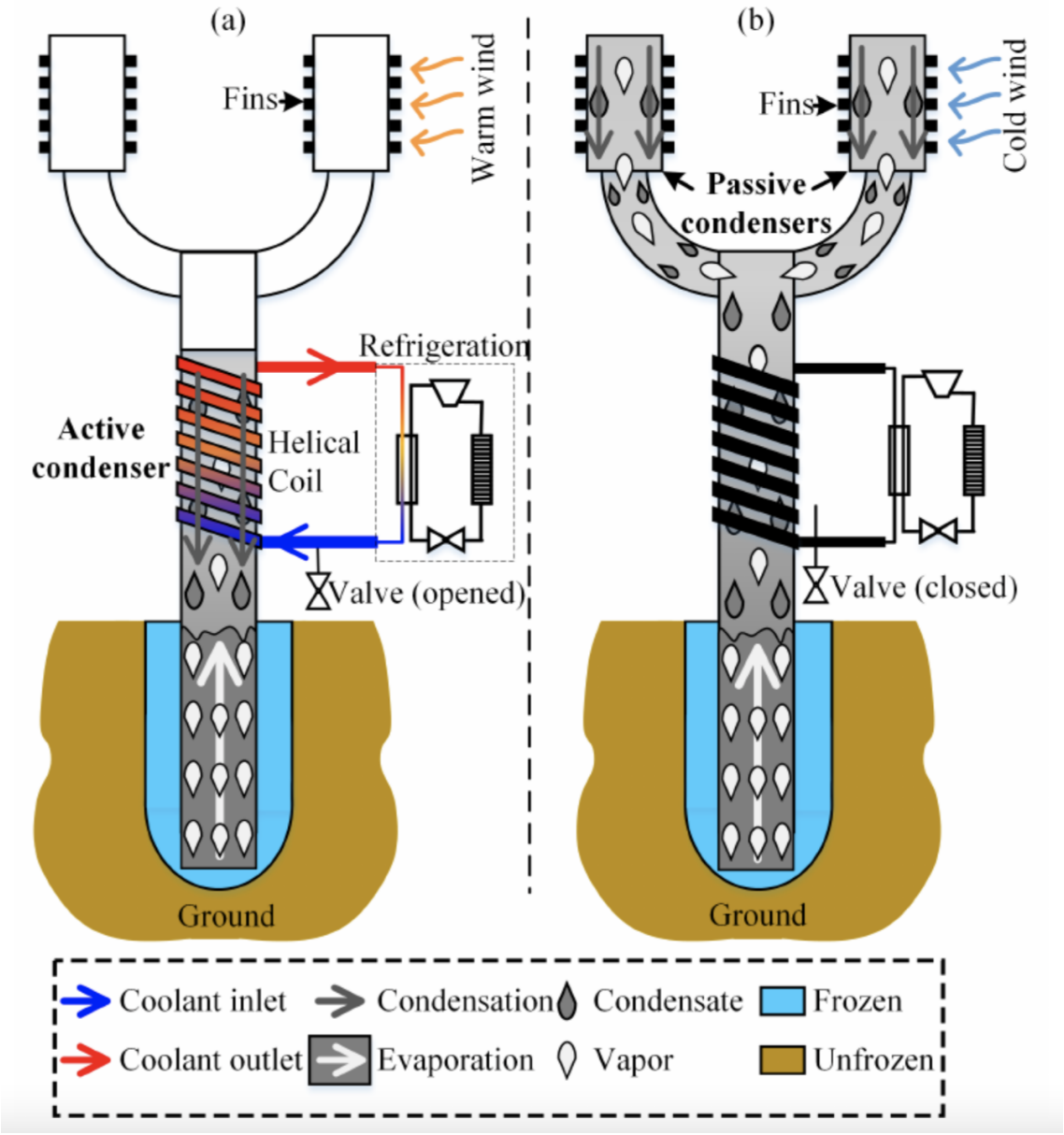

Figure 7: Illustration of a hybrid thermosyphon (Zueter et al., 2021). In a) the thermosyphon is actively cooling the ground. In b) the thermosyphon works passively.

The mechanical cooling unit will cool down the active condenser section of the thermosyphon. This will provide a temperature difference for the system that will

maintain the convection and thus the cooling effect.

Since the first use of thermosyphon in the 1960s, the variety in the design has become much more diverse. It is possible to install thermosyphon in different vertical setups. I can be designed as a loop with the condenser over the ground surface or hairpin where the evaporator and the condenser are under ground surface. The hairpin design it is necessary with an insulation layer between the condenser and the evaporator (Wagner, 2014).

The first and simplest thermosyphon is also referenced to as thermoprobe. They are generally used to keep the ground frozen, but they cannot carry any load. A vertical thermopile can be used if the thermosyphon needs to take a load. The simple thermosyphon/thermoprobe and the thermopile is illustrated in Figure 8.

In a sloped thermosyphon, the evaporator is installed with a slope of about 3-7%, and the condenser is vertical (Wagner, 2014).

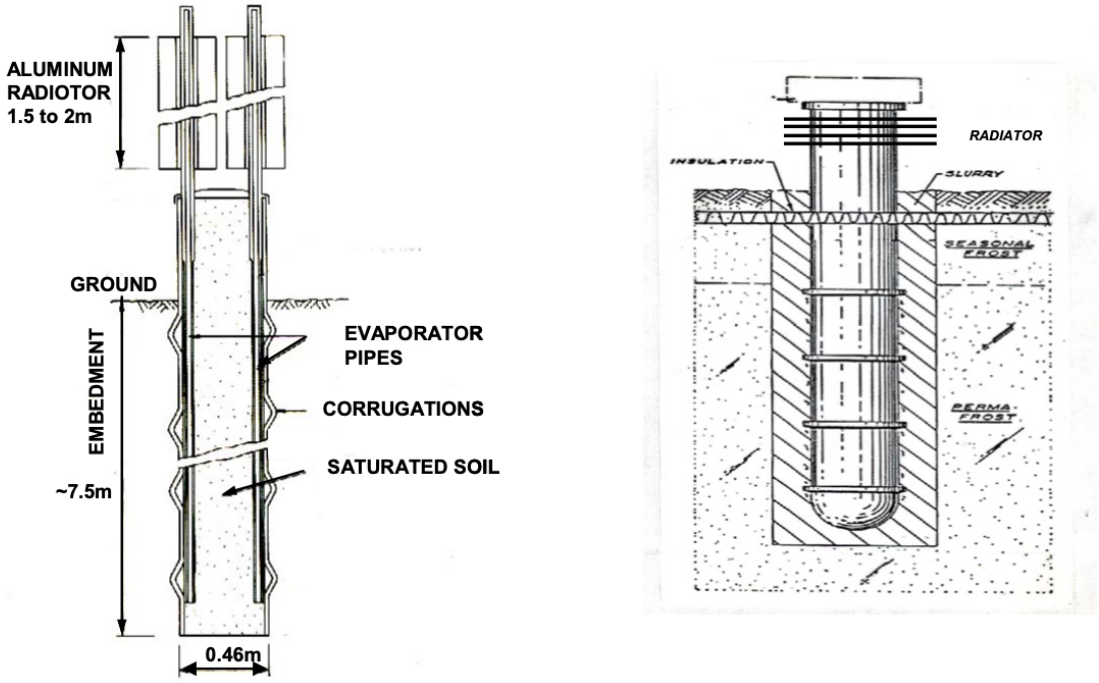

Figure 8: Illustration of a simple thermosyphon to the left and thermopile to the right in the figure (Wagner, 2014).

A flat loop thermosyphon was implemented in the USA and Canada after tests in 1993-1994. A flat loop must be installed on a flat base, making the installation easier. Most of the flat loop thermosyphons are used to provide cooling under buildings and dams (Holubec, 2008). The buildings can be built directly on the

gravel and insulation or constructed with a crawl space between the insulation and the basement.

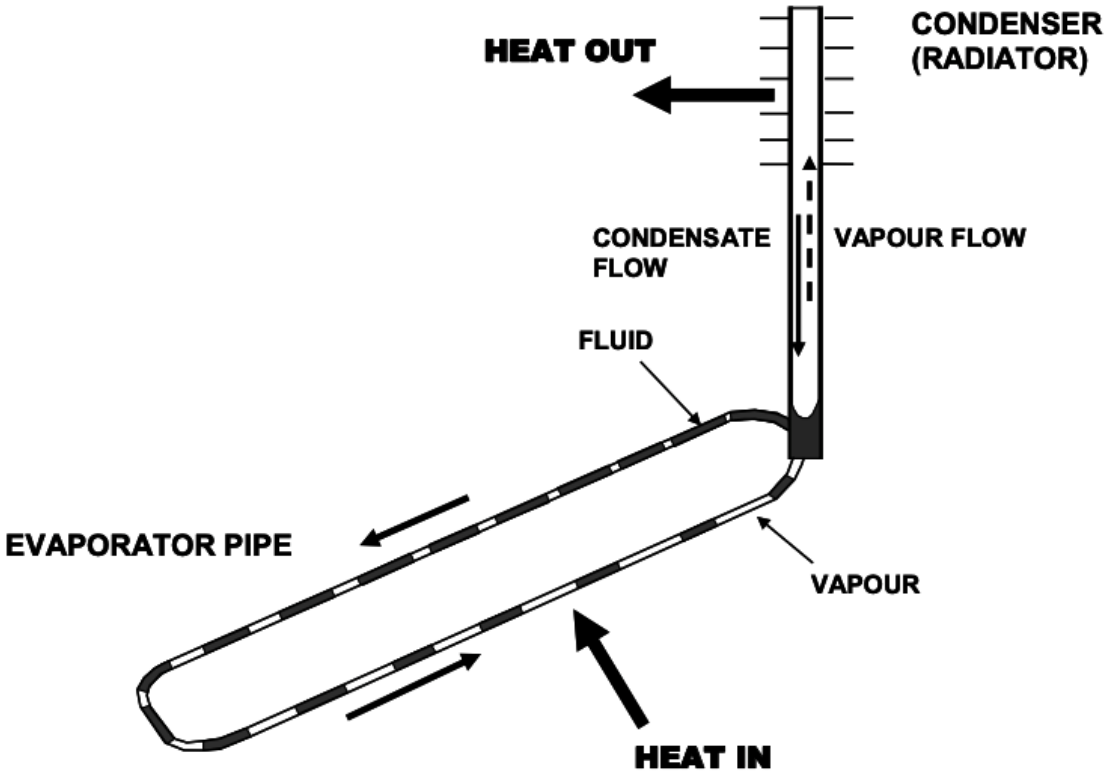

Figure 9: Illustration of the components of a flat loop thermosyphon (Holubec, 2008).

A hairpin thermosyphon is buried with both the condenser and the evaporator underground. The condenser will be above the insulation, and the evaporator will be beneath. This makes the hairpin thermosyphon suitable for roads and runaways, and because of its simple construction, this is one of the cheapest sorts of thermosyphons (Wagner, 2014).

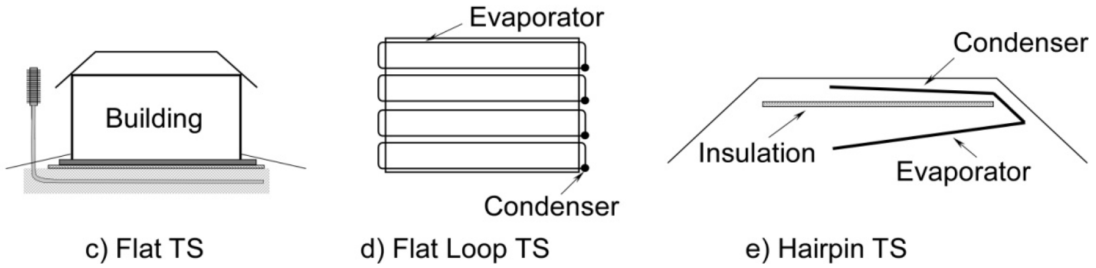

Figure 10: Illustration of the difference between flat-, flat loop- and hairpin thermosyphon(Wagner, 2014).

2.5.5 Application of Thermosyphon

Since the first thermosyphons in 1960, it has been used mostly in arctic areas for stability and support for construction and infrastructure in regions with permafrost. In Canada, Inuvik, Aurora college had 13 flat loops installed to provide cooling for a building foundation. The thermosyphons, insulation, and the granular material was installed one year before the construction of the building started. This gave the thermosyphon the ability to start the cooling before they began the construction of the building. One year after the construction was finished the temperature at 5.5 meters below the surface was 1.8 degrees below normal without thermosyphons (Wagner, 2014). In Deadhorse, Alaska, 42 flat loop thermosyphon were installed in 2008. At this site, the evaporator was 178 meters, and the temperature difference along the evaporator was only 0,5 degrees (Wagner, 2014). An illustration of a thermosyphon for cooling below a building is shown in Figure 11.

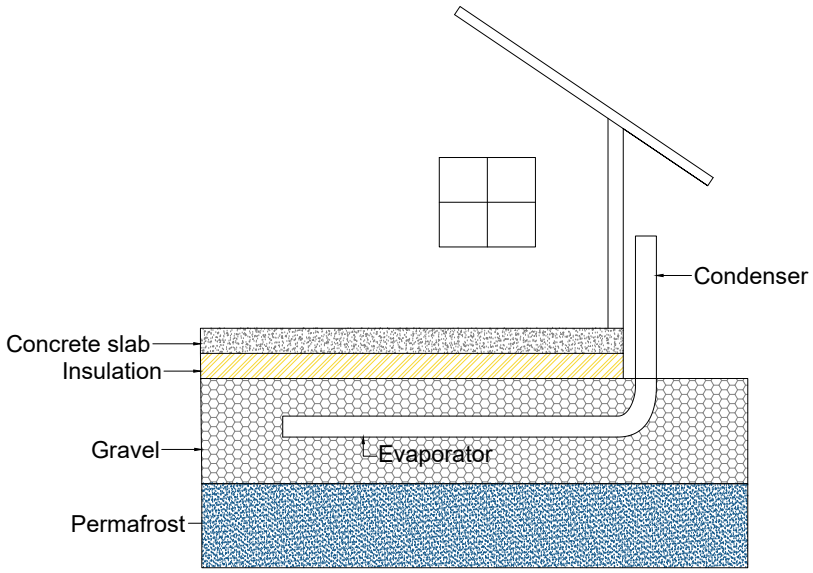

Figure 11: Slab-on-grad thermosyphon installation. Modified from Wagner (2014).

When using thermosyphons it is wanted to add support and stability. This can be done for constructions that doesn't create heat as the antenna in Kwigillingok, Alaska (Wagner, 2014) or in Qinghai–Tibet Power Transmission Line (Guo et al., 2016). It can also be built into the construction as done at Trans-Alaska Pipeline

(Badache et al., 2019). Different configurations of thermosyphons have also been used beneath roads and railways. In (Xu & Goering, 2008) a full-scale field application of hairpin thermosyphons and air convection were tested and successfully protected the embankment from thaw settlement.

Thermosyphon have been used in an attempt to decrease the pollution from nuclear waste, mining and other contamination risks. The use of a hybrid thermosyphon to create a frozen barrier has been investigated. The use of thermosyphon is also recommended the technique to be evaluated for locations with contamination problems. Specialty in a cold climate where the passive solution is enough. The use of hybrid thermosyphon against contamination was also successfully used in the demonstration of a vertical frozen soil barrier at Oak Ridge national laboratory (Lynn et al., 2000).

The main reason why the thermosyphon can be efficient on Svalbard is the low annual air temperature, which makes it possible to operate the thermosyphon passively for large parts of the year. At the same time, it is essential to preserve the permafrost in the area to avoid settlement damage for buildings and infrastructure. Active cooling demands energy and running costs can be significant. Using a thermosyphon the advantage is it can run passively. An example for thermosyphon as a ground freezing technology in regards to green energy is ground cooling for wind mill foundation. Different areas the thermosyphon can be used for in Longyearbyen, Svalbard can be:

- Protection from thaw settlement on roads
- Avoid thawing of permafrost beneath district heating pipes and energy wells
- Avoid thawing of permafrost beneath buildings
- Add support and stability from constructions that do not produce heat

3 Methodology

3.1 Climate data

Temperature data has been collected as observations for the period 2010-2020 and projections for the period 2071-2100 for the emission scenarios RCP45 and RCP85. Data for historical temperatures are measured at Svalbard Airport.

3.1.1 Data for 2010-2020

The air temperature data collected for this thesis from the period 2010-2020 is downloaded from Norwegian Centre for Climate Services (NCCS). Wind data used for all simulations is also downloaded from NCCS. This data is available from MET (MET, 2022). The data set of air temperature observations for the period 2010-2020 is missing some days. To compensate for the missing days temperatures are interpolated from the days before and after. This is to get a complete data set with 365 temperature points per year.

3.1.2 Data for 2071-2100

The data sets for future climate projections are acquired from the Norwegian Meteorological Institute. The data for both RCP45 and RCP85 is available for download at MET's database (MET, n.d.). The data of projections for RCP45 contain eight different temperature estimates. The projections for RCP85 contain five different temperature estimates. The climate models contain temperature estimates from a geographical grid including large parts of the Arctic. The data sets have been handled with the programming language Python to access the data and acquire temperatures for the closest location to Longyearbyen from the grid. The closest location to Longyearbyen in the grid is found using the minimum from calculated Euclidean distance as given in Equation 23 considering longitude and latitude on an equidistant grid (Snyder, 1987). The algorithm for doing this in Python, using the data from the future climate projections is shown in Appendix A.4.

$$d = \sqrt{\cos\frac{lat_{grid} * \pi}{180} * (lon_{grid} - lon_{LY})^2 + (lat_{grid} - lat_{LY})^2} \tag{23}$$

The resolution of the horizontal grid is 0.44°, which is approximately 50 km (Hanssen-Bauer et al., 2019). The different temperature simulation have some variation from the coldest to the warmest estimates. Plot of temperatures for the last decade in the projections, for RCP45 and RCP85, are shown in Figure 45 and Figure 47 in

A.1 and A.2. From the figures one can notice the difference between the coldest and warmest estimates. The temperatures used for the simulation is a sinusoidal curve of temperatures derived from the median temperature from the data sets.

3.2 Ground Modelling for Thermosyphon

Background

The goal of the ground modeling for thermosyphon is to determine the suitability of thermosyphon as a ground-freezing solution. The modeling assesses the suitability of today's climate and the future climate in Longyearbyen. From the theory section, it is clear that temperatures in Longyearbyen have been increasing, and one can argue that this is likely to continue, even though the rate is uncertain. This will affect both the ground's thermal conditions as well as the effectiveness of thermosyphons. This implies that the heat flux, both at the ground surface and for the thermosyphon, change with time due to fact that temperature variations over days, seasons, and years affect both air temperature and the thermosyphon effect. For such a problem one can use numerical software to predict the thermosyphon thermal effect on the permafrost over time. Such numerical models are excellent tools, but these predictions must also be interpreted with care. Simplifications, assumptions, and other input variables will affect the final result. Several different software is available and suitable for modeling the thermal changes, for this thesis COMSOL Multiphysics® (COMSOL Multiphysics®, n.d.) is used. Choosing, and getting access to suitable software was a time consuming process before the work on building a model could begin. Softwares such as PLAXIS and Temp/W are not available at the Department of Geoscience and Petroleum, but a license for COMSOL was eventually acquired. Due to the late arrival and testing of rock samples there was no time to do modelling with thermal properties for rock. The differences in thermal properties between rock and soil, and the effects are discussed in Chapter 5.

3.2.1 COMSOL

COMSOL Multiphysics is a commercial software used for modeling physical problems in all fields of engineering. COMSOL allows modeling in 1D, 2D, and 3D, where a 2-dimensional model will be used for this thesis. COMSOL utilizes the finite element method to estimate real physical problems by solving mathematical equations numerically.

Finite Element Method

The Finite Element Method (FEM) is commonly used for solving numerical equations related to engineering modeling. FEM is used for different fields of engineering such as structural, fluid flow, and as for the case of this thesis; heat transfer. Physical problems are usually expressed from partial differential equations, PDEs. With the FEM method, these equations are approximated and solved numerically. To use the finite element method one must discretize the domain which is relevant to the model. This means splitting the domain into a number of elements, a finite number, often referred to as meshing. An example of a 2D mesh with nodes and elements is illustrated in Figure 12.

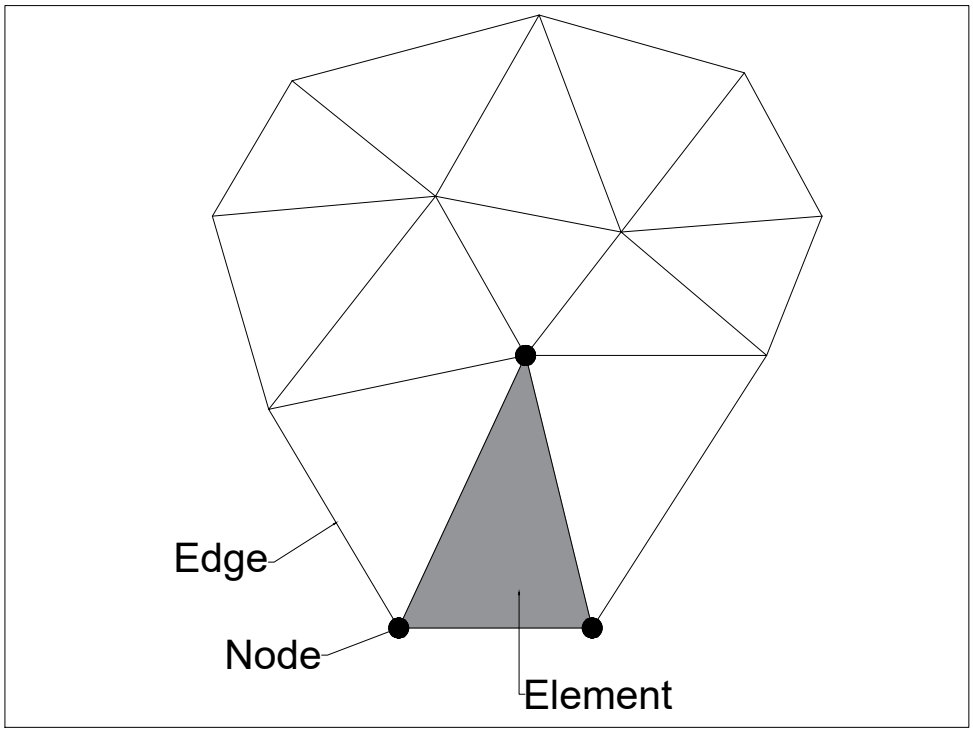

Figure 12: Illustration of 2D mesh for FEM model. Modified from: Lewis et al., 2004.

Each element is surrounded by a number of nodes, and the number of nodes decides the geometry of the elements. For 2D modeling, both triangular and rectangular elements are common. The equations are described for each element and thus give an understanding of the behavior of the domain. The steps for doing a finite element analysis can be summarized as in Figure 13 (Lewis et al., 2004).

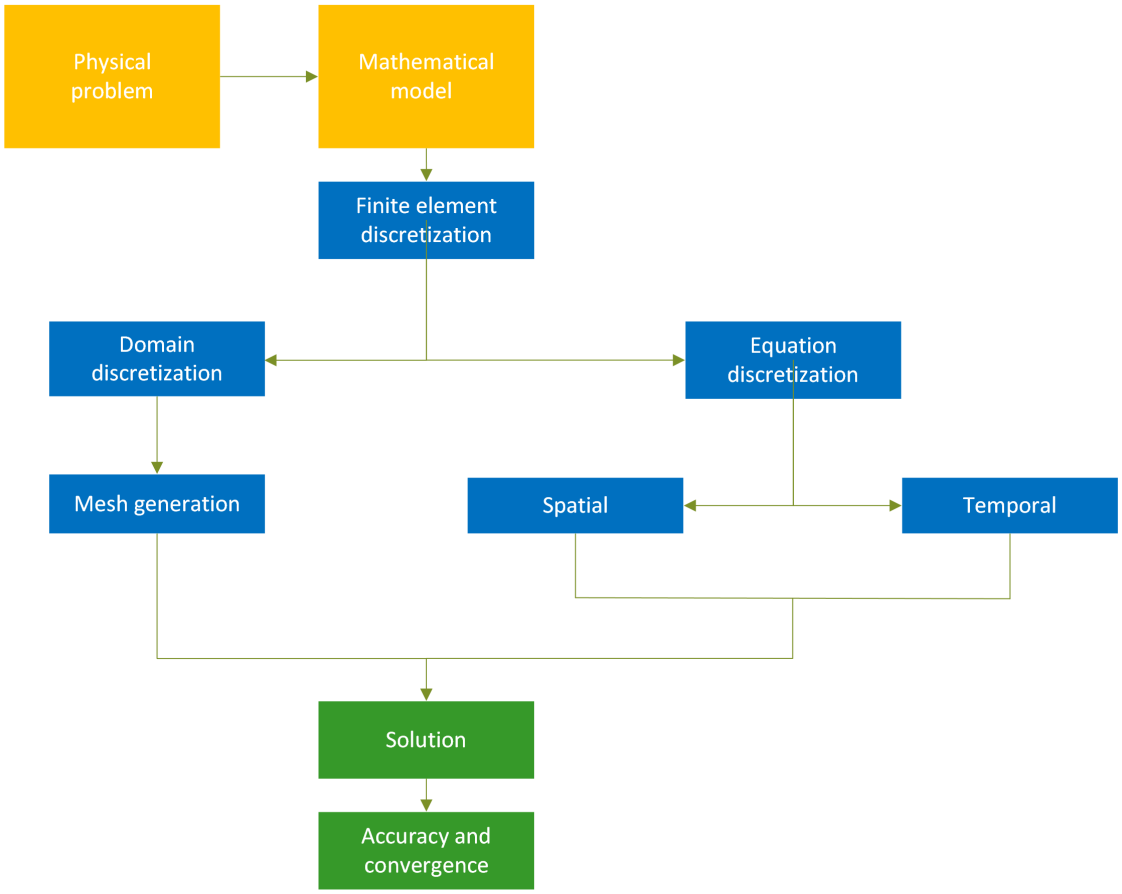

Figure 13: Steps for solving a model using the finite element method. Modified from: Lewis et al., 2004.

3.2.2 Heat Flow in Soil and Rock with COMSOL

COMSOL has an interface for heat transfer in porous media, this is suitable for soil and rock which are the medias of interest for this thesis. The software is also able to handle phase change. This section shortly addresses the theory behind heat transfer in porous media in COMSOL.

Heat Transfer in Porous Media

For this thesis heat transfer happens in fluids and/or in porous media depending on the characteristics of the ground. For porous media, COMSOL describes heat transfer as given by Equation 24 (COMSOL, 2019).

$$(\rho C_p)_{eff}\frac{\partial T}{\partial t} + \rho C_p \mathbf{u}\cdot\nabla T + \nabla\cdot\mathbf{q} = \mathbf{Q} \tag{24}$$

Where:

- $\mathbf{q}$ = -$k_{eff}\nabla T$
- k_{eff} is the effective thermal conductivity [W/(m°C].
- ρ is the fluid density [kg/m^3].
- C_p is the fluids heat capacity at constant pressure [J/(kg°C].
- T is the absolute temperature [C].
- $(\rho C_p)_{eff}$ is the effective volumetric heat capacity [J/kg°C], given as:

$$(\rho C_p)_{eff} = \theta_p \rho_p C_{p,p} + (1-\theta)\rho C_p$$

- θ_p is the volume fraction of solids in the porous material.
- k_{eff} is the effective thermal conductivity.
- $\mathbf{q}$ is the conductive heat flux [W/m^2].
- $\mathbf{u}$ is the velocity field from the Fluid Flow interface in COMSOL [m/s].
- Q is the heat source or heat sink [W/m^3].

  This equation implies that the temperature is the same for the fluid and the solids in the porous media, there is a local thermal equilibrium.

3.2.3 Assumptions

For the heat transfer model displacement in the soil is not taken into account. One can expect displacement in thawed soil under load, but it is assumed that the thermal impact of thermosyphon is similar even without displacement. It is also assumed to be no groundwater flow, vertically or horizontally. Low permeability in frozen ground is assumed to prevent vertical flow of significance. To satisfy energy and mass conservation the density is assumed to be the same for frozen and unfrozen soil, this ensures that mass is conserved locally (COMSOL, 2019). Ice is approximately 9% less dense than water (Andersland & Ladanyi, 1994), meaning frozen soil in reality will have a lower density. With a water content of 30% assuming the same density is considered an acceptable simplification for this thesis. Thermal expansion of soil particle's is not considered, the thermal volumetric expansion of solid particles is of magnitude 10^{-5} (Carmichael & Klein, 2021) and considered to have little impact on the thermal modelling. Sun exposure on the thermosyphon condenser could effect the cooling potential, but as the thermosyphon mainly provides cooling during

winter, when the sun exposure is low in Longyearbyen, this not considered as a big uncertainty.

3.2.4 Model Setup

This section will explain the setup of the model and the choices behind the model. A model with only ground surface boundary will be presented. A model simulating heat flux from a building in the form of a concrete slab is also presented.

Thermal Parameters

The soil parameters that are used represent heterogeneous silty sand, this is a simplification of the situation in Longyearbyen. This is seen as reasonable because the use of thermosyphon, in this model, is not site-specific but it is a possible freezing technology for different locations and thus different soil conditions. The thermal parameters used in the model, which are modified from the report by Bekele and Sinitsyn (2017), are the following:

- Unfrozen thermal conductivity = 1.8 $[Wm^{-1}C^{-1}]$
- Frozen thermal conductivity = 1.6 $[Wm^{-1}C^{-1}]$
- Unfrozen heat capacity = 2.056 $[kJkg^{-1}C^{-1}]$
- Frozen heat capacity = 0.8 $[kJkg^{-1}C^{-1}]$
- Density = 1800 $[kgm^{-3}]$
- Water/ice content = 30 [%]

Geometry and Mesh

The domain is a two-dimensional domain. This is seen as sufficient for the horizontal thermosyphon scenario. With a 2D domain, the model will have a significantly lower computational cost than a 3D domain. The 2D model will give a good insight into the heat distribution from both the thermosyphon and the effect from the ground surface boundary. For more problems with more complex geometry, for example, several vertical thermosyphon, a 3D model might be necessary to describe the problem in an appropriate way.

The size of the ground domain is decided by trial and error, and with assumptions from theory. The size of the domain is set to 40x40 meters, this will give sufficient width and depth so that the boundaries do not affect the thermosyphons in the domain. For the diameter of the evaporator in the model we assume 7.5 cm, from the theory, this is a reasonable assumption. The length of the evaporator is assumed to

be 4 meters. The depth of the thermosyphon is set to 2 meters, this is deeper than the active layer with today's climate but shallower than the predicted active layer thickness with future climate changes. From future climate models, the assumed active layer thickness is approximately 2.5 meters in the period 2071-2100. The model will include three thermosyphons with a distance of 1 meter between them. An illustration of the domain and the geometry of the model is shown in Figure 14.

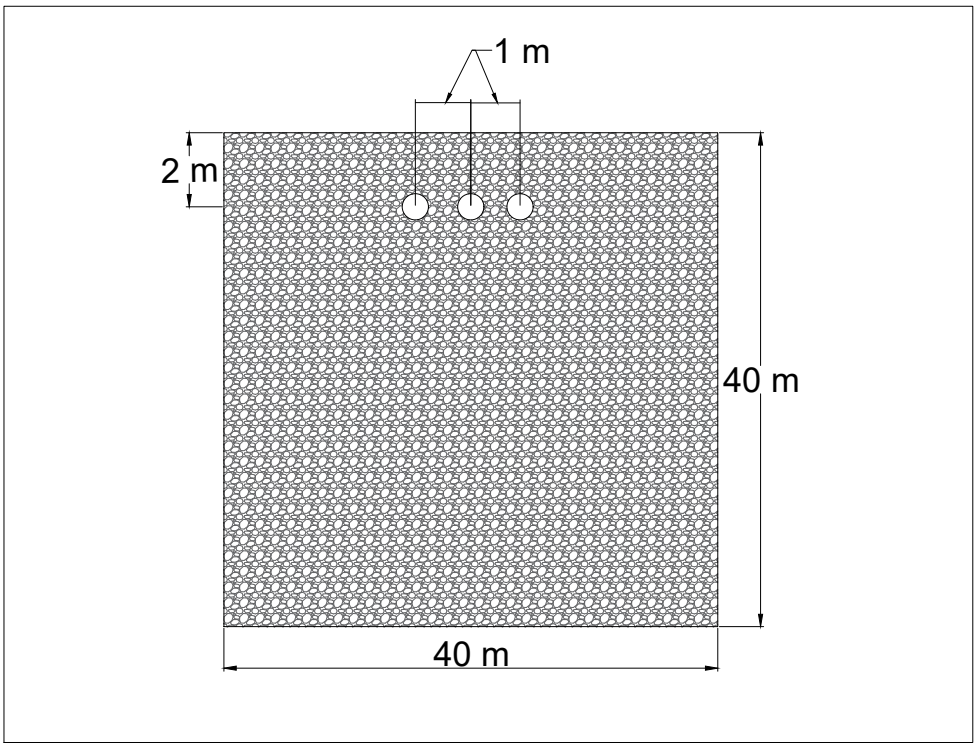

Figure 14: Illustration of the model domain and geometry.

Defining an appropriate mesh is important for the model to be accurate. COMSOL will generate a mesh automatically, but it can be necessary to adjust the meshing of the domain to fit the situation one wishes to evaluate. The standard mesh geometry in COMSOL is triangular and this is the geometry used for the model. An example of a triangular mesh is shown in Figure 15.

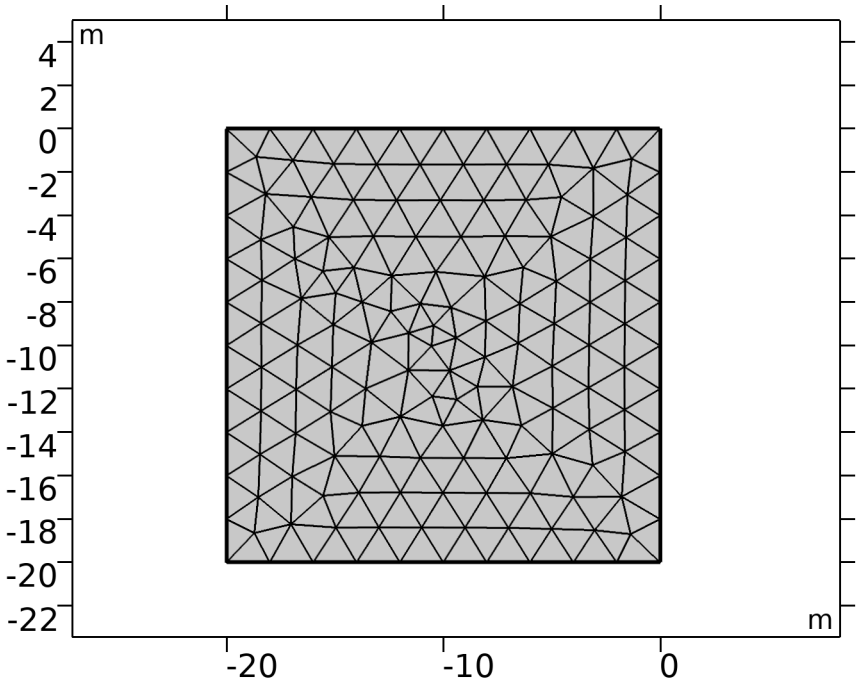

Figure 15: Illustration of a free triangular mesh in COMSOL.

For the domain in this model, it is beneficial to make the mesh finer in the upper parts of the domain. This is because the temperature gradients here are higher than in the deeper part of the domain. For the phase change, it is also beneficial with a finer mesh, which allows a smaller phase change temperature interval.

Initial Conditions

The initial conditions for the temperature profile need to be decided for all the scenarios. It is possible to estimate the initial conditions for the different scenarios using Equation 2. For the equation, one is able to set a thermal regime for the ground using the mean annual temperature and amplitude for the time period of interest. The phase of the sinus equation can be shifted so that 15. February is assumed to be the coldest day of the year. From the temperature data, the time of year for the minimum temperature is not equal from the different decades. The issue with setting the initial conditions using an analytical expression is that it estimates the ground's thermal regime with a steady climate. This will lead to a high estimate for the ground temperatures because the permafrost itself will cool the ground and resist temperature change due to the energy needed to thaw the permafrost. For this reason, using an analytical expression for setting initial conditions is not seen as sufficient.

The variables for the different climates in Equation 2 are the surface temperature

amplitude and the mean annual temperature. These variables are given from the temperature data for the different decades and climate scenarios. The surface temperature amplitude and mean annual temperature are given in Table 8 for all scenarios.

Table 8: Amplitude and mean annual temperature, degrees in celsius.

	2010-2020	**RCP45**	**RCP85**
Tm	-2.5	-1.3	2.3
As	11.2	9.2	7.2

From the table, one can notice the amplitude in the period 2080-2090 is less than the amplitude for the period 2000-2010. This is due to the fact that climate predictions estimates temperatures in the winter season to increase more than in the summer season, thus reducing the temperature difference and amplitude.

The initial conditions for today's climate are set using ground temperature data from Endalen in Svalbard and adjusting these. The data is available from the Geological Survey of Norway (NGU, no date). The model ran for 5 years with today's temperature data and the ground temperature from Endalen on 01.01.2010. The acquired ground temperature profile from the model is set as initial conditions for the simulation in the period 2010-2020.

The initial conditions for future climate for the different emission scenarios are found by running the model for a 60-year period from 2020 to 2080. The air temperatures used for this period are a sinus function with interpolated mean annual air temperature and interpolated amplitude. Ground temperature plots of the final year in the 60-year simulation for both RCP45 and RCP85 can be seen from Figure 44 in Appendix A.1 and Figure 46 in A.2, respectively.

Boundary Conditions

The domain in the model must have boundary conditions for all the boundaries. For a 2D domain, this implies boundary conditions for all four sides of the domain. The domain, given a square 2D geometry, will have a left and right boundary, a bottom boundary, and a top boundary. The thermosyphon will also have a boundary condition with the surrounding soil or rock, which represents a heat sink.

Ground Surface Boundary

The ground surface boundary condition is dependent on several factors and accurate approximations for the ground surface boundary is demanding to find.

For estimating the ground surface temperature the two methods in the theory are considered. The surface energy balance boundary condition makes it possible to get a mathematical description of the energy transfer between the ground and the atmosphere, but it is driven by several processes and it needs a lot of site data. Accessing data to satisfy the ground surface balance equation accurately is not considered feasible for this thesis. The second option is the n-factor boundary condition. This method does not require the same amount of site-specific data. The ground temperature is calculated from the Equation 7, and the input is the air temperature and the freezing and thawing n-factor. But there is also a downside to this method. By using the n-factor, changes within the seasons are not taken into account (Heller, 2021).

The ground surface boundary condition chosen for the model is an empirical equation for convective heat transfer in combination with surface-to-ambient radiation. The convective heat transfer for the ground surface can be described from J*ü*rges equation (Nam et al., 2008) as shown in Equation 25.

$$\begin{cases} \text{h} = 5.8 + 3.9\text{v}; \ (\text{v} < 5 \text{ m/s}) \\ h = 7.1v^{0.78}; (v > 5m/s) \end{cases} \tag{25}$$

Where:

- v - wind speed [m/s]

The surface-to-ambient radiation is described with an inward heat flux from COMSOL as given in Equation 26 (COMSOL, 2019) .

$$-n \cdot q = \epsilon\sigma(T_{amb}^4 - T^4) \tag{26}$$

where:

- ϵ - surface emissivity
- σ - Stefan-Boltzmann constant (predefined physical constant)
- T_a^4 - air temperature
- T - surface temperature

The emisstisivity is set to 0.9 (Nedbal et al., 2020).

Left and Right Boundary

The left and right vertical boundaries in the model are thermally insulated. A thermally insulted boundary has no heat flux through the boundary, this means that the temperature gradient over the boundary is zero (COMSOL, 2019). This will allow the temperature near the boundary to change with time which is necessary for the transient model in this thesis. It is essential to ensure that the model is wide enough so that end effects do not affect the thermosyphon.

Bottom Boundary

There are three options for the bottom boundary condition considered for this thesis:

- Constant temperature
- Thermal insulation
- Constant heat flux

At greater depth, the temperature in the ground will not change because of seasonal changes in air temperature, which allows setting the bottom boundary at a constant temperature. The depth where seasonal temperature fluctuations are zero is called zero annual amplitude (ZAA). For depths greater than ZAA the temperature is often linear or close to linear with a constant geothermal heat gradient. Over time the temperature at the depth of ZAA and deeper can change due to increased air temperature and more heat transfer to the ground. This implies that when simulating for a few seasons assuming a constant temperature bottom boundary is reasonable if the domain is of appropriate depth. The constant temperature for the bottom boundary could be estimated using Equation 2 with z = -40m and time = 1 day. If the initial conditions are not set from the analytical expression, one can set the constant temperature equal to the temperature of the initial condition at the bottom of the domain, y = -40m. The issue with the constant temperature boundary is the effect of the thermosyphon which can change the heat transfer towards depth in the ground due to the cooling effect. It is possible that this will affect the temperature at depths of ZAA and the temperature will no longer be constant. As a consequence, the constant temperature boundary condition can induce errors in the estimates. A constant temperature boundary can be considered suitable for simulating only the ground surface boundary and its effect on the ground temperature. For simulating with the thermosyphon this is not seen as the best option. Since it is desirable to have the same boundary condition for all simulations, a constant temperature bottom boundary is not seen as appropriate.

The second option is assuming the bottom boundary to be thermally isolated, adiabatic. This is with an assumption that the geothermal heat flux does not affect the temperature in our domain to a significant degree. Using an insulated bottom boundary the temperature will be able to change at the boundary and the effect of the thermosyphon will not have the same issue as with a constant temperature boundary condition.

Using a constant heat flux is an option for the bottom boundary. For depths deeper than ZAA the temperature is increasing with a near-constant temperature gradient towards depth. This makes it possible to estimate the ground heat flux from the geothermal gradient and thus assume a constant heat flux for the bottom boundary. The vertical heat flux can be estimated using Equation 27.

$$q = -k\frac{dT}{dZ} \tag{27}$$

Where:

- q = heat flux [W/m^2]
- k = thermal conductivity [W/mK]
- $\frac{dT}{dZ}$ = geothermal gradient [K/m]

From Equation 27, using a thermal conductivity of 1.8 W/mK and a thermal gradient of 0.03 - 0.035K/m the heat flux is in the range of 54 - 63 mW/m^2. These values are within the range of measured heat flow on the mainland (Slagstad et al., 2009). Using a constant heat flow as the bottom boundary is considered the best representation of the real physical problem for this thesis. For the bottom boundary in the model, a constant heat flux of 60mW/K is assumed.

Thermosyphon Boundary

The boundary condition for the thermosyphon will be set according to the Equation 21 and Equation 22 as discussed in the theory section. The parameters needed to decide the boundary heat flux are the following:

- Wind speed
- Air temperature
- Area of condenser
- Area of the evaporator

The air temperature will be decided from either historical air temperature data or climate predictions, depending on the time perspective of interest. The temperature data for the period 2010-2020 is taken from measurements at Svalbard Airport, these data are available from Norwegian Centre for Climate Services (MET, 2022). Temperature data for the future climate is obtained from the Norwegian Meteorological Institute. The different emission scenarios have several simulations, 5 for RCP45 and 8 for RCP85, the temperature data is used for the modeling in COMSOL is the median from the different climate models. For wind speed the same data will be used for all models, the theory section argues that wind speed predictions are uncertain and the wind speed change in the future will not be massive. For this reason, the wind speed data that is used in the model is historical data from the period 2010-2020 measured at Svalbard Airport. Both wind and air temperature data are given with a resolution in days, for wind the values are the average of the mean speed and the air temperature is the average daily temperature.

All the temperature data used in the modeling is derived from the average temperature for each day for each of the 10-year periods. The average temperature for 01.01, 02.01, etc. Then this average data is used to define a cosine function with amplitude given by max and min temperatures and the period being 365 days. The min and max of the cosine function are determined by finding the day with maximum average temperature and then shifting the phase of the cosine function accordingly. For the wind data, the same is done, a cosine function derived from the average wind speed is used in the modeling. This is to eliminate big changes in temperature between days for more dependable modeling. The graph of the cosine function for the temperature in the period 2010-2019 is shown in Figure 16.

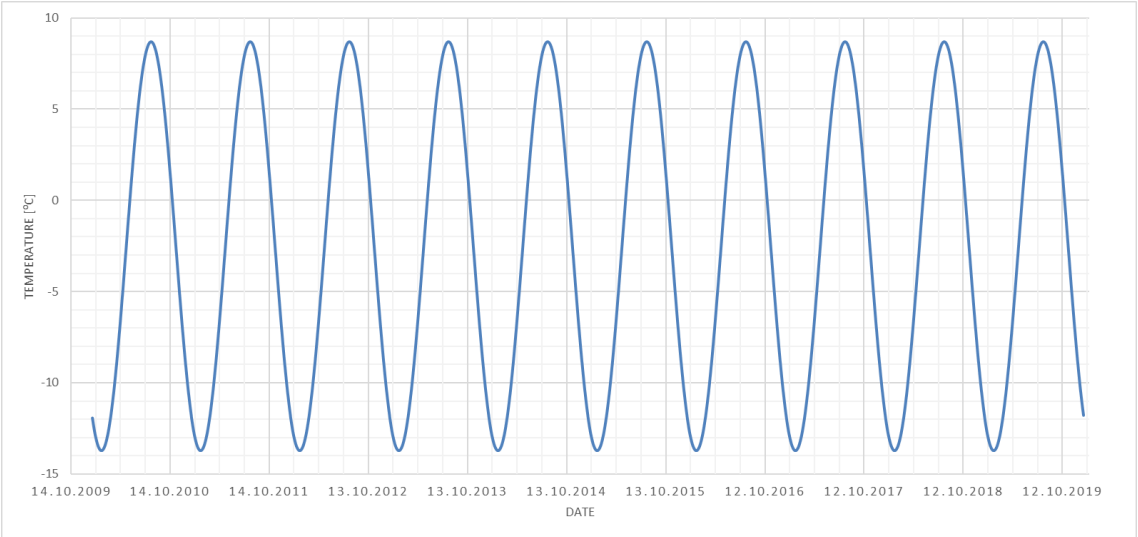

Figure 16: Cosine function of the air temperature used in the model for the period 2010-2019. Data from (MET, 2022).

The surface area of the condenser is set to 13 m^2. This is in accordance with the typical surface area for the condenser part of a thermosyphon as addressed in the theory.

3.2.5 Phase Change

Phase change makes heat transfer problems more complicated and more computationally heavy, at the same time the latent heat from permafrost thawing is significant. The case when simulating in this thesis will be to account for the thawing and freezing of rock and soil. The latent heat needed to change ice to water is 334 kJ/kg, this energy demand should be considered to make the model as representable as possible for the actual physical situation. For the change in soil or rock, from frozen to unfrozen, or vice versa, the latent heat for thawing or freezing to happen will be decided by the degree of water in the media. Phase change occurs at approximately 0°C, or a few degrees below, depending on the salinity of the water. In COMSOL it is possible to add a subnode to account for the phase change of a material. COMSOL handles the phase change between two materials by setting a temperature interval where the phase change happens. Over this interval, the material is modeled by a function that represents the fraction of each phase (COMSOL, 2019). An illustration of the phase change is shown in Figure 17

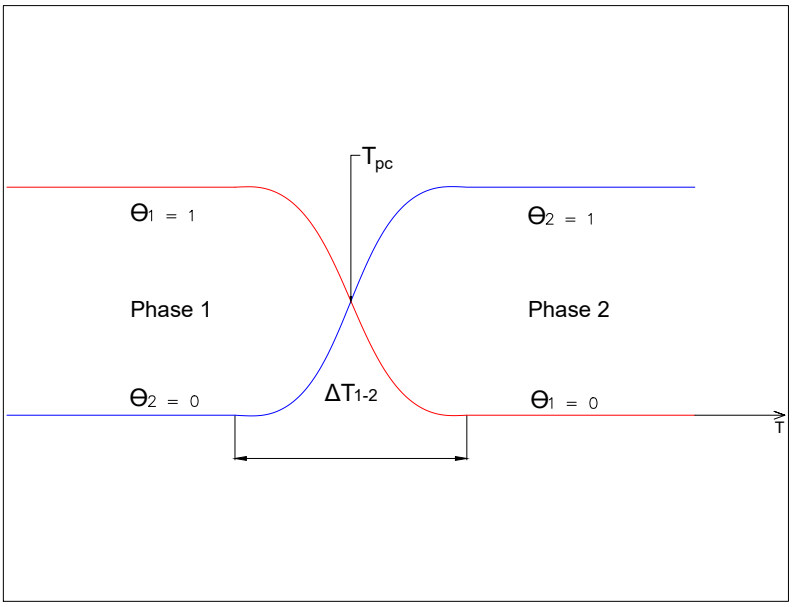

Figure 17: Illustration of the phase change function in COMSOL. Modified from COMSOL, 2019.

- Θ is the function deciding the fraction of each phase
- T_{pc} is the temperature at which phase change happens, approximately 0°C for water.
- ΔT is the temperature interval over which one decides the phase change to happen over, this is a parameter on chooses and sets in COMSOL.

Over this interval, the properties of the material are decided as a combination of the two different materials, and the fraction of each phase is decided by the function Θ. The ΔT value chosen for modeling is 1 Kelvin, this is seen as sufficient accuracy and works well when running the model. The phase change temperature in the model is chosen for -1°C because salinity is common in pore water in the Svalbard area.

To simulate the phase change as accurately as possible, the latent heat for phase change between unfrozen and frozen soil, as well as the freezing temperature of the ground must be determined. Using Equation 11 one can determine the volumetric latent heat for the soil.

Using the following parameters, as found in the theory section:

- $\rho_d = 1800\text{kg/m}^3$
- $w = 30\%$
- L' = 334 kJ/kg

This gives a volumetric latent heat of 180 360 kJ/m^3 or given as specific latent heat, 77kJ/kg of saturated soil.

3.3 Validation of the Model

To validate the model one option is to compare the zero annual amplitude measured with the zero annual amplitude of the model. Since the evaluation of the thermosyphon is not cite-specific in this thesis it is seen as sufficient to validate against ZAA and active layer depth. From Figure 18 one can see the ground's temperature profile for each month

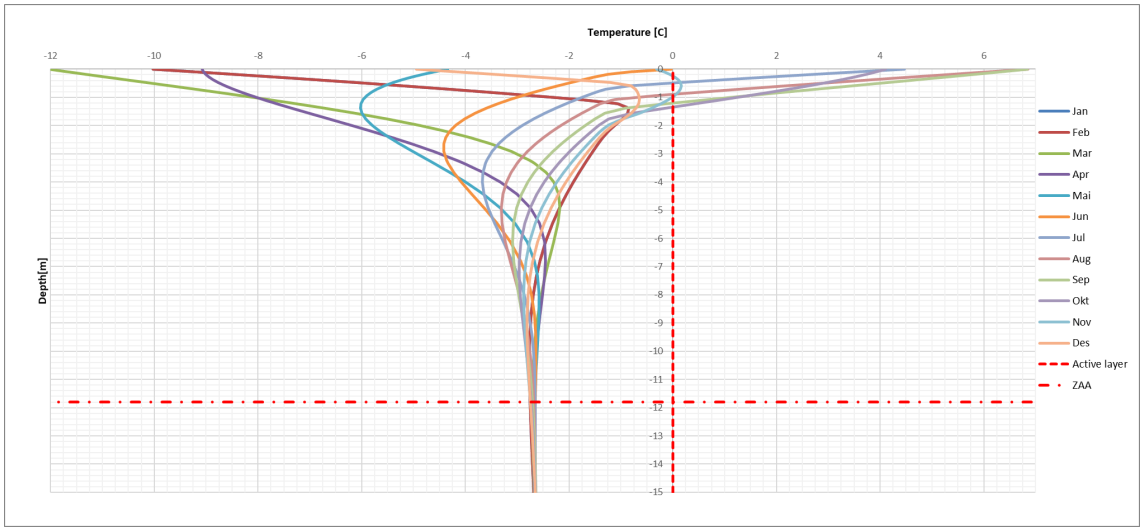

Figure 18: Ground temperature profile for the first day of each month for one year in the period 2010-2020. Plotted from model data for the 5th year of the simulation.

The ZAA is plotted in Figure 18 at 11.8 meters in depth. The depth of zero annual amplitude can be defined as the depth where the temperature variations over one season are less than 0.1°C (Harris et al., 2017). Data from the model estimates this depth to be 11.8 meters. The depth of the active layer is approximately 1.4 meters assuming the active depth layer at 0°C. Generally, the thickness of the active layer in the area is 1-2 meters (Hanssen-Bauer et al., 2019) which supports the active layer depth from the model.

One can also compare the model from this thesis to other ground temperature models.

From the report Climate in Svalbard 2100 the permafrost is estimated to thaw down to 5 meters depth, but still be present below 10 meters (Hanssen-Bauer et al., 2019). From Figure 19 one can see this is within the estimated thaw depth from the modeled temperatures in this thesis. This is supportive of the model. At the same time, the estimated from the climate report, 5 - 10 meters, is of the same magnitude as the thaw depth it self.

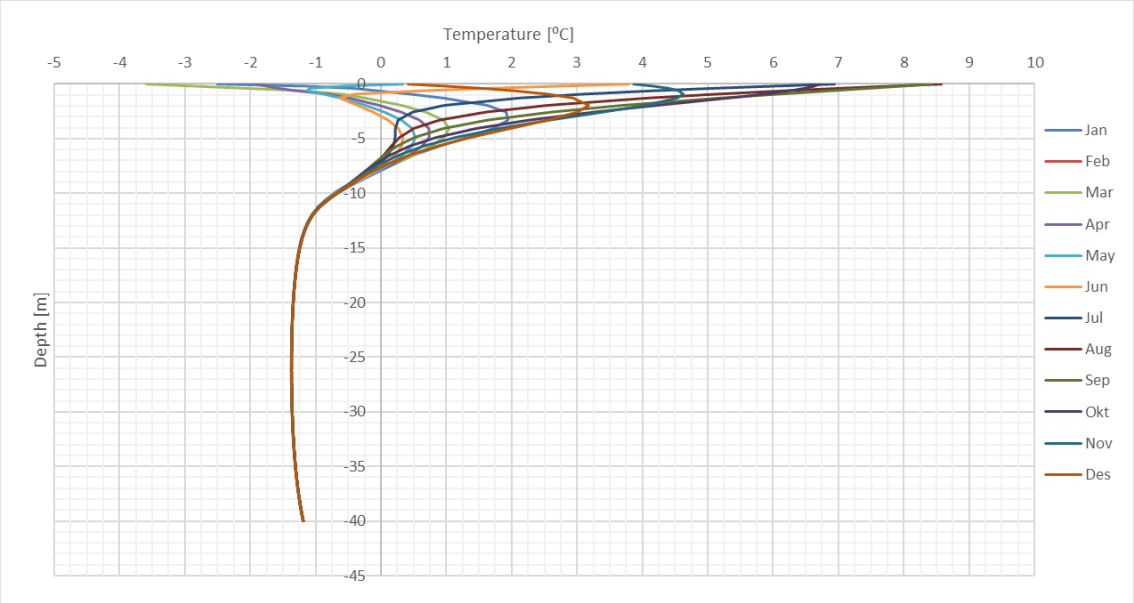

Figure 19: Ground temperature profile for the first day of each month for one year. Plot of the year 2079, the final year in the 60-year simulation done by the FEM model in COMSOL.

3.4 Building Foundation Case

Under this section, a building foundation case with thermosyphons as cooling is presented. This is simulated for today's climate and the emissions scenario RCP45.

3.4.1 Model Design

To show the effect of using a thermosyphon under a building it is used a slab-on-grad foundation. This foundation requires insulation installed between the floor slab and the gravel where the thermosyphon is located. The geometry is illustrated in Figure 20 where the building is designed as 10x10 meters concrete slab with 11 horizontal thermosyphons with the center of the evaporator at 0.15 meters into the gravel. To illustrate the heat flux from the building to the ground it is used a constant temperature boundary condition set to 20°C.

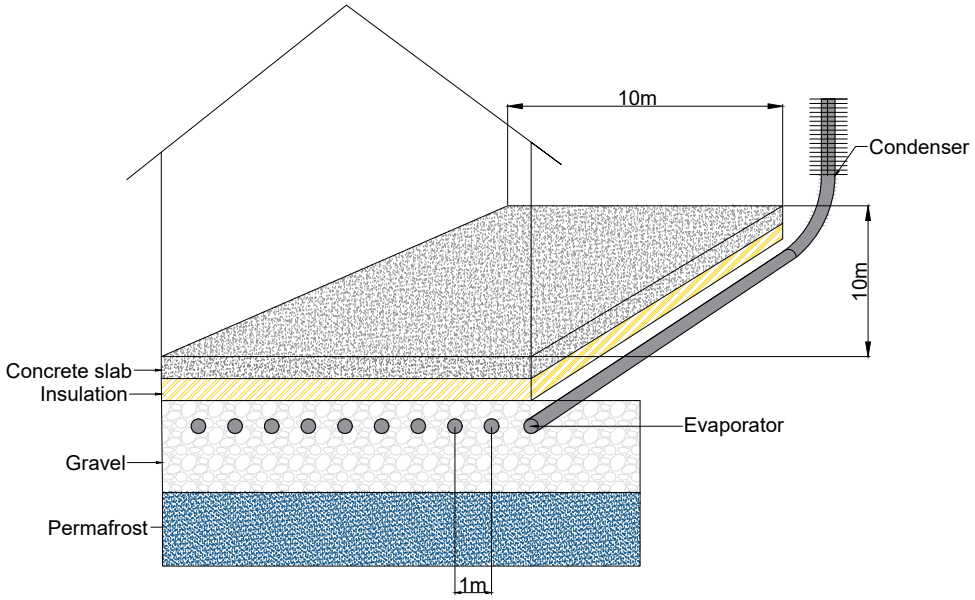

Figure 20: Illustration of the situation the model represents with thermosyphon for foundation cooling.

The gravel fill should be at least 1.5 meters, but it is recommended to be the summer period thaw depth. It should also be used non-frost-susceptible gravel, with a particle limit of 0.075 meter (CSA, 2014). This can allow thawing in the gravel through the gravel, but keep the permafrost in the gravel undisturbed. In the model, it is excavated 2 meters of soil and filled with gravel with the properties in Table 9.

Table 9: Thermal Properties for Gravel (Goering, 2003).

Material	**Density** $[kg/m^3]$	**Thermal Conductivity** $[W/(mK)]$	**Heat capacity** $[J/(kgK)]$
Gravel	1625	0.346	628

The insulation layer between the concrete slab and the gravel is recommended to be 0.1-0.2 meters. The most used thickness is 0.15 meters, which is the thickness used in the model. The insulation is also extended 1 meter outside the concrete slab as recommended to reduce the thawing effect from the side of the building. (CSA, 2014). For the concrete slab, the thickness is 0.1 meters. The thermal properties of

the insulation and concrete are found in COMSOL Material Library and listed in Table 10.

Table 10: Thermal Properties for XPS and Concrete from COMSOL Material Library .

Material	**Density** $[kg/m^3]$	**Thermal Conductivity** $[W/(mK)]$	**Heat capacity** $[J/(kgK)]$
XPS	34	0.41	1450
Concrete	2300	1.8	880

3.5 Laboratory Measurements of Rock Samples

3.5.1 Background

The testing of the thermal properties from the rock samples is done at the lab of the Norwegian Geological survey (NGU). The intention of conducting the tests of thermal properties is to be able to compare these against the model established for soil. The test are done on dry samples at 25°.

3.5.2 Test Material

For the study of thermal properties on rock samples from Svalbard, six samples have been collected from mainly three different places on Svalbard. The information about these are listed in Table 11. The samples are cut and tested in dry conditions in Trondheim.

Table 11: Information about the samples from Svalbard.

Sample	**Classification**	**Age**	**Lithostratigraphic units**	**Location**
NSL-2022-1	Dolerite dyke	Late jurassic to early Cretaceous	Diabasodden Suite	Botneheia
NSL-2022-2 A	Chert	Late Permian	Kapp Starostin Formation	Eskerfossen
NSL-2022-2 B	Chert	Late Permian	Kapp Starostin Formation	Eskerfossen
NSL-2022-2 C	Chert	Late Permian	Kapp Starostin Formation	Eskerfossen
NSL-2022-4 A	Sandstein	Early Cretaceous	Carolonefjellet Formation	Longyearbyen, Flyplassvei
NSL-2022-4 B	Sandstein	Early Cretaceous	Carolonefjellet Formation	Longyearbyen, Flyplassvei

The exact location of the different rock samples is shown in Figure 21. The samples

at location Botneheia are collected from two locations a few hundred meters apart, where NSL-2022-2B and C are collected from the same location. The same applies to the samples from Longyearbyen, NSL-2022-4A and B, which are also collected from the same location.

Figure 21: Map over where the samples are collected (Norwegian Polar Institute, no date).

3.5.3 Test Method

The C-Therm TCi system is based on the modified transient plane source method (MTPS). The MTPS technique apply a known current through the sensor coils heating element. Around the heating element, a guard ring makes sure that the heat exchange is close to one dimensional. Therefore the temperature in the sample will increase, which induce a decrease of voltage in the sensor. The drop in temperature is monitored, and graphed as illustrated in Figure 22, by using the voltage drop, and then calculate the thermal properties. The MTPS technique is a non-destructive test, the results is ready in seconds and the sample can be minimum 17 mm in diameter.

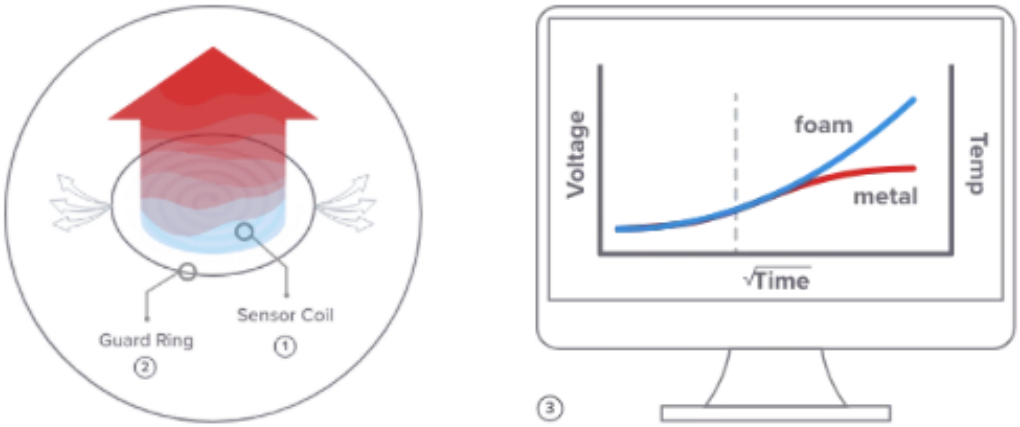

Figure 22: How the sensor is working to the left, and the plot of the results to the right . In 1) The sensor coil is illustrated. In 2) the surrounding guard ring is illustrated (C-Therm Technologies Ltd, no date).

Before the test is performed the sensor temperature needs to be calibrated. The sensor temperature is factory calibrated with TCR (Temperature coefficient of resistivity) calibration to find the resistance of the sensor at a given temperature (C-Therm Technologies Ltd, no date).

Figure 23: Illustration of the C-therm TCi sensor (C-Therm Technologies Ltd, no date).

The test measures directly the thermal conductivity and effusivity, and calibrate them against other samples where the thermal conductivity and effusivity is known. Each of these materials will have a different change in voltage when the temperature changes.

This can look something like the curve in Figure 24.

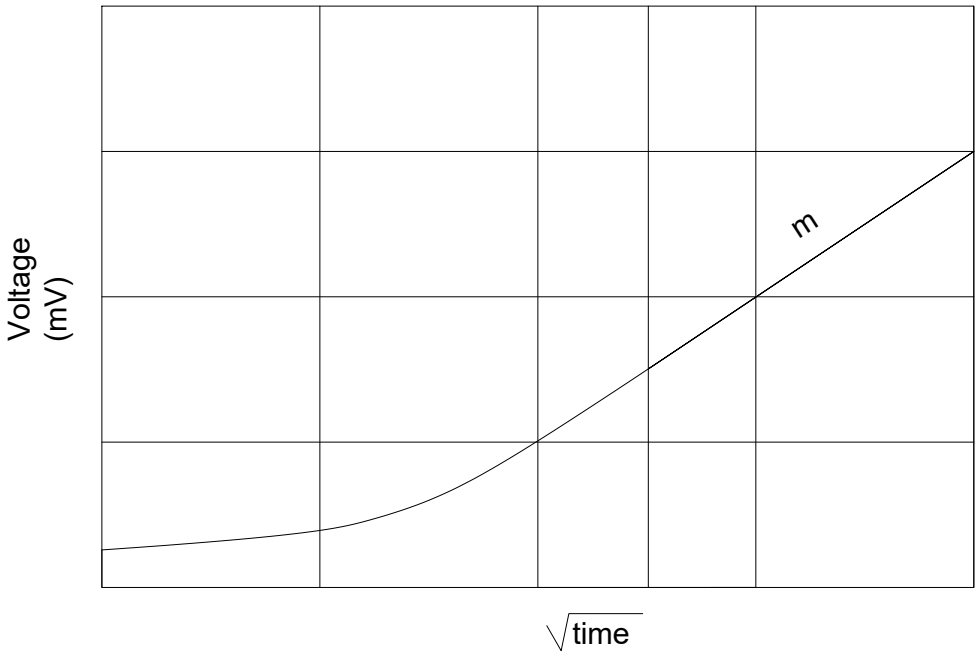

Figure 24: Graph of the change in voltage over time under calibration, modified from (C-Therm Technologies Ltd, no date).

The slope, m, in Figure 24 is then used in Equation 28 to sensor calibrate for effusivity.

$$\frac{1}{m} = Me_2 + C \tag{28}$$

Where:

- m = The slope of the calibration line, shown in Figure 25.
- C = The 1/m value for vacuum.
- e_2 = The thermal effusivity of the measured material.

A graph for the sensor calibration is illustrated in Figure 25. The Graph is found by using samples with known effusivity.

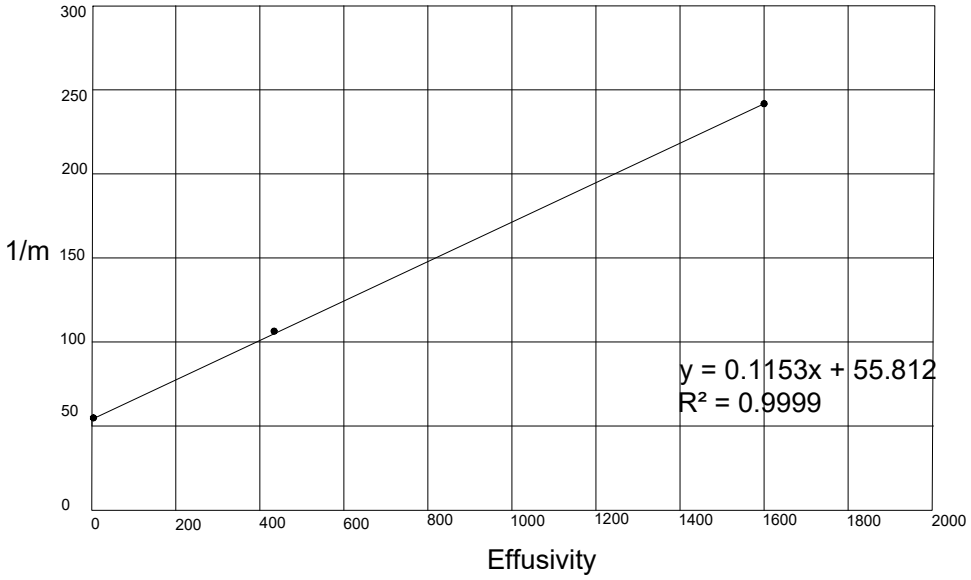

Figure 25: Graph of the 1/m effucivity calibration curve, modified from (C-Therm Technologies Ltd, no date).

The thermal conductivity is measured with the same principle, but with the calibration equation that is shown in Equation 29.

$$\frac{1}{m - m^*} = slopek + intercept \tag{29}$$

Where:

- Slope = The slope of the calibration line, shown in Figure 26.
- Intercept = The intercept in Figure 26 between the thermal conductivity and the 1/(m-m*)
- k = The thermal conductivity of the measured material.
- m* = The calibration factor to linearize 1/m values with the known thermal conductivities from calibration.

The m value is found from using calibration materials from materials with known thermal conductivity. The m^* is attractively changing to provide a god fit for the data.

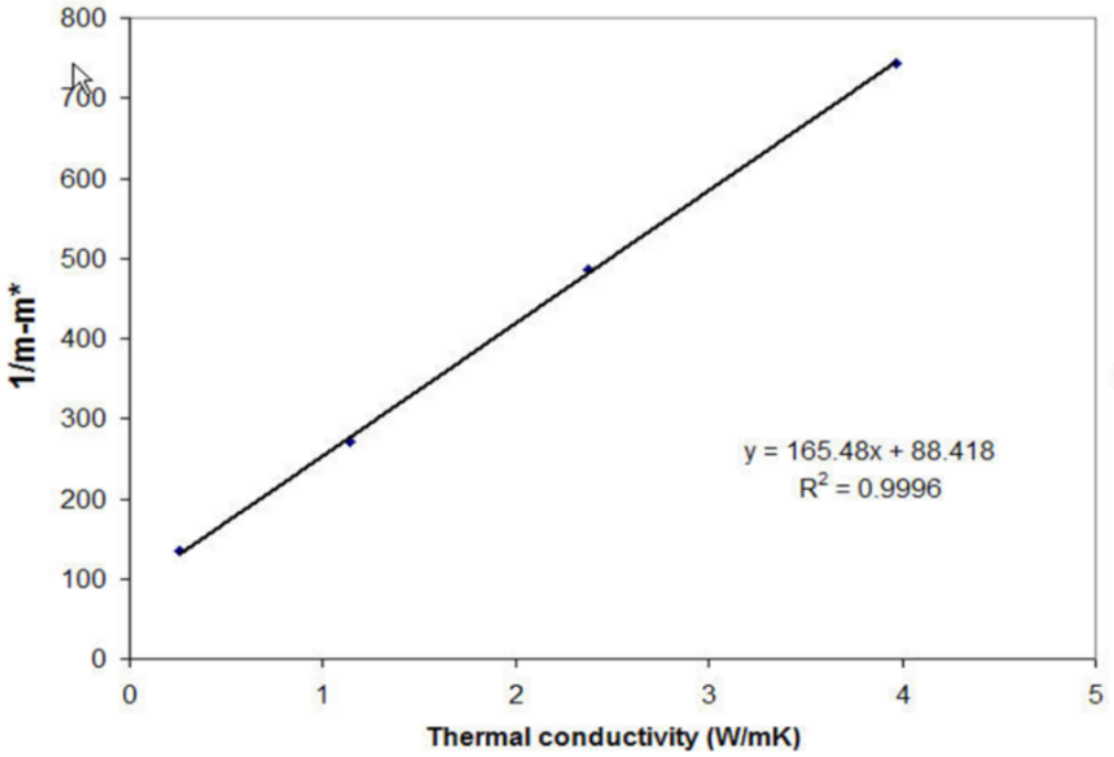

Figure 26: Graph of the thermal conductivity calibration curve (C-Therm Technologies Ltd, no date).

If the density and the specific heat capacity is known, the thermal conductivity can be calculated with Equation 30 (C-Therm Technologies Ltd, no date).

$$k = \frac{e_2^2}{\rho C_p} \tag{30}$$

Where:

- ρ = Density
- C_p = Specific heat capacity
- e_2 = Measured effucivity of the sample

In the MTPS method it is mainly three types of error when measuring the thermal conductivity: The contact between sample and the sensor, equipment error and calibration error. The surface of the sample needs to be of a high quality and it is also recommended to use a fluid between the sensor and the sample to lower the contact resistance (C-Therm Technologies Ltd, no date). If there are bubbles of air between the sample and the sensor this can make a big impact on the results. Also,

a lot of fractures will be disturbing to the test results, because the fracture will make a big impact since only a small volume of the sample is tested.

4 Results

The results from the COMSOL model will compare temperatures in the ground when thermosyphon are installed and temperatures without thermosyphon cooling. The results also compare the thermosyphons effect on ground temperatures with today's climate and expected future climate. In this section the ground temperatures and cooling effect from a the model simulating cooling of a foundation are presented. Results from thermal conductivity measurements are also presented in this section.

4.1 Thermosyphon Today

To illustrate the effect of the thermosyphon on the grounds thermal regime temperatures have been plotted for 4 different points over a 10 year period from the model. Figure 27 shows the placement of the points where the temperature is measured.

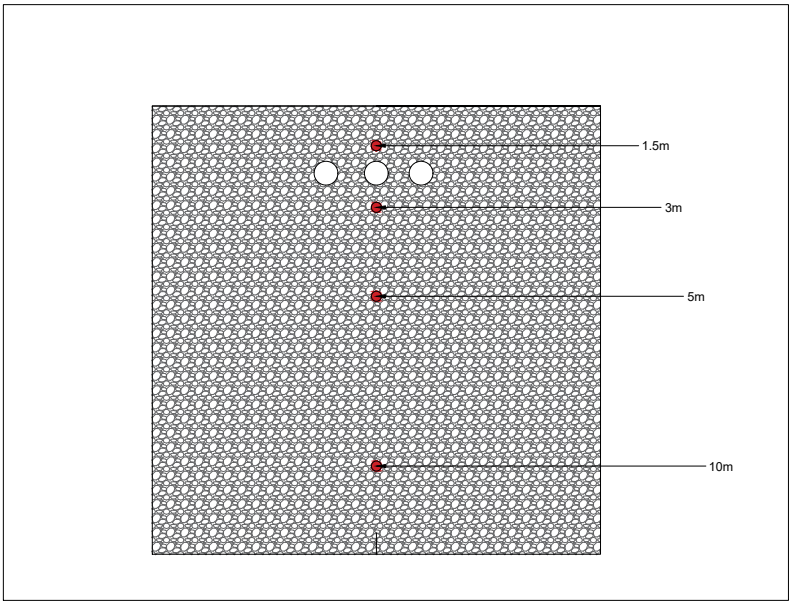

Figure 27: Shows the points where temperatures are plotted in the domain. Not to scale.

Figure 28 and Figure 29 show plots of ground temperature over time. The plots show temperatures at different depth for a 10 year period without thermosyphon

and with a thermosyphon running passively. From the illustration one can see the thermosyphon has an effect on the grounds thermal regime.

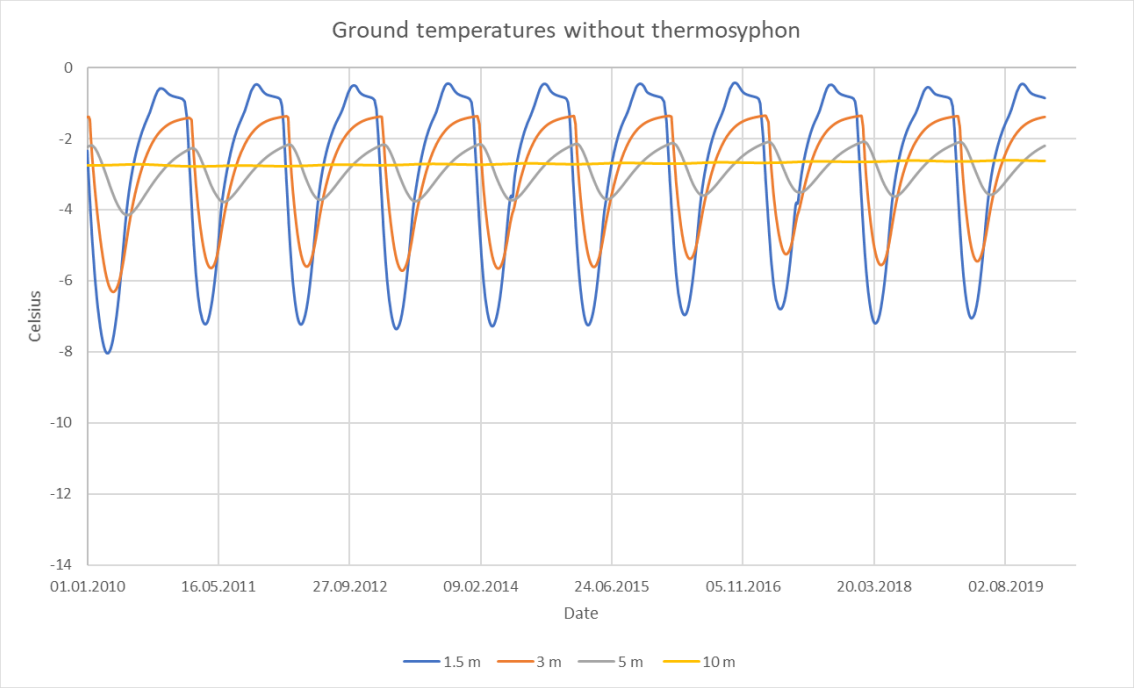

Figure 28: Shows the temperature at different depths for a 10 year period with no thermosyphon to provide cooling.

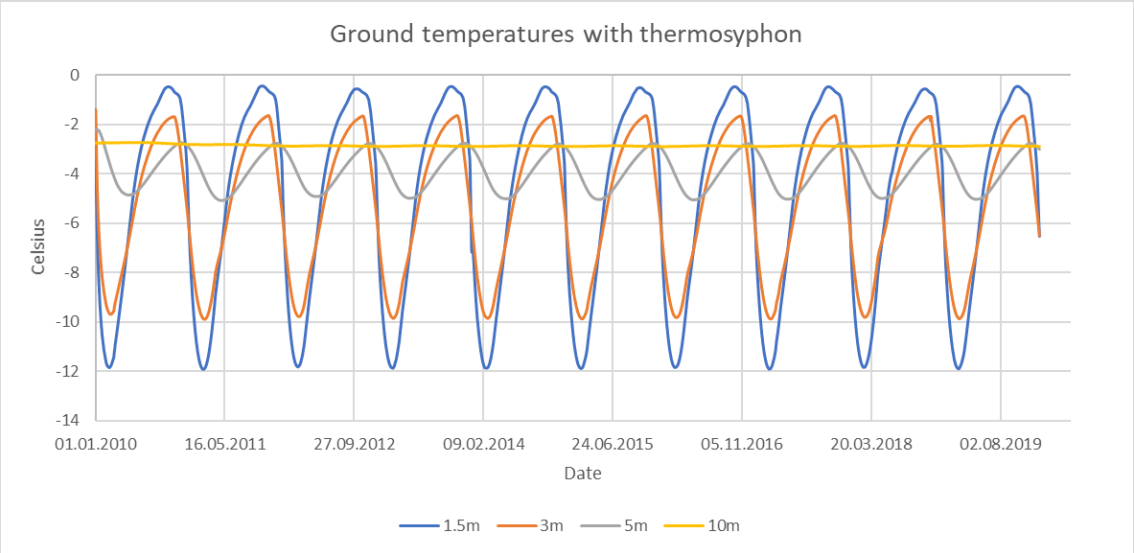

Figure 29: Ground temperatures with thermosyphon running passively for a 10 year period.

From Figure 28 and 29 the temperatures observed from the model are decreasing throughout the 10 year period when a thermosyphon is installed. The model shows

the biggest decrease in ground temperature during the winter period, during warmer parts of the year the temperature difference is less. The temperatures through one year are clearer in Figure 30.

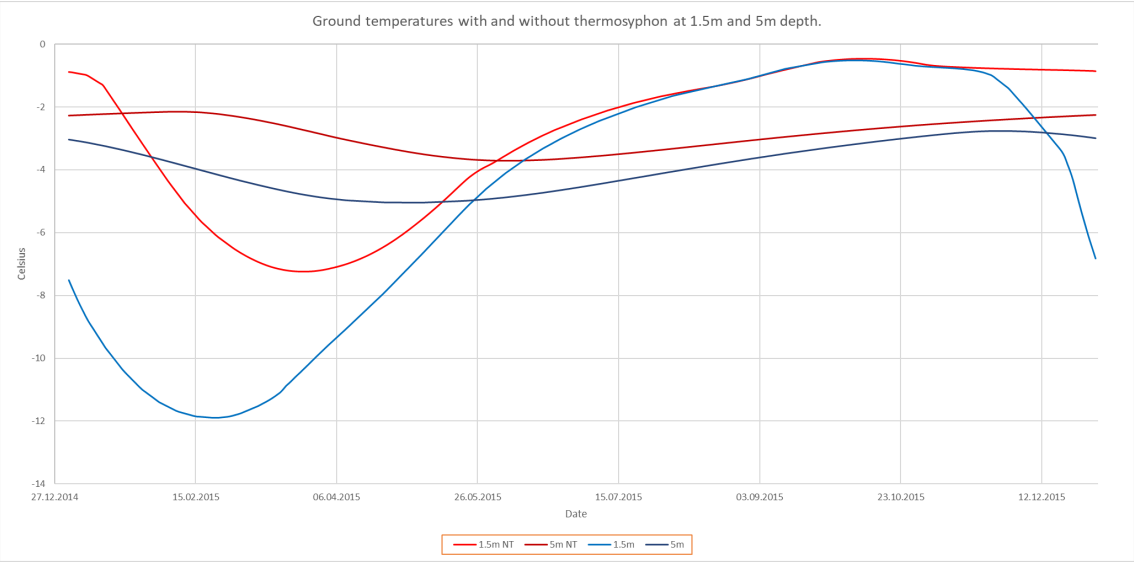

Figure 30: Ground temperatures with and without thermosyphons for 1.5 and 5 meters depth. NT indicates "no thermosyphon"

From Figure 30 temperatures are shown at 1.5 meter and 5 meters depth for one year. Temperatures from the model with the thermosyphon running passively are shown as blue lines, while the red lines illustrate the temperatures without cooling from thermosyphons. From the plot it is clear that the thermosyphons provide cooling through cold parts of the year at both 1.5 meters and 5 meters depth. At 1.5 meter the thermal impact is greatest thus the temperature difference when using a thermosyphon is largest. At 5 meter the temperature is also reduced, but less than at shallower depth. The largest temperature difference at 5 meters depth is approximately 2.3°C on 17th of March. At 1.5 meters depth the largest difference is approximately 8.2 °C on 14th of January.

4.2 Thermosyphon Future

Under this section the thermosyphon effect is presented for both the middle emission scenario, RCP45 and the high emission scenario, RCP85.

Modelling the period 2080-2090 for RCP45

From Figure 31 and Figure 32 one can see the difference in temperature from the modelling results after installing the thermosyphon. The ground temperature

decreases with a thermosyphon at all depths, 1.5 meters, 3 meters, 5 meters and 10 meters. From the figures one can notice the decrease is larger during winter and less during summer. At 1.5 meters depth the temperature during winter season is approximately 5°C lower after installing a thermosyphon compared to the ground temperature without a thermosyphon. For warmer parts of the year the ground temperature difference is less than 0.5°C. Over the 10 year period the temperature shows a small decreasing trend.

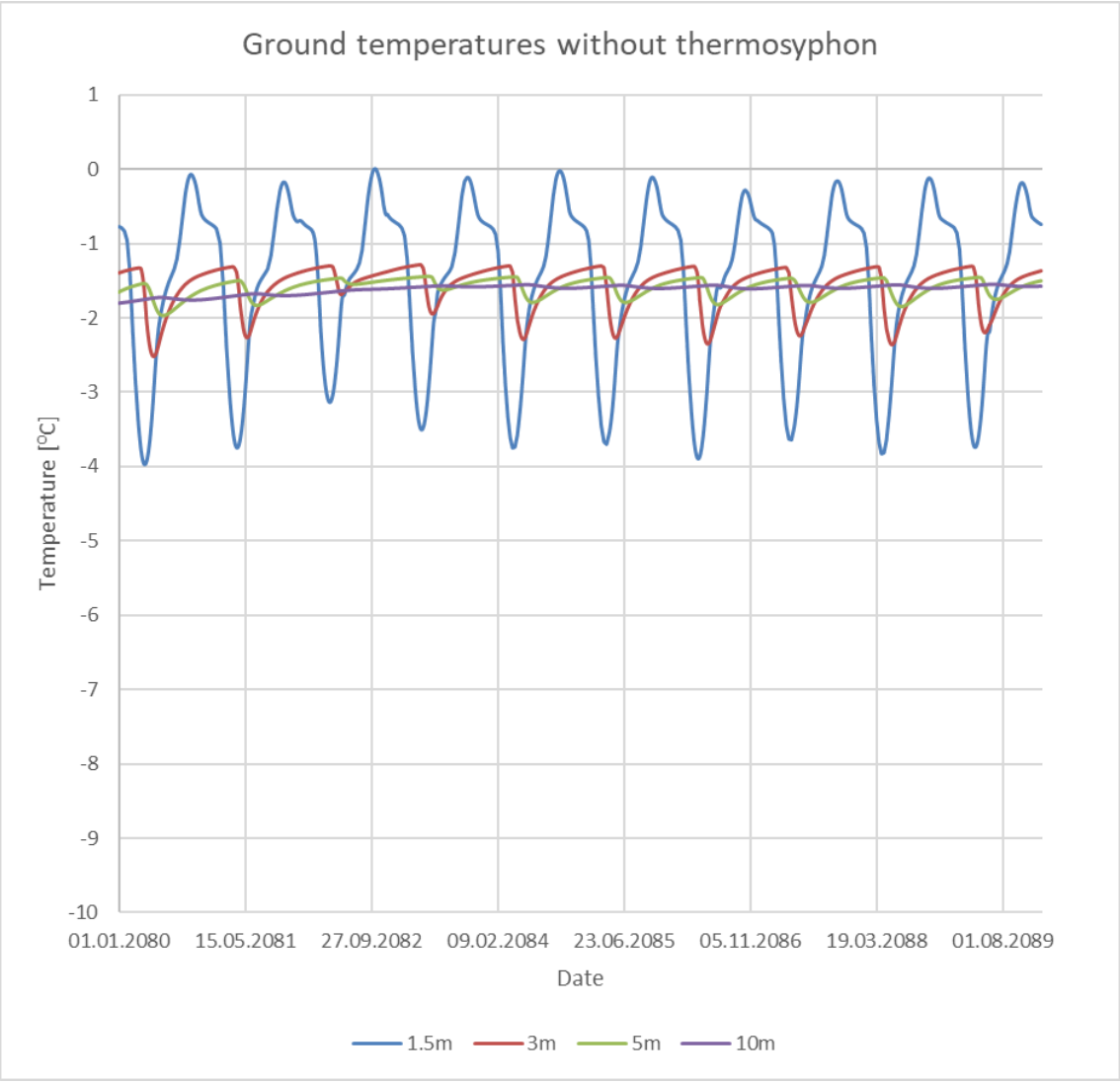

Figure 31: Shows the temperature at different depths for a 10 year period with no thermosyphon to provide cooling, for RCP45.

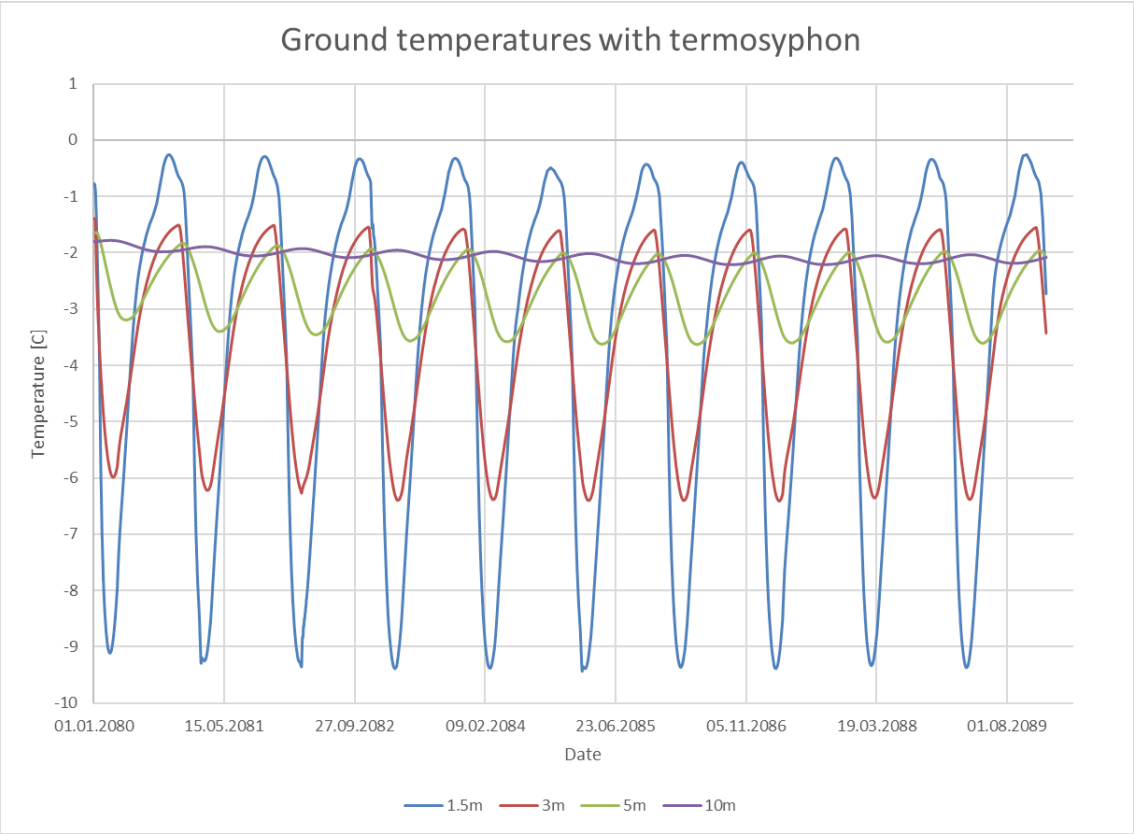

Figure 32: Ground temperatures with thermosyphon running passively for a 10-year period, for RCP45.

Modelling the period 2080-2090 for RCP85

From Figure 33 and Figure 32 one can see the difference in temperature with and without a thermosyphon for the highest emission scenario and thus the highest temperatures increase. The temperature difference with and without thermosyphon is similar for both warm and cold parts of the year, the magnitude of the temperature difference is 1°C. Over the 10 year period the ground temperature with a thermosyphon is increasing, but the increase is smaller compared to the model without thermosyphon.

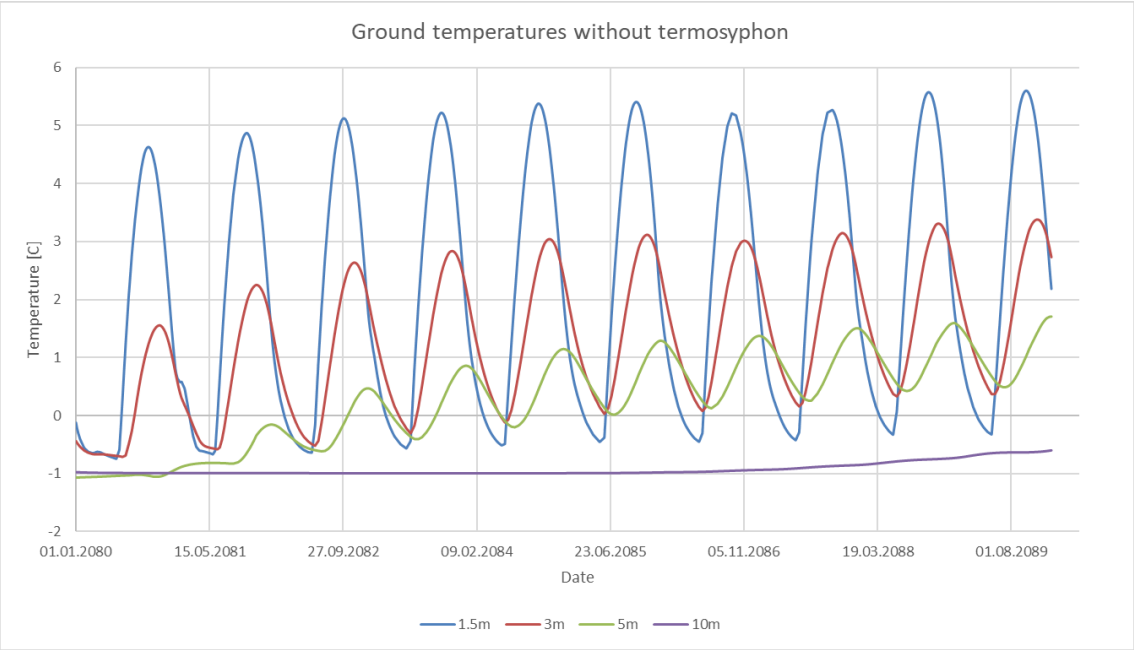

Figure 33: Shows the temperature at different depths for a 10-year period with thermosyphon to provide cooling, for RCP85.

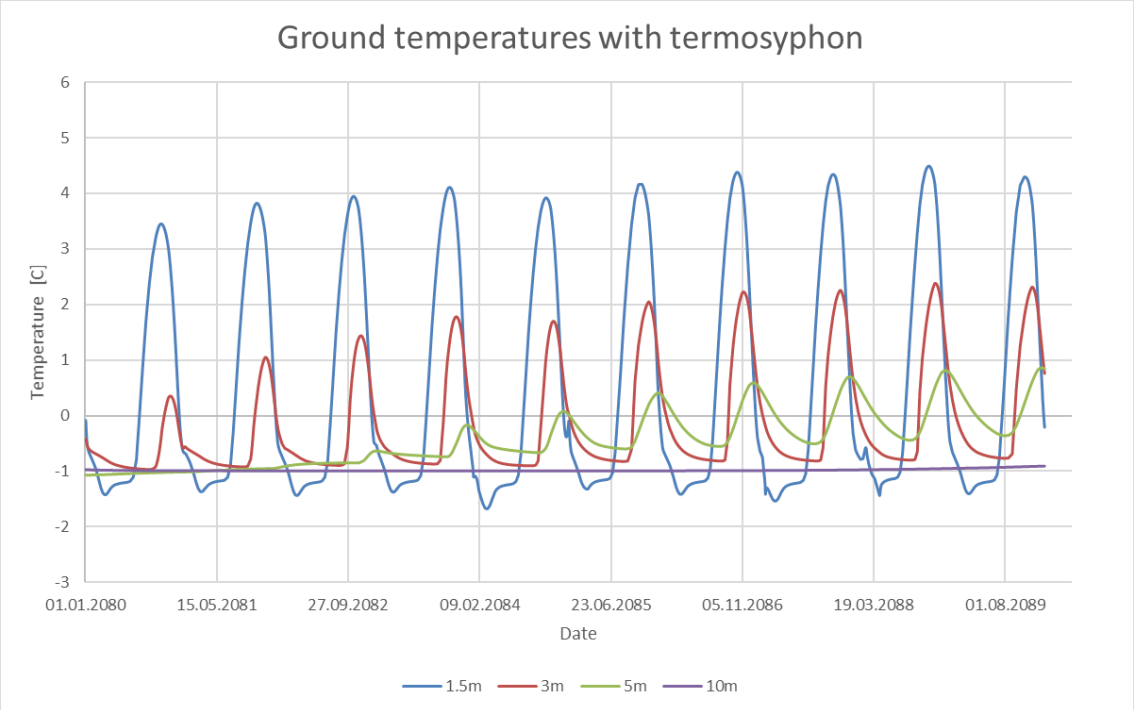

Figure 34: Shows the temperature at different depths for a 10-year period with thermosyphon to provide cooling, for RCP85.

4.3 Building Foundation Case

In this part of the results, the use of thermosyphon as cooling under a foundation is presented. The results are presented for the current situation and for the future middle emission scenario, RCP45.

4.3.1 Building Foundation Today

Figure 35 and 36 show the ground temperature plots without and with a thermosyphon, respectively. The figures illustrate that the passive thermosyphon has an effect on the ground temperature. Without the use of thermosyphons, the temperature increases throughout the period, nor does it appear to stabilize. With thermosyphons, temperatures rise in the first few years before they appear to stabilize.

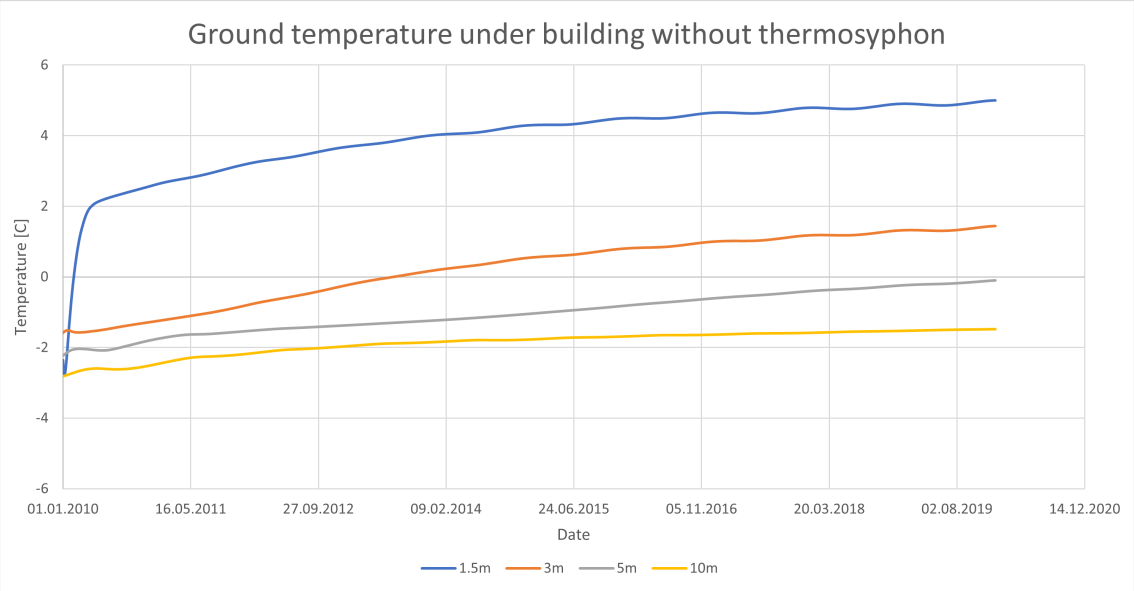

Figure 35: Graph over ground temperatures beneath building without thermosyphon at 1.5, 3, 5, and 10 meters depth.

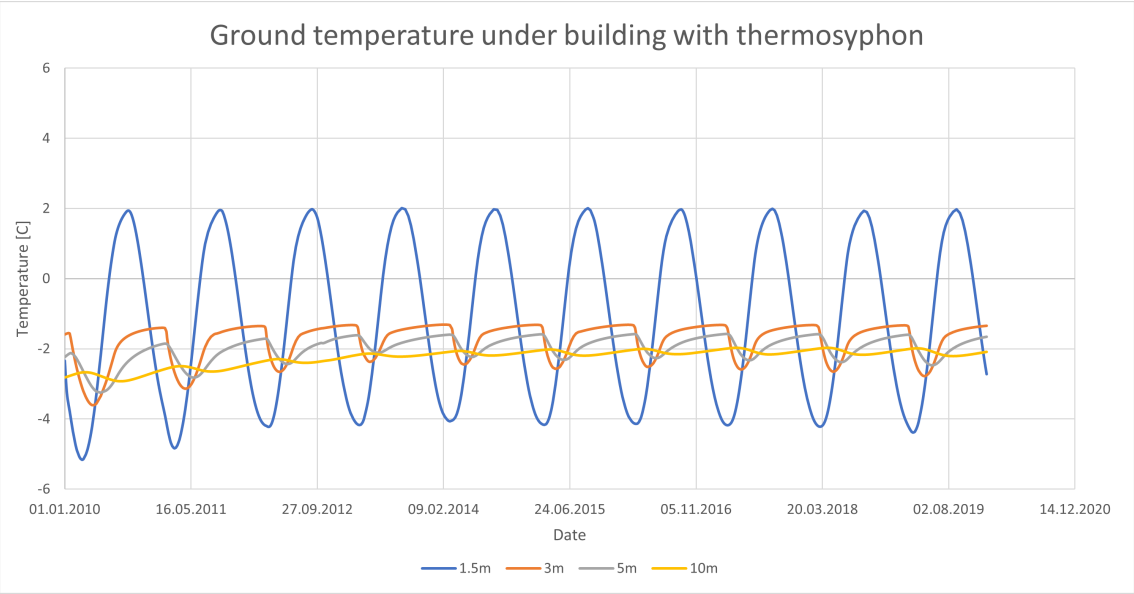

Figure 36: Graph over ground temperatures beneath building with thermosyphon at 1.5, 3, 5, and 10 meters depth.

Figure 37 and Figure 38 show ground temperature profiles with a building foundation represented for the period 2010-2019. The thawing is illustrated with the light blue area where the temperatures are between -1 °C and 0 °C. Without thermosyphons, this area gets deeper and deeper every year. At the end of the simulation the thaw depth reaches almost 7 meters with no thermosyphon to provide cooling. With the use of thermosyphons, which is illustrated in Figure 38, the light blue area stays within the gravel and thus the model estimates little or no thawing in the permafrost. Still, the temperature increases the first years after the construction of the building, even with thermosyphons.

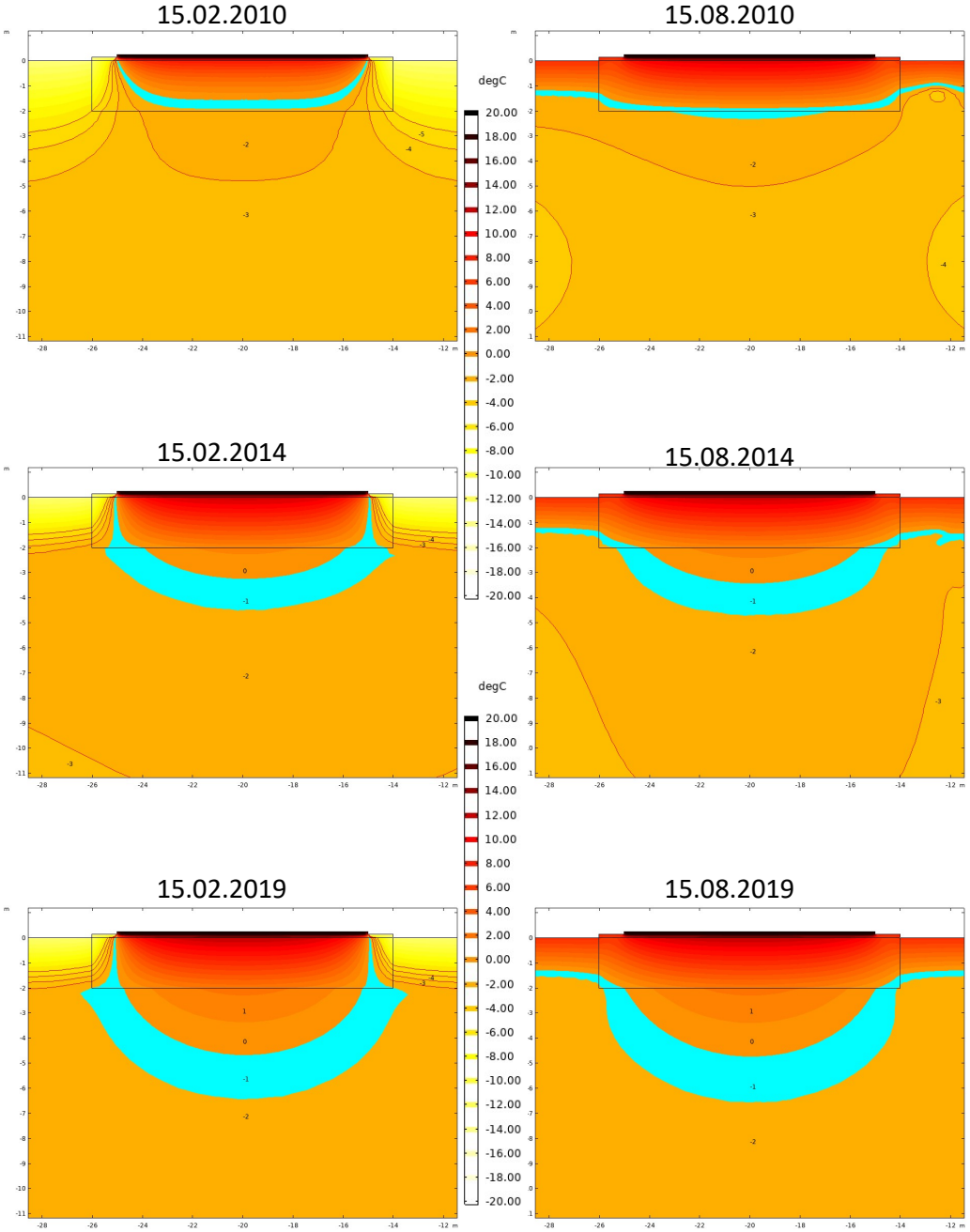

Figure 37: Ground temperatures beneath building without thermosyphon at 15th of February and 15th of August the first, fifth and tenth year.

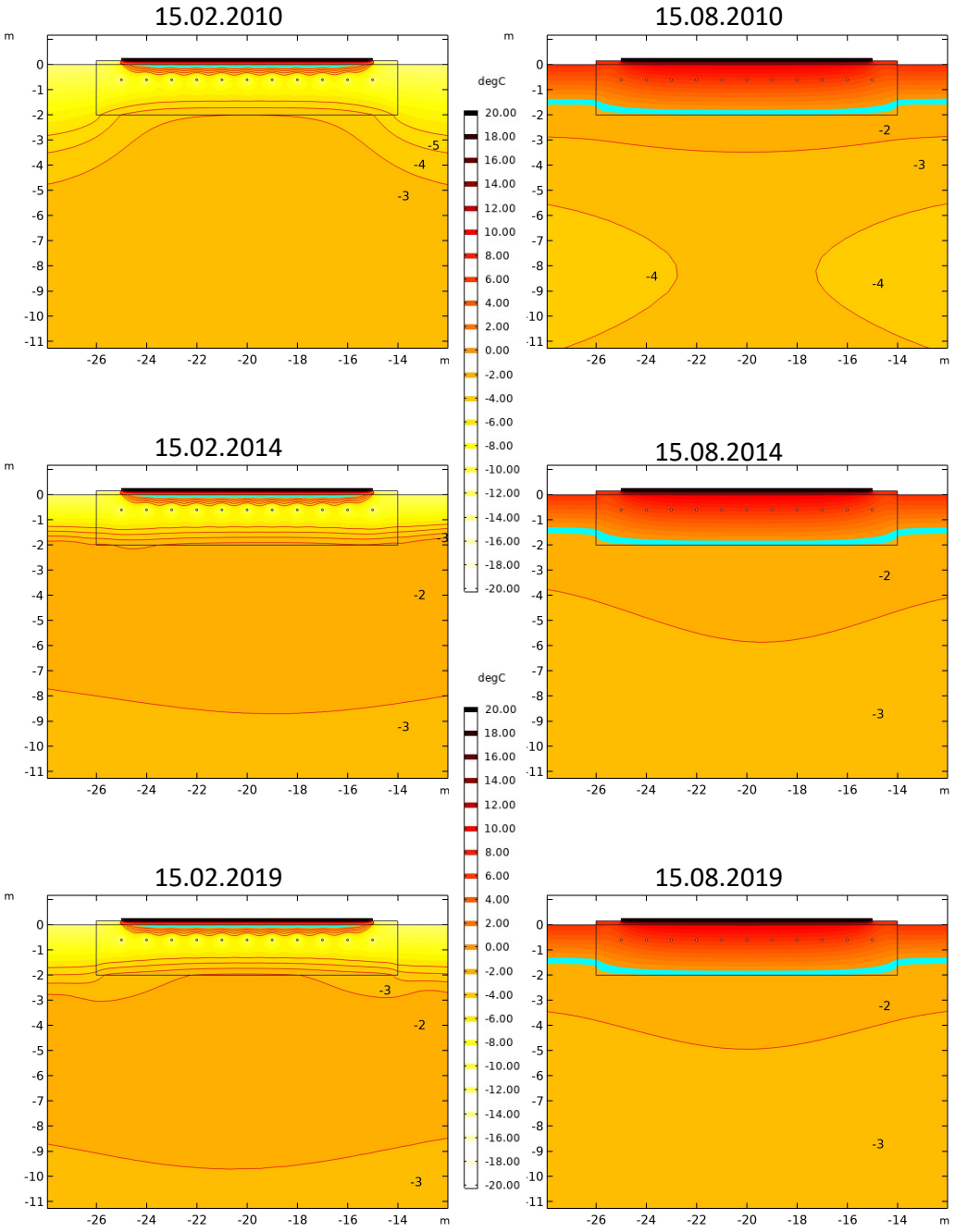

Figure 38: Ground temperatures beneath building with thermosyphon at 15th of February and 15th of August the first, fifth and tenth year.

4.3.2 Building Foundation in the Future

The modelling of thermosyphons for a building foundation case shows potential cooling effect from the heat exchanger. From Figure 39 and 40 one can observe that the model estimates a reduction in the ground temperature after installing thermosyphons beneath the foundation. Without thermosyphon the ground temperatures annually oscillation is close to invisible. With the use of thermosyphons the annual oscillations are observed only in the gravel at 1.5 meters, but the increase in the temperature at 3,5 and 10 meters are also reduced.

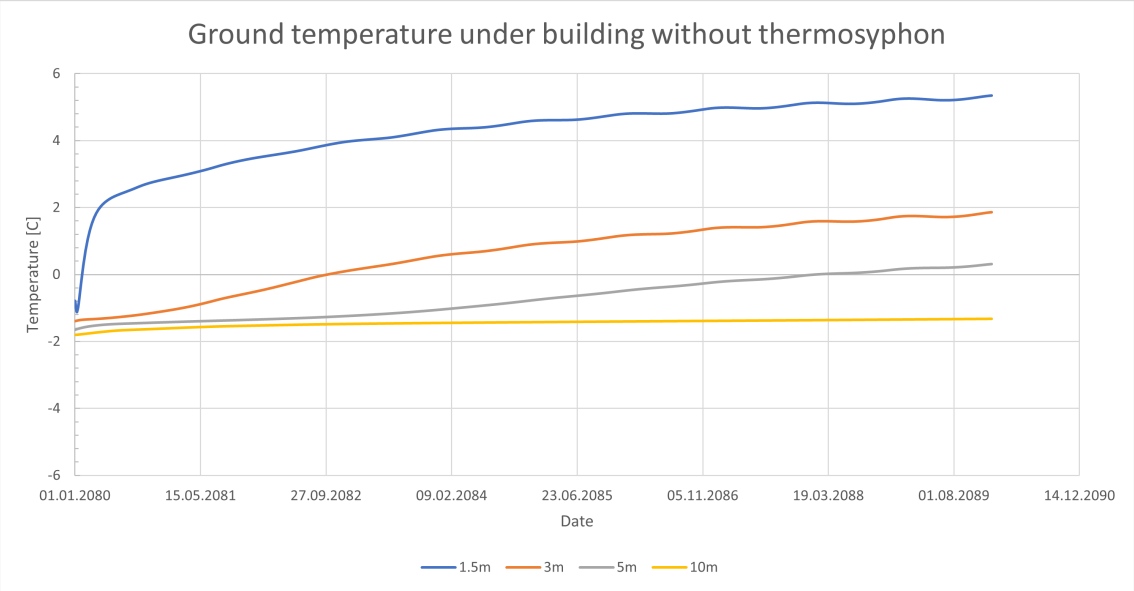

Figure 39: Plot of ground temperatures at under the building foundation without thermosyphon at 1.5, 3, 5, and 10 meters depth.

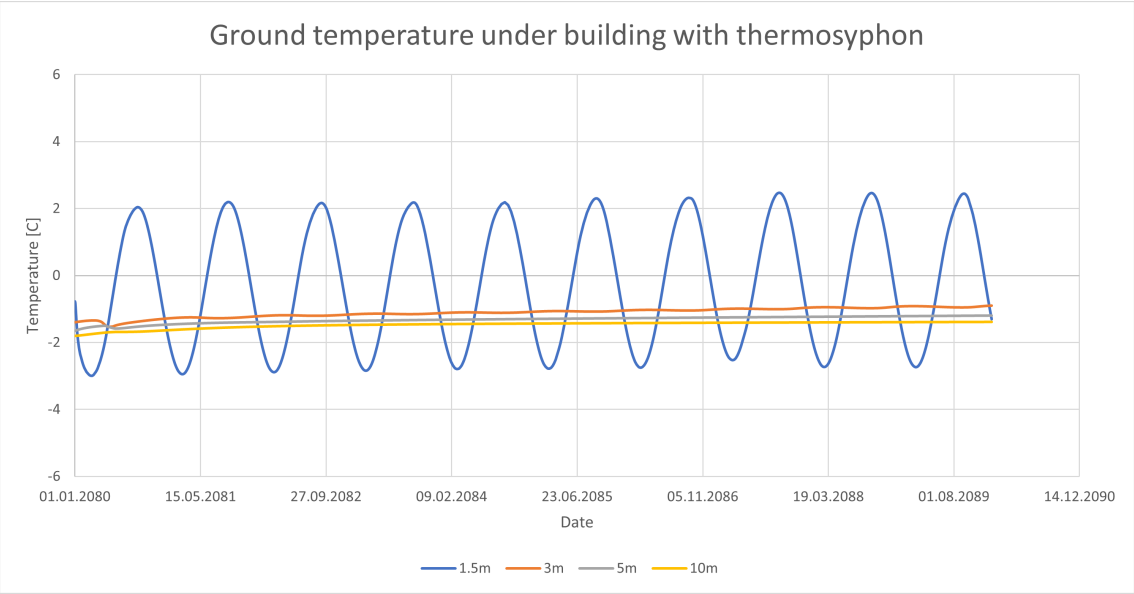

Figure 40: Plot of ground temperatures under the building foundation with thermosyphon at 1.5, 3, 5, and 10 meters depth.

Figure 41 and 42 show a temperature profile of the ground temperatures with a building foundation represented for the medium emissions scenario, RCP45, without and with thermosyphon to provide cooling. The bright blue section illustrates the freezing front, with a temperature range -1°C to 0°C.

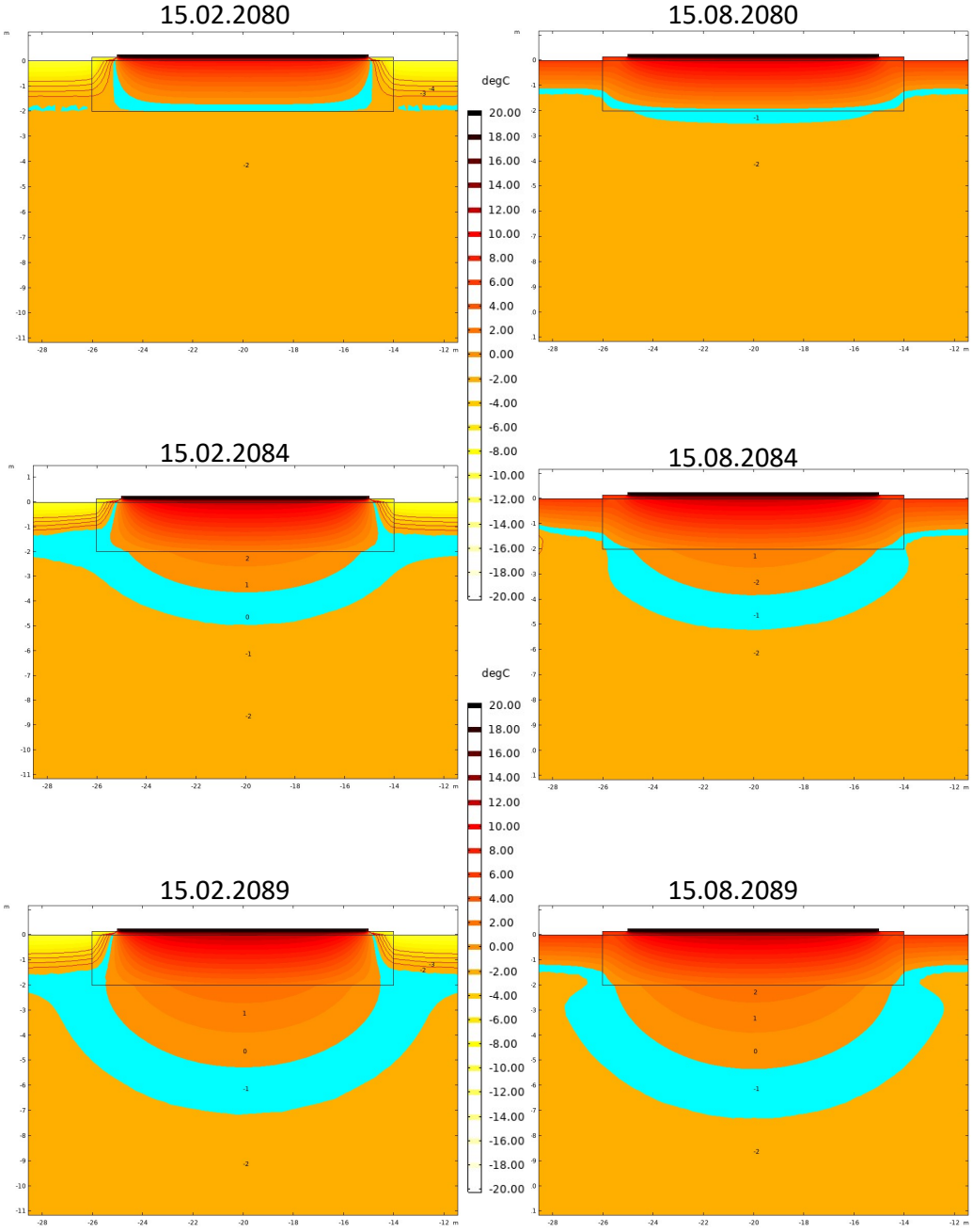

Figure 41: Ground temperatures beneath building without thermosyphon at 15th of February and 15th of August in 2080, 2084 and 2089.

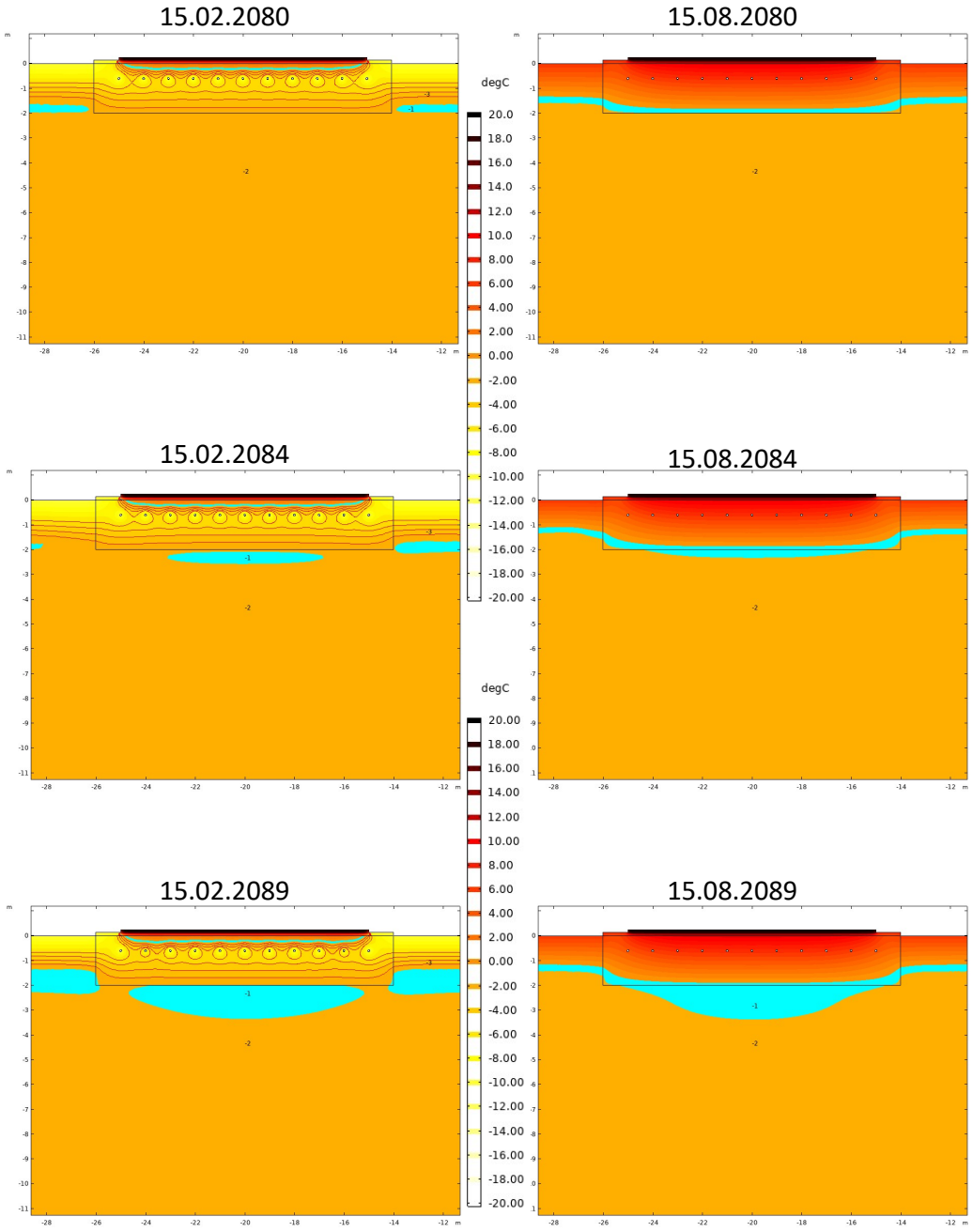

Figure 42: Ground temperatures beneath building with thermosyphon at 15th of February and 15th of August in 2080, 2084 and 2089.

The undisturbed soil below the gravel is exposed for thawing, even when using passive thermosyphons to cool the ground. The thawing depth is estimated to be reduced from the modelling. The thaw depth is estimated to be 7 meters at the end of the simulation with no thermosyphon, compared to a thaw depth of 3.5 meters with thermosyphons installed. A reduction in thaw depth of approximately 3.5 is estimated when running thermosyphons passively for the emissions scenario RCP45.

4.3.3 Quantifying Energy Extraction from Thermosyphon

Figure 43 illustrate the extracted energy from the ground in 2014 and in 2084. In the model, the passive thermosyphons had a heat extraction of 3057 kWh and 2754 kWh in 2014 and in 2084, respectively. A decrease of approximately 10% with increased temperatures for future climate.

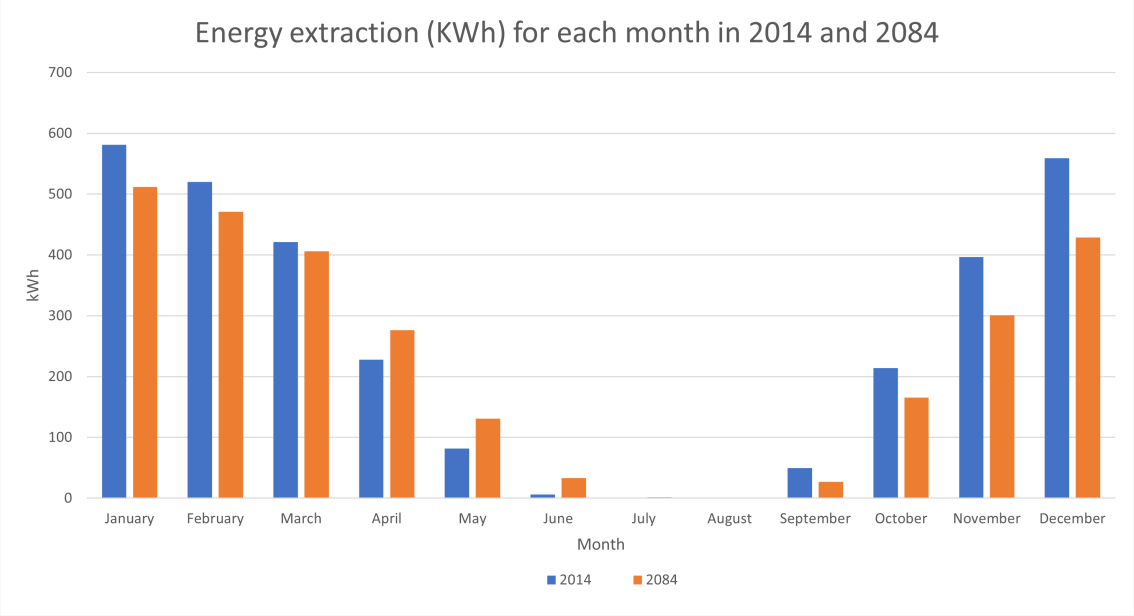

Figure 43: Energy extraction from the thermosyphons in year 2014 and 2084.

From 2014 to 2084 the decrease in heat extraction is largest in January, November and December with 23%, 32% and 43% respectively. While in March, April and June, heat extraction increases by 16%, 16% and 9%, respectively.

4.4 Thermal Conductivity of Rock Samples

Thermal conductivity is measured from six samples from different locations on Svalbard. After being transported to Trondheim, the thermal conductivity and

specific heat capacity have been measured with C-therm's sensor shown in Figure 23. The measurements were performed in three different places on each sample, and then calculated an average. The results and the variation between the three different measurements are shown in Table 12. To prevent air bubbles between the sample and the sensor, water has been used as a contact medium.

The results have been obtained through the use of the calibration method Ceramics-HR. For sample NSL-2022-2 C, it was not possible to obtain any representative measurements as the sample was strongly fractured. Pictures of the samples are shown in Figure 49 in Appendix B.1. The density is not measured, but calculated from Equation 15.

Table 12: Measured thermal conductivity and specific heat from samples from Svalbard. Sample NLS-2022-1 to NLS-2022-4-B are measured using the Ceramics-HR calibration method. The values for frozen and unfrozen soil are taken from Table 7.

Sample Name	**Sample material**	**Thermal Diffusivity** $[m^2/s]$	**Density** $[kg/m^3]$	**Specific Heat Capacity** $[J/kgK]$	**Thermal Conductivity** $[W/mK]$
NSL-2022-1	Dolerite Dyke	1.36E-06	1997	994	2.7
NSL-2022-2 A	Chert	2.11E-06	2009	1085	4.6
NSL-2022-2 B	Chert	2.03E-06	2016	1075	4.4
NSL-2022-2 C	Chert				
NSL-2022-4 A	Sandstone	1.45E-06	1994	1003	2.9
NSL-2022-4 B	Sandstone	1.80E-06	2018	1046	3.8
	Frozen Soil	1.11E-06	1800	800	1.6
	Unfrozen Soil	0.49E-06	1800	2056	1.8

In Table 12, the thermal diffusivity of the laboratory-measured samples of hard rock has a higher thermal diffusivity than the unfrozen and frozen soil. And it is highest for the chert in samples NSL-2022-2 A and B. The high measured diffusivity is reasonable because of the high thermal conductivity of 4.4 [W/mK] and 4.6 [W/mK] in samples NSL-2022-2 A and B, respectively. The thermal properties of the dolerite dyke (NSL-2022-1) can be compared to the sandstones (NSL-2022-4-A and B), but the results from the two different sandstones have a significant gap in thermal conductivity.

Compared to the frozen and unfrozen soil, the hardrock samples have a higher thermal conductivity and the frozen soil has a lower specific heat capacity because of the high water content in the soil. The hard rock samples have not been measured at lower temperatures or in a saturated state.

5 Discussion

5.1 Rock Samples

Because of the late arrival of rock samples and testing, there was no time to do modelling with the thermal properties of the rock samples. Still, by comparing the rock's thermal properties with the soil properties used in the modeling one can get an idea of what the expected difference would be. Assuming the water content is small and thus not affecting the thermal properties significantly for frozen and unfrozen rock we can compare the differences. Higher thermal diffusivity gives a more rapid temperature change in the material. The thermal diffusivity is higher for all rock samples compared to both frozen and unfrozen soil, thus we expect more rapid temperature change in rock. This is expected to be the case for both thawing during summer and freezing during winter, as well as freezing from the thermosyphons. In addition, the lower water content in rock will mean less resistance to temperature change due to phase change. One can expect the heat to propagate faster from rock to the thermosyphon than to soil. At the same time, the rock is expected to reach colder temperatures faster than soil, thus the cooling effect from the thermosyphon is not clear for soil versus rock. From the differences in thermal properties between rock and soil, the temperature fluctuations in the ground are expected to be greater for rock. It is important to be aware that the properties for bulk rock mass can be different. These tests are performed on relatively small rock samples and they do not necessarily give a good picture of a large rock volume. For a greater volume of rock, there can be fracturing, including ice lenses and higher water content, which will affect the thermal properties of the rock. These uncertainties makes it challenging to argue exact expectations for thermosyphons effect in soil versus rock.

5.2 Today's Climate, RCP45 and RCP85 Simulations

From Figure 28 and Figure 29 one can notice peaks of the curves not being symmetric. This is most visible in the figure with no thermosyphon, Figure 28, but one can find this in both plots. The reason for this is the phase change and latent heat in COMSOL, as shown in the modeling section this is defined as a function of the fraction of each phase of the media over a temperature interval. The latent heat will "resist" temperature change and thus making the flat spots in the temperature plots. If one chooses latent heat as 0 kJ/kg the temperatures will be symmetric, one can also notice the bottom of the curves being symmetric. This is shown by example in Figure 48 in A.3. Here the temperature is below the phase change temperature and

thus no latent heat affects the temperature change.

From the modeling results, it is clear that a thermosyphon will have a cooling effect on the ground's temperature. For the simulations without a building foundation, the thermosyphons show an effect on the ground temperatures. This effect is present in today's climate and both climate scenarios. The effect is less for increased air temperatures with higher mean annual temperatures for future climate projections. This is also in accordance with what one would expect. For today's climate and for the climate scenario RCP45 the thermosyphons seem to provide a cooling trend for the ground temperatures. This gives an indication that the thermosyphons can be useful to preserve permafrost with only passive cooling if this is needed. From the results, one can notice the difference in temperature throughout the season for different depths. For shallower depths, 1.5 meters, the cooling effect from the thermosyphons does not last through the summer season. The ground temperature with and without thermosyphons is the same during summer. For greater depth, 5 meters, the temperature difference seems to be permanent as shown in Figure 30. This indicates that passive thermosyphons can be used for permanent cooling of permafrost, especially at depth.

For the highest emissions scenario, RCP85, the ground temperatures are increasing over the 10-year period even with the thermosyphon installed. Passive cooling with thermosyphon might not be an efficient cooling option for the warm climate which is projected for high emissions. Temperatures in the winter increase more than in the summer and the thermosyphon will have a lower potential to provide cooling during colder parts of the year. At the same time, the mean annual temperature will increase and thus contribute to warmer ground temperatures. For this emissions scenario, RCP85, the mean annual air temperature is projected to be above 0°C and thus thawing of permafrost will happen over time. Both the modeling results from this thesis and theory suggest permafrost thawing to an extent of 5 to 10 meters in Longyearbyen by 2100. From Figure 19 one can notice the ground being permanently thawed, even during winter, for a depth of 3-6.5 meters. With such thaw depths, sufficient cooling of permafrost for constructions and infrastructure might be demanding to provide. Extensive thawing of the permafrost will require more cooling to keep the ground frozen, at the same time, thermosyphons will provide less passive cooling with increased air temperatures. When thawing happens for the upper 5-10 meters of the permafrost, other foundation solutions than foundation cooling might be more appropriate. Buildings and infrastructure constructed in the future, will most likely have foundation methods similar to the mainland if the upper parts of the permafrost thaws. Construction in today's climate with expectations of

extensive thawing due to higher air temperatures with high emissions (RCP85) in the future, might require foundation in solid rock or longer friction piles. A combination of thermosyphons and piling is not discussed in detail in this study, but could be considered as an option. Load bearing thermosyphon piles, thermopiles, or vertical thermosyphons in combination with piles is an interesting solution that potentially can provide a strong foundation with increased air temperatures. Still, other Arctic areas might have a need for ground cooling and thermosyphons can have applications in other areas than Longyearbyen and Svalbard, even with the highest emissions scenario.

5.3 Building Foundation Case

In the modeling case with a concrete slab representing heat flux from a building, the thermosyphons show a passive cooling effect. For today's climate, the thermosyphons seem to provide sufficient cooling to prevent permafrost thawing. With no thermosyphon installed the heat from the building increased the ground's temperature and permafrost thaw happens down to a depth of approximately 5 meters during summer. After installing the thermosyphons the ground shows lower temperatures and thawing only happens in the gravel below the building. This cooling comes from only passive operation of the thermosyphons so no additional energy is required to get such an effect. In the winter season, without thermosyphons, the ground still increased temperatures. The modeling shows permafrost thawing during wintertime when a building heats the ground. Installing thermosyphons provides cooling during winter and the heating from the concrete is prevented. This is an indicator that thermosyphons are useful for ground cooling in Arctic climates.

For the emissions scenario RCP45 the ground shows significant thawing in the modeling case with a building. With no thermosyphons to provide cooling, the ground temperature from modeling indicates thawing down to approximately 6 meters for the final year of the simulation. With thermosyphons installed the thawing is reduced by several meters, but the modeling still suggests there will be thawing in the undisturbed soil. This is not desirable. To provide sufficient cooling for such temperatures one could use a heat pump to run the thermosyphon actively during the warmer parts of the year. This can ensure that the ground stays frozen even when the climate gets warmer. With a heat pump one might be able to utilize the heat from the condenser of the thermosyphon. Even during the summer in Longyearbyen, buildings will need heating and hot water, thus running a heat pump to provide heating for the building and at the same time ground cooling is an

interesting option. Using solar panels to provide power for the heat pump during the summer could improve the efficiency and the environmental aspect even further. These kinds of solutions, utilizing a combination of energy sources, with geothermal heat, ground cooling and solar power are interesting and highly recommended for further work.

The modeling results from both today's climate and RCP45 suggest that thermosyphons have the potential to provide ground cooling. The cooling effect is 3057KWh and 2754KWh for today's climate and RCP45, respectively. For comparison, the average electricity consumption for a household in Norway is 16 000 KWh (Aanensen & Holstad, 2018). The reduction for RCP45 is approximately 10%, which may seem small compared to the difference in thawing. This can be explained by higher ground temperatures for RCP45 giving lower change in the temperature difference, ΔT, for the thermosyphon, thus maintaining much of the cooling effect. The modeling results indicate that a passive thermosyphon is sufficient as ground cooling below a building as presented is the case, with the climate for the period 2010-2020. For the future emissions scenario, RCP45, a passive thermosyphon is not sufficient. From this one can argue that only installing passive thermosyphons, and not choosing a hybrid solution might be short-sighted. One should also consider the fact that temperatures might increase more than RCP45, as is the case with RCP85. For the highest emissions scenario, ground cooling might not be something to consider at all because the mean annual air temperature is above freezing and permafrost has or will thaw permanently. The future temperatures are uncertain and the actual air temperatures could end up somewhere between RCP45 and RCP85.

6 Conclusion

This study suggests that thermosyphons can provide ground cooling for today's climate and future emissions, RCP45 and RCP85. The effect is less for future climate scenarios due to the increased air temperature. For the highest emission scenario, RCP85, both theory and modeling for this study show permafrost thawing to a depth of 5-10 meters. Thus horizontal thermosyphons are not seen as a suitable option for ground cooling in this scenario. Today's climate and RCP45 modeling show that thermosyphons give the ground temperature a cooling trend over the 10-year simulation. The cooling effect is present throughout the entire year for only greater depths. Modeling for 2015 shows a permanent decrease in temperature at 5 meters depth, but at 1.5 meters, the temperature during summer is the same with and without thermosyphons installed.

The modeling case with a building represented the thermosyphons providing sufficient cooling for today's temperatures. The ground is cooled and the undisturbed soil is not thawed from the heat provided by the building when thermosyphons are installed. Without thermosyphons to provide cooling the modeling shows permafrost thaw. For the emissions scenario RCP45, the modeling suggests that passive cooling with thermosyphons is insufficient to prevent permafrost thawing under a building. The temperature is lower when the heat sink is installed, but the modeling shows thawing in the permafrost also with thermosyphons. For this reason, a hybrid solution with thermosyphons is recommended. A hybrid solution can provide sufficient ground cooling even with increased mean annual air temperatures in future climates.

Summary:

- Thermosyphons have several applications and can provide ground cooling.
- The passive cooling effect from thermosyphons is reduced with increased temperatures for future climate change.
- A hybrid thermosyphon solution is preferable to have the option to provide cooling during summer, and with increased temperatures due to global warming.
- Theory and modeling suggest permafrost thawing to depths of 5-10 meters for the highest emissions scenario. For such a case, ground cooling might not be necessary for Longyearbyen.

7 Recommendations for Further Work

Further investigations are needed to improve and develop the topic. Such investigations can both improve, criticize and support the work in this thesis. Including a broader use of thermosyphons to further expand the applications of the technology is also advantageous. Some suggestions for further work within the topic is listed in this section.

- Developing numerical models for other cases where permafrost cooling is necessary is an option for further work. Such cases can be geothermal wells in permafrost, windmill foundation and waste control. Also an interesting aspect for such cases is evaluating ground temperature and soil strength. Looking at a specific case and using modeling with cite specific data to calibrate a numerical model and dimension an appropriate thermosyphon cooling system is useful. In such work one can also implement hybrid cooling for the thermosyphon for additional cooling effect.
- Elaborating and improving the numerical model from this study is useful. This can include making the model in 3 dimensions as well as improving the models parameters. Other thermosyphon setups such as vertical or incline evaporators. Including temperature variation for parameters and groundwater flow to see how this influences the results. Improving the model can also include a more detailed domain. A layered ground domain with different soil properties for depth as well as including both soil and rock for depth according to borehole data can be done. Using the thermal properties of rock from this study is a good option. One could also simulate a rock domain i combination with ice lenses in the rock.
- Improving the ground surface boundary is of great value to make a numerical model more accurate. This is applicable for several topics, both foundation cooling simulation and permafrost modelling with climate change can utilize improved ground surface boundary. Such work can be recording ground surface temperatures in relation to other climate factors such as air temperature, wind, precipitation and sun exposure. Another option is to collect necessary data for Svalbard or a similar environment to estimate the ground surface energy balance accurately.
- Evaluating a combination of heat pump for ground cooling and building heating purposes. An option is to look at the feasibility of exploiting heat from the thermosyphon to provide heating for buildings or hot water etc. and at

the same time using the heat pump for ground cooling in combination with thermosyphons.

- Evaluating feasibility for the use of load-bearing thermosyphon piles or vertical thermosyphons in combination with piling. This can include modeling of both thermal modeling and modeling of displacement and settlements. Such a solution can also be considered in combination with a heat pump as described above.

References

Aanensen, T., & Holstad, M. (2018). Tilgang og anvendelse av elektrisitet i perioden 1993-2017.

Abdalla, B., Fan, C., McKinnon, C., & Gaffard, V. (2015). Numerical study of thermosyphon protection for frost heave. *International Conference on Offshore Mechanics and Arctic Engineering*, *56512*, V05AT04A025.

Andersland, O. B., & Ladanyi, B. (1994). *An introduction to frozen ground engineering.* Chapman Hall.

Badache, M., Aidoun, Z., Eslami-Nejad, P., & Blessent, D. (2019). Ground-coupled natural circulating devices (thermosiphons): A review of modeling, experimental and development studies. *Inventions*, *4*(1), 14.

Bekele, Y., & Sinitsyn, A. (2017). Impact of changing climate on infrastructure in Longyearbyen: stability of foundations on slope terrain–Case study. *Rock and Soil Mechanics*, *2017*, 11–22.

Bratlie, U. H. H. (2018). *An experimental study of thermal properties of permafrost soils* (Master's thesis). NTNU.

Carmichael, R. S., & Klein, . C. (2021). Encyclopedia britannica. (rock). https://www.britannica.com/science/rock-geology

Cengel, Y. A., & Ghajar, A. J. (2014). *Heat and mass transfer: Fundamentals and applications.* McGraw-Hill Higher Education.

COMSOL. (2019). Heat transfer module user's guide. *COMSOL version*, *5.5*.

COMSOL Multiphysics®. (n.d.). Comsol multiphysics® v. 5.5. (COMSOL AB, Stockholm, Sweden.). www.comsol.com.

CSA. (2014). Thermosyphon foundations for building in permafrost regions. *National Standard of Canada, CAN/CSA-S500*, *14*, 44.

C-Therm Technologies Ltd. (no date). How to measure thermal conductivity: Method selection guide [Accessed: 2022-04-25].

de Witt, M., Stefánsson, H., & Valfells, Á. (2019). Energy security in the Arctic: Policies and technologies for integration of renewable energy. *Arctic Yearbook 2019.*

Dobler, A. (2019). Convection permitting climate simulations for Svalbard—Background-report for Climate in Svalbard 2100. *NCCS Rep*, *2*, 27.

Etzelmüller, B., Schuler, T. V., Isaksen, K., Christiansen, H. H., Farbrot, H., & Benestad, R. (2011). Modeling the temperature evolution of Svalbard permafrost during the 20th and 21st century. *The Cryosphere*, *5*(1), 67–79.

Flyen, A., & Mattson, J. (2017). *Permafrost og fundamenteringsforhold for kulturminner i Longyearbyen*. Norsk institutt for kulturminneforskning (NIKU). https://niku.brage.unit.no/niku-xmlui/handle/11250/2607975

French, H. M. (2017). *The periglacial environment* (Fourth edition). John Wiley & Sons.

Geo Slope. (2014). Thermal modeling with temp/w. *September 2014 Edition*.

Geo Slope. (2021). Heat and mass transfer modeling with geostudios.

Gilbert, G., Instanes, A., Sinitsyn, A., & Aalberg, A. (2019). *Characterization of two sites for geotechnical testing in permafrost: Longyearbyen, Svalbard*. Norges Geotekniske Institutt(NGI).

Goering, D. J. (2003). Passively cooled railway embankments for use in permafrost areas. *Journal of Cold Regions Engineering*, *17*(3), 119–133.

Guo, L., Yu, Q., You, Y., Wang, X., Li, X., & Yuan, C. (2016). Cooling effects of thermosyphons in tower foundation soils in permafrost regions along the Qinghai-Tibet Power Transmission Line from Golmud, Qinghai Province to Lhasa, Tibet Autonomous Region, China. *Cold Regions Science and Technology*, *121*, 196–204.

Hanssen-Bauer, I., Førland, E. J., Mayer, H. H. S., Sandø, A. B., & Sorteberg, A. (2019). *Climate in svalbard 2100 - a knowledge base for climate adaptation*. The Norwegian Centre for Climate Services (NCCS).

Harris, S. A., Brouchkov, A., & Guodong, C. (2017). *Geocryology: Characteristics and use of frozen ground and permafrost landforms*. CRC press.

Heller, S. T. (2021). *A Numerical Simulation of Permafrost Thermal Regime under a Heat Pump Chilled Foundation in Longyearbyen, Svalbard* (Master's thesis). NTNU.

Holubec, I. (2008). *Flat loop thermosyphon foundations in warm permafrost*. Government of Northwest Territories Thermosyphon Foundations in Warm Permafrost—Report. https://www.inf.gov.nt.ca/sites/inf/files/flat_loop_thermosyphon_foundations_in_warm_permafrost.pdf

Humlum, O., Instanes, A., & Sollid, J. L. (2003). Permafrost in Svalbard: a review of research history, climatic background and engineering challenges. *Polar research*, *22*(2), 191–215.

Instanes, A., & Rongved, J. (2018). *Forventede klimaendringers påvirkning på byggegrunn i Longyearbyen-området*. Instanes AS.

Isaksen, K., Førland, E., Dobler, A., Benestad, R., Haugen, J., & Mezghani, A. (2017). *Klimascenarioer for Longyearbyen-området, Svalbard*. Norwegian Meterological Institute, MET.

Johansen, Ø. (1975). *Thermal conductivity of soils*. Ph.D. diss., Norwegian Technical University, Trondheim; also US Army Cold Regions Research and Engineering Laboratory Translation 637, July 1977.

Johansson, M., Christensen, T. R., Akerman, H. J., & Callaghan, T. V. (2006). What determines the current presence or absence of permafrost in the Torneträsk region, a sub-arctic landscape in northern Sweden? *AMBIO: A Journal of the Human Environment*, *35*(4), 190–197.

Kim, M.-H., Pettersen, J., & Bullard, C. W. (2004). Fundamental process and system design issues in CO2 vapor compression systems. *Progress in energy and combustion science*, *30*(2), 119–174.

Krautblatter, M., Funk, D., & Günzel, F. K. (2013). Why permafrost rocks become unstable: A rock–ice-mechanical model in time and space. *Earth Surface Processes and Landforms*, *38*(8), 876–887.

Ladanyi, B., & Andersland, O. (2004). *Frozen ground engineering* (2nd). Wiley.

Lewis, R. W., Nithiarasu, P., & Seetharamu, K. N. (2004). *Fundamentals of the finite element method for heat and fluid flow*. John Wiley & Sons.

Long, E. L., & Zarling, J. P. (2004). Passive techniques for ground temperature control. *Thermal analysis, construction, and monitoring methods for frozen ground (D. C. Esch Ed.)*, 77–165.

Lynn, S. W., Rock, S., & Rhodes, C. (2000). Evaluation of a vertical frozen soil barrier at Oak Ridge Rational Laboratory. *Remediation Journal*, *10*(3), 15–33.

Mantelli, M. B. H. (2021). *Thermosyphons and heat pipes: Theory and applications* (1th). Springer.

MET. (n.d.). *Climate in svalbard, arc44*. Retrieved February 5, 2022, from https://thredds.met.no/thredds/catalog/KSS/Climate_in_Svalbard/ARC-44/catalog.html

MET. (2022). *Observasjoner og værstatsitikk fra norsk klimaservicesenter*. Retrieved February 5, 2022, from https://seklima.met.no/observations/

Nam, Y., Ooka, R., & Hwang, S. (2008). Development of a numerical model to predict heat exchange rates for a ground-source heat pump system. *Energy and Buildings*, *40*(12), 2133–2140.

Nedbal, V., Láska, K., & Brom, J. (2020). Mitigation of arctic tundra surface warming by plant evapotranspiration: Complete energy balance component estimation using LANDSAT satellite data. *Remote Sensing*, *12*(20), 3395.

NGU. (no date). *Permafrost - Svalbard*. Retrieved April 6, 2022, from https://geo.ngu.no/kart/permafrost_svalbard_mobil/

Norwegian Polar Institute. (no date). *Map over rock samples from svalbard*. Retrieved May 6, 2022, from https://toposvalbard.npolar.no

Plaxix. (2017). *Modelling of Thermosyphons Foundation System Using Plaxis 2D*. Retrieved February 22, 2022, from https://communities.bentley.com/cfs-file/__key/communityserver-wikis-components-files/00-00-00-05-58/Validation_2D00_Modelling_2D00_of_2D00_Thermosyphons_2D00_Foundation_2D00_System_2D00_Using_2D00_PLAXIS_2D00_2D_2D00_2017.pdf

Regjeringen. (2021). *Ny energiløsning for Longyearbyen*. Retrieved May 14, 2022, from https://www.regjeringen.no/no/dokumentarkiv/regjeringen-solberg/aktuelt-regjeringen-solberg/oed/pressemeldinger/2021/ny-energilosning-for-longyearbyen/id2827886/

Slagstad, T., Balling, N., Elvebakk, H., Midttømme, K., Olesen, O., Olsen, L., & Pascal, C. (2009). Heat-flow measurements in Late Palaeoproterozoic to Permian geological provinces in south and central Norway and a new heat-flow map of Fennoscandia and the Norwegian–Greenland Sea. *Tectonophysics*, *473*(3-4), 341–361.

Snyder, J. P. (1987). *Map projections–a working manual* (Vol. 1395). US Government Printing Office.

van Huissteden, J. (2020). *Thawing Permafrost: Permafrost Carbon in Warming Artic*. Springer Nature Switzerland AG.

Wagner, A. (2013). Creation of an artificial frozen barrier using hybrid thermosyphons. *Cold Regions Science and Technology*, *96*, 108–116. https://doi.org/10.1016/j.coldregions.2013.08.008

Wagner, A. (2014). *Review of thermosyphon applications*. Cold Regions Research and Engineering Laboratory (CRREL).

Xu, J., & Goering, D. J. (2008). Experimental validation of passive permafrost cooling systems. *Cold Regions Science and Technology*, *53*(3), 283–297.

Zueter, A. F., Newman, G., & Sasmito, A. P. (2021). Numerical study on the cooling characteristics of hybrid thermosyphons: Case study of the Giant Mine, Canada. *Cold Regions Science and Technology*, *189*, 103313.

Appendix A COMSOL Model

A.1 RCP45

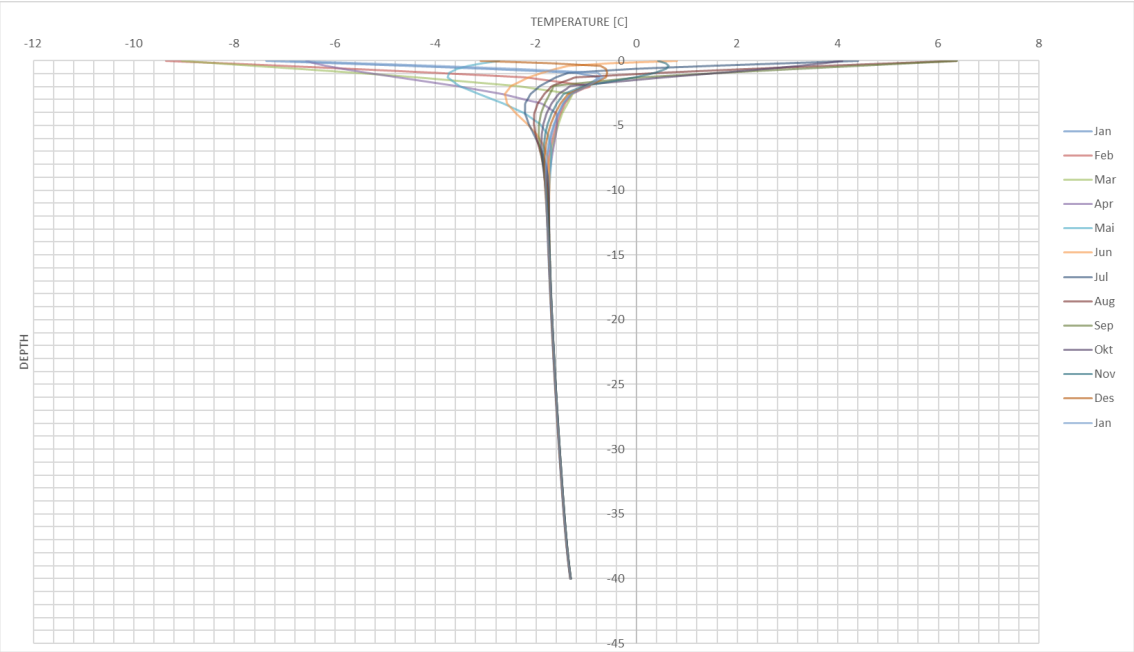

Figure 44: Ground temperature profile for the final year in a 60-year simulation from 2020-2080 for RCP45.

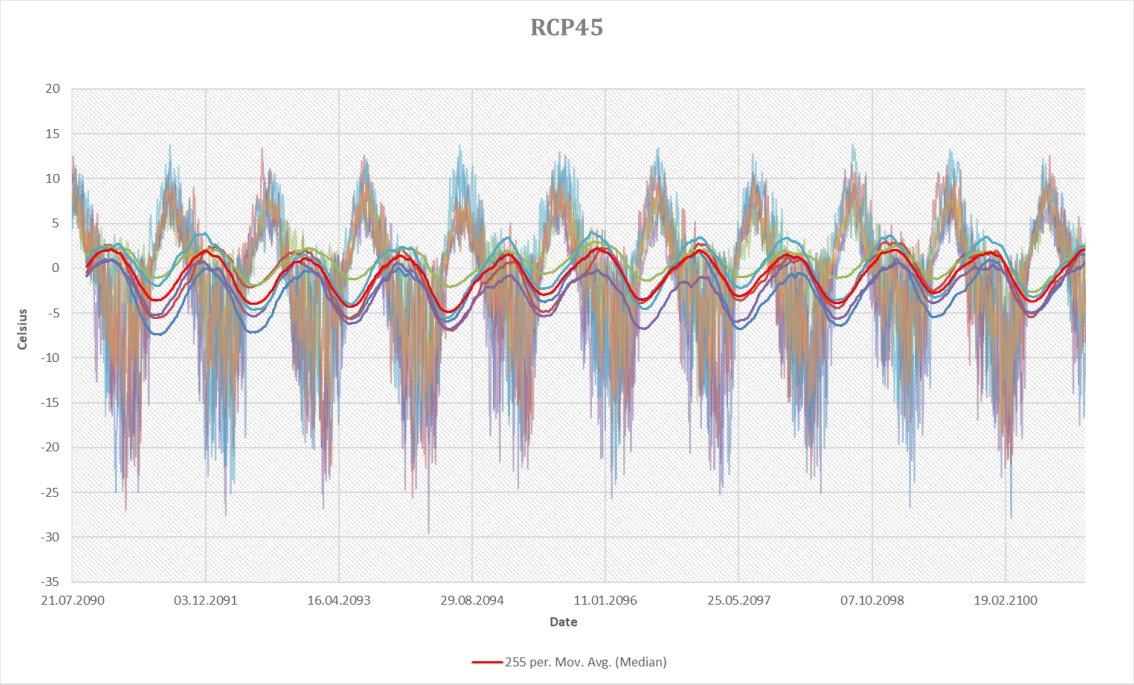

Figure 45: Temperatures, moving average and median temperature for future projections.

A.2 RCP85

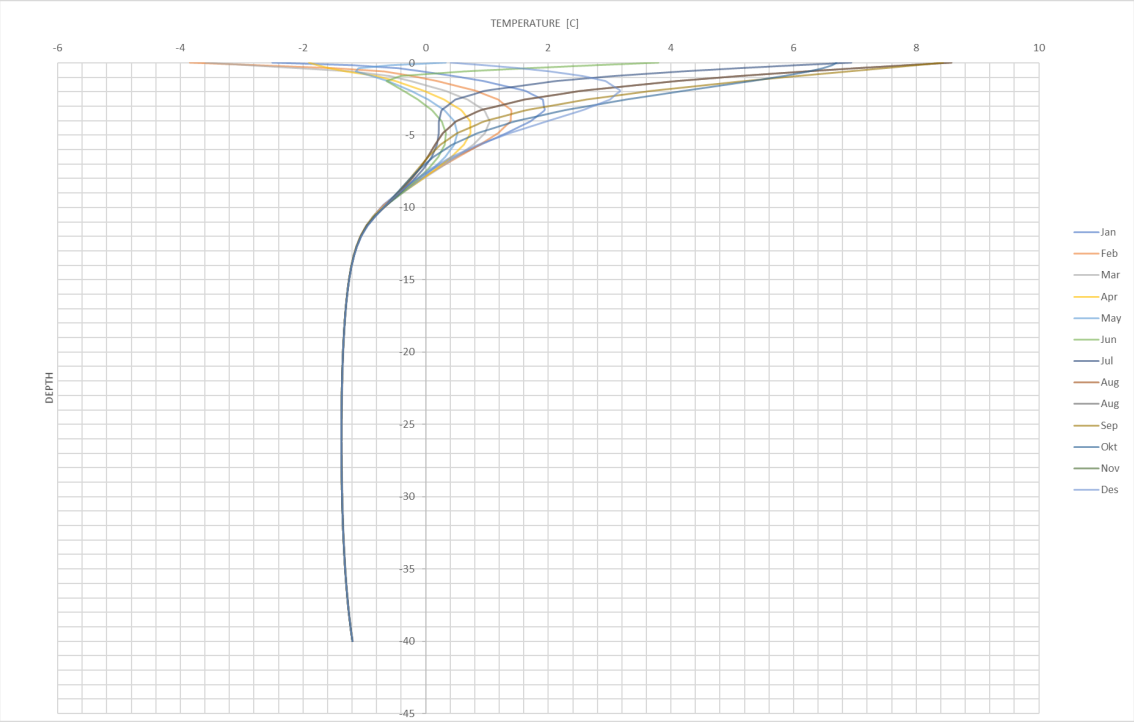

Figure 46: Ground temperature profile for the final year in a 60-year simulation from 2020-2080 for RCP85.

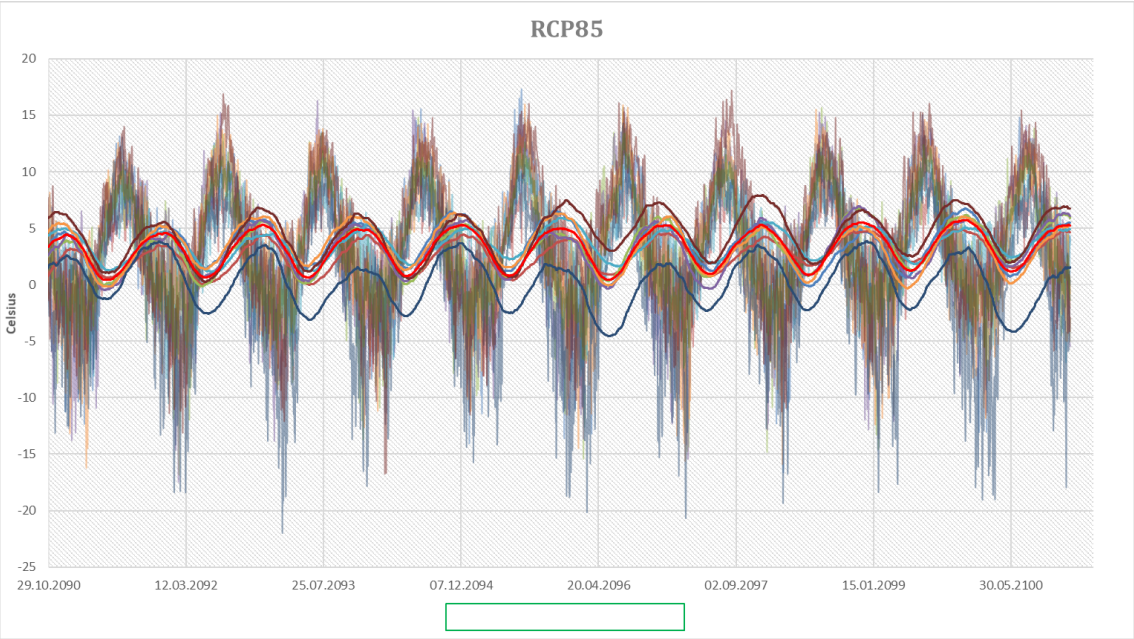

Figure 47: Temperatures, moving average and median temperature for future projections for RCP85.

A.3 RCP45 Without Latent Heat

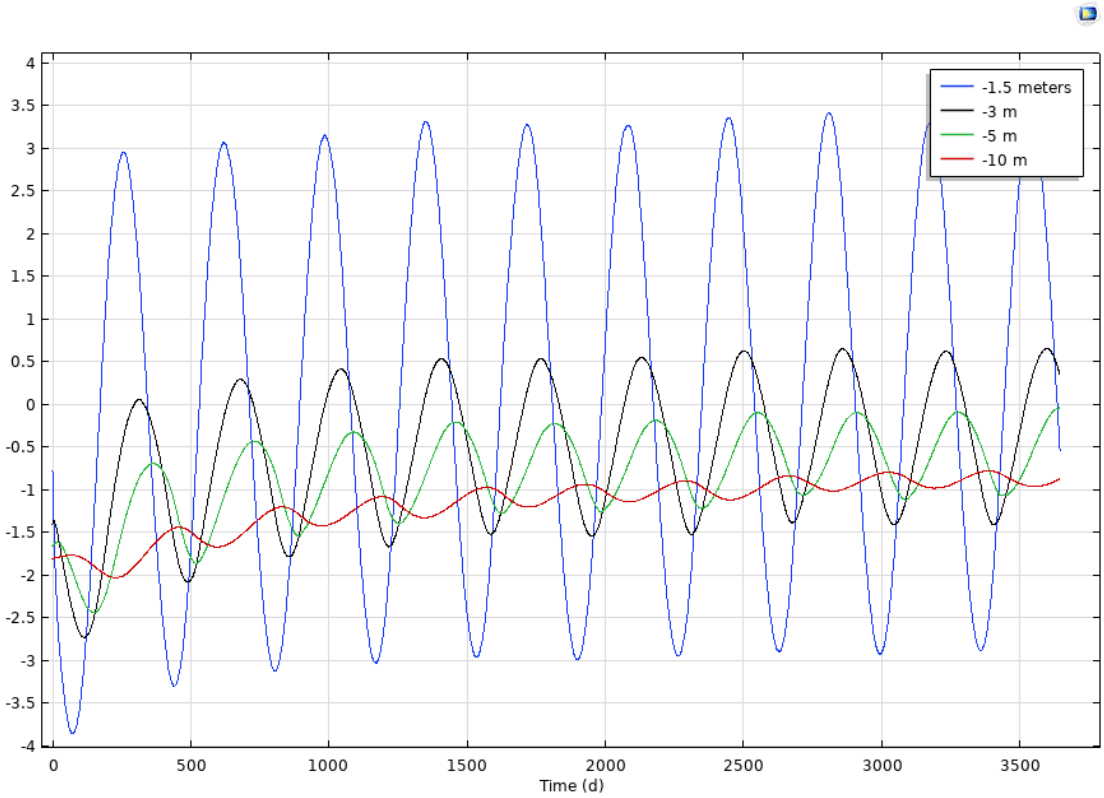

Figure 48: Simulation with no latent heat.

A.4 Code for Data Collection

```
import numpy as np
filer_4_5 = [...] #contains data for the different simulations
data=[]
lon_pt = 15.55 #actual coordinates for Lonyearbyen
lat_pt = 78.22

#collect data from rcp45
for i in range(len(filer_4_5)): #indexing through the different simulations
    ds = data[i] #setting ds as the indexed simulation
    lat = ds['lat'][:,:] # getting all latitudes from the simulation
    lon = ds['lon'][:,:] # getting all longditudes from the simulation
    lon = ds['lon'][:,:]

    # Calculating distances between grid and Longyearbyen coordinates:
    dist = np.sqrt((np.cos(lat/180*np.pi)*(lon-lon_pt))**2+(lat-lat_pt)**2)
    #Finding index for the smallest distances:
    cord = np.where(dist==np.min(dist))
```

Appendix B Rock samples from Svalbard

B.1 Picture of Rock samples

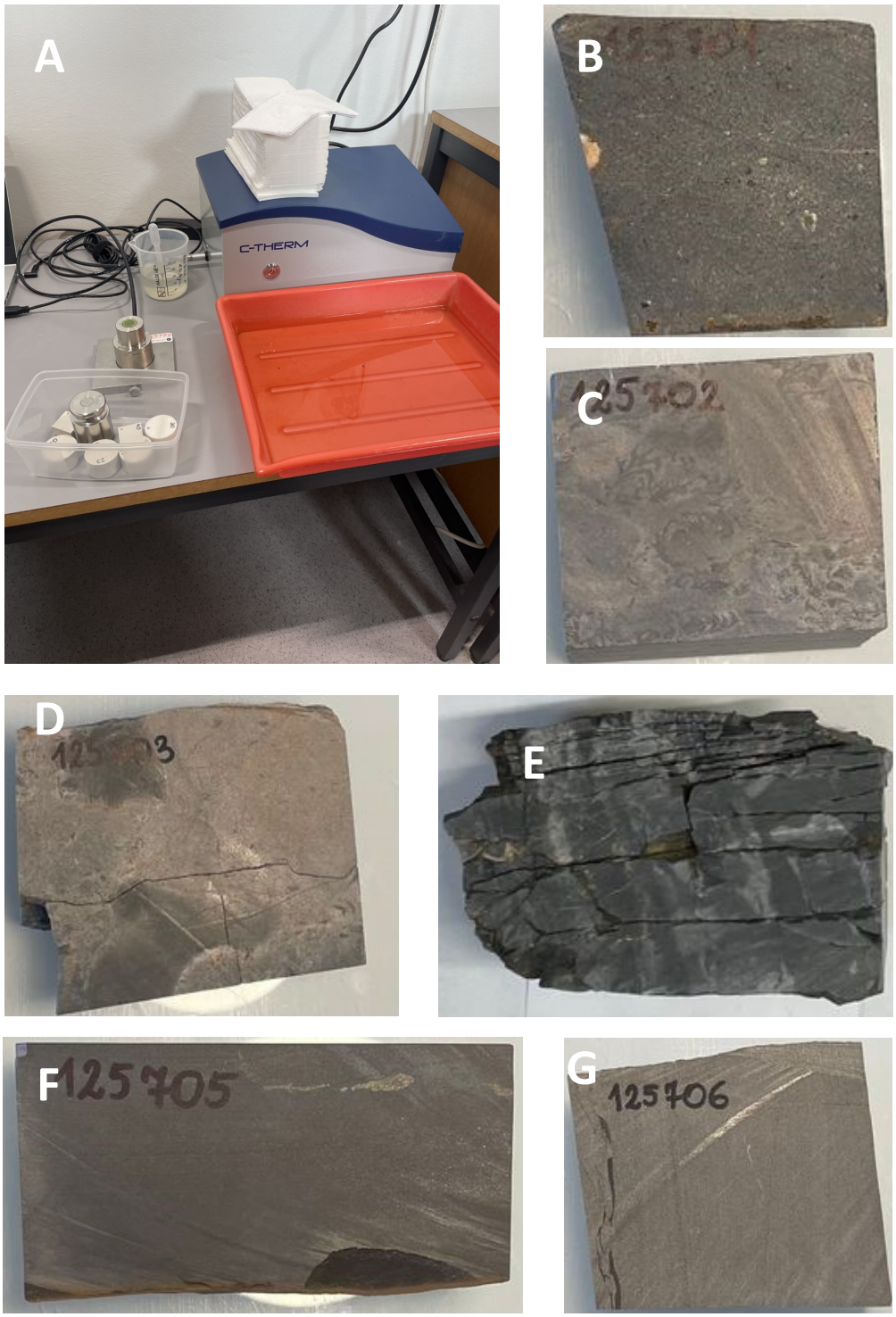

Figure 49: A) The image of the device used to measure thermal conductivity. B-G) Picture of the rock samples named NSL-2022-1 to NSL-2022-4 B, respectively.

Håkon Myhre Aftret og Vetle Martnes Daleng

Suitability of Thermosyphon as a Ground Freezing Technology in Longyearbyen

NTNU
Norwegian University of
Science and Technology